Studies on the intracellular transport system for maternal factors in the ascidian egg

Hirokazu Ishii

DOCTORAL DISSERTATION

Studies on the intracellular transport system for maternal factors in the ascidian egg

by

Hirokazu Ishii

Graduate of Frontiers of Innovative Research in Science and Technology (FIRST), Konan University, Kobe, Japan

March 2014

Supervisor

Professor Takahito Nishikata

Frontiers of Innovative Research in Science and Technology (FIRST), Frontier Institute for Biomolecular Engineering Research (FIBER), Konan University, Kobe, Japan

Summary

細胞はその活動において、RNA やタンパク質などの必要とされる種々の分子を合成し、それぞれ必要とされる特定の細胞内領域へと輸送している。こういった細胞内物質輸送メカニズムは多彩であり、細胞の極性や機能、形態などの制御、発生過程における細胞分化や、その後の生命活動にとって必要不可欠であり、様々な視点からその分子メカニズムが研究されている。中でも、神経細胞における軸索輸送に代表されるような微小管とそのモータータンパク質、つまりダイニンやカイネシンとがつくる微小管系輸送システムは、小胞体の輸送だけにとどまらず、細胞内の一般的な物質輸送システムとしても重要であると考えられている。

ホヤ卵は典型的なモザイク卵として知られ、受精直後から第一卵割直前までの間に、細胞質ドメインとも言える卵細胞質の大きなまとまりが、大きくその局在パターンを変える細胞質再配置が起こる。これは、ひとつの細胞内物質輸送システムであり、種々の母性因子が発生運命地図に対応した卵領域へと輸送される。細胞質再配置は大きく二つの段階に分けて理解されており、第一細胞質再配置はアクチン、第二細胞質再配置は微小管に依存した物質輸送システムであることが明らかにされている。この細胞質再配置は、小胞体やミトコンドリアを含むマイオプラズムが、細胞質ドメインとしての大きなまとまりを保ったままダイナミックに後極へと輸送される点で特徴的であり、個々の分泌小胞をカーゴとしてモータータンパク質が運搬していく上記の微小管系物質輸送システムとは大きく異なっている。このホヤ母性因子の細胞内物質輸送システムでは、これまでにない新規で特徴的なメカニズムが働いている可能性があるが、その分子メカニズムはほとんど明らかにされていない。

そこで本研究では、ホヤ卵細胞質再配置のメカニズムを解明し、細胞内物質輸送の新たなメカニズムと概念を明らかにすることを目的とし、以下の 2 つのアプローチにより研究を進め、以下のような結果を得た。

<u>アプローチ 1</u> ホヤ母性タンパク質 p58 の解析:

ホヤ卵母性因子のひとつである p58 は、ブタ中間径フィラメント抗体に認識される抗原タンパク質としてはじめて報告された。p58 はマイオプラズム全域に局在し、細胞質ゾル中の繊維状タンパク質 myoplasmin-C1 などと複合体を形成している。p58/myoplasmin-C1 複合体は、細胞骨格ドメインの構成に重要な因子のひとつとして注目されており、細胞質再配置メカニズムへの関与も期待された。そこでまず私は、p58 を認識する NN18 抗体を用いた免疫学的手法により、p58 が F_0F_1-ATPase α-subunit と同一であることを明らかにした。一般的に、F_0F_1-ATPase はミトコンドリア内膜に局在して ATP を産生するタンパク質複合体として知られている。しかし、ホヤ卵では F_0F_1-ATPase の α サブユニットおよび β サブユニットだけが、ミトコンドリア外のマイオプラズム表層領域に局在しているという驚くべき事実が明らかとなった。さらに興味深いことに、これらのサブユニットはミトコンドリア内とは異なる構成の新規な複合体を形成して細胞骨格と結合していた。私はこの新規な複合体を exo-ATPα/β と名付けた。

<u>アプローチ 2</u> ミトコンドリア阻害剤 sodium azide (NaN_3)を用いた解析:

ホヤでは卵母細胞への遺伝子導入法が確立されておらず、母性因子の機能解析法には限界があった。そこで、forward chemical genetics としてホヤ卵にいくつもの化合物を添加し、細胞質再配置を阻害する阻害剤を探索して、そのターゲット分子を同定することを試みた。その結果、ミトコンドリア呼吸鎖阻害剤として知られる NaN_3 が、微小管依存的な第二細胞質再配置におけるマイオプラズムの輸送を阻害することを明らかにした。このとき、微小管の脱重合は見受けられず、NaN_3 が微小管の重合に直接影響を与えるものではないことが示唆された。別の呼吸鎖阻害剤である oligomycin には、細胞質再配置に対する阻害効果は見受けられず、NaN_3 が呼吸鎖以外の細胞質再配置に重要な分子を阻害したことが明らかとなった。また、NaN_3 が卵割期胚における spindle midzone の形成や spindle orientation といった spindle dynamics に関わる微小管依存的メカニズムも阻害することがわかった。Spindle dynamics に対する同様な阻害効果は、ウニ胚やヒト培養細胞においても見受けられ、NaN_3 が異なる動物種間で保存されている分子

をターゲットにして、微小管依存的な共通メカニズムを阻害していることが示唆された。

本研究で明らかにした、exo-ATPα/β の存在は、常識的なミトコンドリア内膜の F_0F_1-ATPase に対する理解を根底から覆し、細胞生物学をはじめとした様々な分野に多大なインパクトを与えるものである。exo-ATPα/β の機能は不明であるが、exo-ATPα/β の局在するマイオプラズム表層領域は、微小管依存的な第二細胞質再配置に特に重要な卵領域であることが示唆されている。今後、exo-ATPα/β の構成分子や、その機能を明らかにしてゆくことで、exo-ATPα/β と細胞質再配置との関わり、そしてその分子メカニズムの解明に繋がることが期待される。さらにホヤ卵表層領域には、spindle orientation に重要な分子の局在も報告されており、exo-ATPα/β との関連も興味深い。

また本研究では、第二細胞質再配置を微小管重合阻害剤以外の阻害剤（NaN_3）で阻害することにはじめて成功した。これは、ホヤ細胞質再配置における微小管依存的なメカニズムを解析する上で重要な実験系となる。NaN_3 の阻害効果は、同様の濃度で spindle dynamics にも大きな異常をもたらすことから、NaN_3 がこの 2 つの異なる微小管依存的な細胞内イベントを、共通のメカニズムで阻害したことが示唆される。またさらに、この NaN_3 の spindle dynamics に対する効果は、同じ濃度でホヤ、ウニ、ヒトの細胞で同様に再現されることから、そのメカニズムが幅広い生物種で保存されたメカニズムであることも示した。分子レベルの解析が容易なヒト培養細胞を材料に微小管依存的メカニズムに関わる NaN_3 のターゲット分子を同定し、ホヤでの相同分子を明らかにして細胞質再配置における役割を解析していく、という今後の新たなアプローチは、細胞質再配置のメカニズムを解明していくための重要な研究基盤となるに違いない。

さらに細胞質再配置および spindle orientation と、spindle midzone に対する NaN_3 の阻害効果は、細胞表層と midzone との関わりに対する阻害効果と考えることも可能であり、不明な点の多い細胞表層と midzone という二つの領域の関連性が浮かび上がってきた。exo-ATPα/β の構成分子および機能解析と、NaN_3 のターゲット分子の同定は、細胞内物質輸送の新たなメカニズムを明らかにするだけでなく、細胞分裂における spindle dynamics の解明という新たなテーマにも

発展する可能性を持っている。

Contents

1 BACKGROUND

1.1 Intracellular transport system

In cells, numerous molecules such as RNAs and proteins are transported to the particular intracellular regions where the molecules exert their roles in cellular activities. Alternatively, a number of molecules are metabolized or degraded following the transports. These intracellular transport systems are essential for the cellular functions, polarity and structure of the cell, normal cellular activities, and cell differentiation during development. Above all, microtubule transport system including microtubule and its motor proteins, dynein and kinesin, is the most important mechanism and well understood. For example, in axonal transport, synaptic vesicles are transported to the plus end of axonal microtubules as a cargo of the plus-end motor protein, dynein. Recently, this microtubule-based transport system is not restricted to the axonal transport, but also important for various cell types (Aridor & Hannan 2000; Vale 2003; Hirokawa *et al*. 2009; Hirokawa 2011; Nakajima *et al.* 2012; Franker & Hoogenraad 2013).

1.2 Spindle microtubules

Mitotic cell division is usually divided into five discernible phases; prophase, metaphase, anaphase, telophase, and cytokinesis. The mitotic spindle is a microtubule-dependent apparatus, which is important for chromosome segregation and

composed by three sets of microtubules. The kinetochore microtubules connect the chromosomes to the spindle poles. The astral microtubules connect the poles to the cell cortex. The interpolar microtubules interdigitate between each pole to form an antiparallel microtubule array in the spindle midzone, where the chromosome passenger complex containing aurora B kinase is localized (Vader *et al.* 2006; Ruchaud *et al.* 2007; Sharif *et al*. 2010). The spindle midzone microtubules contribute to positioning the cell-division plane between the segregating chromosomes (Glotzer 2005; Fuller *et al.* 2008). The cell-division plane is also regulated by the orientation of the mitotic spindle relative to cell polarity axes. In principle, the spindle orientation is achieved through signaling pathways that provide a molecular link between cell cortex and astral microtubules (Lu & Johnston 2013). On the other hand, how signals are transmitted over length scales of micrometers between midzone microtubules and the cell cortex is unclear. Fuller *et al.* (2008) proposed that feedback between aurora B kinase activation and midzone microtubules generates a gradient of post-translational marks that provides spatial information for events in anaphase and cytokinesis.

1.3 Mitochondria control numerous cellular processes

Mitochondria are the key organelles producing cellular energy, ATP (adenosine triphosphate), through oxidative phosphorylation in complexes I through V of the mitochondrial respiratory chain. In addition to producing ATP, mitochondria are involved in controlling numerous cellular processes, such as apoptosis (Suen *et al.* 2008), cell-cycle control (Mandal *et al.* 2005; Mitra *et al.* 2009), cell growth

(Sciacovelli *et al.* 2013) as well as germ cell differentiation (Amikura *et al.* 2005). The eggs of many animals contain aggregates of tightly packed mitochondria, which are called nuage, mitochondrial cloud or Balbiani body, often associated with germ plasm (Kloc *et al*. 2004; Dumollard *et al*. 2006; Zhou *et al*. 2010). The ascidian myoplasm offers an accessible system to address questions concerning networks of mitochondria, such as their regulation, function, and how they are properly partitioned during cell division.

1.4 Mitochondrial ATP synthase (F_0F_1-ATPase)

The complex V of the mitochondrial respiratory chain is known as ATP synthase (F_0F_1-ATPase), which is comprised of two basic units, a water-soluble catalytic moiety called F_1-ATPase and a detergent-soluble unit called F_0. The physiological function and mechanisms of F_0F_1-ATPase, their conformations as well as the inhibition sites of various inhibitors are well understood. For example, oligomycin binds to the ring of subunit c in the F_0 of the F_0F_1-ATPase and inhibits the synthesis of ATP (Hong & Pedersen 2008; Symersky *et al*. 2012). The azide anion of sodium azide (NaN_3) binds to the catalytic site in the β-subunit of F_1-ATPase and inhibits the ATP hydrolase activity but not its synthetic activity (Bowler *et al*. 2006; Hong & Pedersen 2008). Azide also inhibits cytochrome *c* oxidase (complex Ⅳ) by binding to the metal sites, heme a_3 and Cu_B, that form the oxygen reduction site (Yoshikawa *et al*. 1998; Fei *et al*. 2000). Thus, both oligomycin and NaN_3 are expected to inhibit mitochondrial respiration.

1.5 Forward chemical genetics

Forward chemical genetics is an experimental approach to screen for small-chemical compounds, which have biologically activities, and to identify the target molecules. Examples of compounds screened by forward chemical genetics are the immunosuppressant rapamycin and the proteasome inhibitor lactacystin (Martel *et al.* 1977; Omura *et al.* 1991; Schreiber 1991). The target molecules of rapamycin and lactacystin are the mTOR (mammalian target of rapamycin) protein and the 20S proteasome, respectively (Cafferkey *et al.* 1993; Kunz *et al.* 1993; Brown *et al.* 1994; Sabatini *et al.* 1994; Sabers *et al.* 1995; Fenteany *et al.* 1995). These chemical inhibitors progressed the understanding of the functions of mTOR signaling pathway and proteasome.

In the field of ascidian development, chemical inhibitor is one of the most useful tools to reveal the mechanism of the development. The information of the small chemicals used in the field of ascidian biology is summarized in Ascidians Chemical Biological Database (ACBD; http://chordate.bpni.bio.keio.ac.jp/acbd/top.html), where more than 800 articles from 1970 to 2009 are integrated and annotated. In the ACBD, there is no small chemical that inhibits the cytoplasmic and cortical reorganization except for cytoskeletal inhibitors.

2. INTRODUCTION

2.1 Ascidian egg is a typical mosaic egg

Ascidians are the sister group to vertebrates (Delsuc *et al.* 2006), and their embryos develop rapidly into tadpole larvae exhibiting the typical chordate body plan (Lemaire *et al*. 2008; Satoh 2003). Over a century ago, Conklin closely observed the cell lineage and the cytoplasmic organization of *Cynthia* (*Styela*) *partita*, and described the "yellow crescent" at the posterior pole just before the first cleavage (Conklin 1905a). As this yellow cytoplasm was distributed into larval muscle cells, he designated this cytoplasm as "myoplasm" (Conklin 1905b, Gilbert 2010). Until the 1990's, the myoplasm was recognized as a cytoplasmic region containing pre-localized egg cytoplasmic information responsible for specifying larval tail-muscle cells (Satoh *et al.* 1990; Satoh 1994).

2.2 Maternal factors localized in the ascidian myoplasm

Ultrastructurally, myoplasm is composed of pigment granules, an aggregation of mitochondria, endoplasmic reticula, fine granular materials, and a cytoskeletal framework (Berg & Humphreys 1960; Jeffery & Meier 1983). Speksnijder *et al.* (1993) revealed the endoplasmic reticulum (ER) network within the ascidian egg cytoplasm and the stuck of the ER in the myoplasm. Gualtieri & Sardet (1989) revealed the cortical ER (cER) domain in the cortex of the myoplasm by the techniques of confocal

microscopy and isolated cortices. High-resolution confocal microscopy and in situ hybridization revealed the co-localization of postplasmic mRNA and the cER (Sardet *et al.* 2003; Sardet *et al.* 2005; Prodon *et al.* 2005).

When the maternal *macho-1* mRNA, ascidian muscle determinant, was discovered at the end of the last century (Nishida & Sawada 2001), the cortical region of the myoplasm, where *macho-1* mRNA is localized, was thought to be the sole location of maternal information. Moreover, many maternal mRNAs, so-called "type-I postplasmic RNAs" (Makabe *et al.* 2001), or "postplasmic/PEM RNAs" (Prodon *et al*. 2005) are also localized to the cortical region. These findings pointed out the importance of the cortical region of the myoplasm for the establishment of the anteroposterior axis, unequal cleavage, cell fate determination, and a number of cellular processes.

Mitochondria are very few in the cortical region of the myoplasm (Speksnijder *et al.* 1993; Ishii *et al.* 2012). Most of the mitochondria are localized to the internal region of the myoplasm (mitochondria-rich myoplasm). The mitochondria localized in the mitochondria-rich myoplasm are distributed into larval muscle cells and are thought to play a role in producing ATP (Nishida 2005).

2.3 The transport system of ascidian maternal factors: cytoplasmic and cortical reorganization

The ascidian myoplasm is also known as a cytoskeletal domain with filamentous networks consisting of intermediate filaments, microfilaments, and microtubules (Jeffery 1985, 1995; Jeffery & Meier 1983). The myoplasmic cytoskeletal domain is

localized to the periphery of the unfertilized eggs, except for a small patch on the animal pole. After fertilization, during the first cell cycle, cytoplasmic and cortical reorganization (previously called ooplasmic segregation) occurs in two phases (Fig. 2.1; Sardet *et al*. 1989; Roegiers *et al*. 1999; Sardet *et al.* 2003; Sardet *et al.* 2007). Immediately after fertilization, the first phase of reorganization occurs and concomitantly the myoplasm and sperm nucleus are brought to the vegetal pole region. During the first phase of reorganization, the cortical microfilament network shrinks towards the vegetal pole region. The microfilament inhibitor cytochalasin B inhibits the first phase of reorganization, suggesting that the first phase of reorganization occurs via a microfilament-dependent mechanism (Reverberi 1975; Chiba *et al.* 1999). The second phase of reorganization brings the myoplasm to the future posterior side and establishes the anteroposterior axis (Sardet *et al.* 1989; Roegiers *et al*. 1999; Nishida 2005). During the second phase, the sperm aster migrates to the posterior pole along the egg cortex, and then leaves the cortex and migrates to the center of the egg (Sawada & Schatten 1988; Sardet *et al.* 1989; Roegiers *et al.* 1999). When microtubule polymerization is prevented by the inhibitor griseofulvin, the myoplasm and the sperm nucleus stay at the vegetal pole region, suggesting that the second phase is microtubule-dependent (Chiba *et al.* 1999). During the second phase of reorganization, some astral microtubules were found to extend themselves along the posterior cortex and were suggested to be important for the reorganization (Chiba *et al.* 1999).

The cytoplasmic and cortical reorganization is regarded as an intracellular transport system that transports the cytoskeletal domain including numerous maternal factors.

Since the ascidian reorganization is one of the most dynamic phenomena in intracellular transport systems, the molecular mechanism could be characteristic and novel. However, because very few experimental tools have been available for the knockdown of maternal factors during ascidian oogenesis, the molecular mechanisms of this cytoplasmic and cortical reorganization are not yet fully understood.

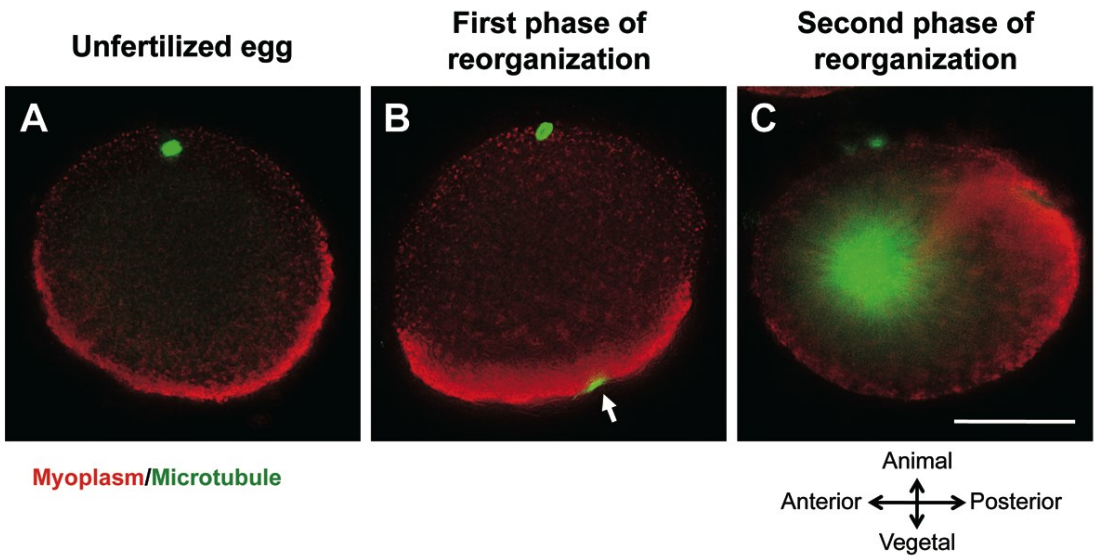

Figure 2.1 Cytoplasmic and cortical reorganization in the ascidian *Ciona intestinalis*. Vertical sections of *Ciona* eggs were stained for myoplasm (red) and microtubule (green). (A) Unfertilized egg. (B) 1-cell-stage embryo at the end of the first phase of reorganization (5 mpf). (C) 1-cell-stage embryo at the end of the second phase of reorganization (45 mpf). The anteroposterior axis is established after the second phase of reorganization. The region where the myoplasm is localized becomes posterior side. The animal pole is up and the vegetal pole is down. Arrow indicates sperm aster. Scale bar, 50 μm.

2.4 An ascidian maternal factor “p58”

Swalla *et al.* (1991) first reported an ascidian maternal factor p58, which was recognized by the NN18 monoclonal antibody. This NN18 antibody recognizes the medium molecular weight (160 kDa) neurofilament subunit and labels exclusively neurofilaments in vertebrates as well as crab (Balaratnasingam *et al*. 2011; Arboleda *et al*. 2011; Franke *et al*. 1991; Corrêa *et al*. 2004). In the ascidian embryo, NN18 recognizes a 58 kDa protein and strongly labels myoplasm in eggs from numerous species (Roegiers *et al*. 1999; Swalla *et al*. 1991; Jeffery & Swalla 1992; Chiba *et al*. 1999; Marikawa 1995). Immunoblots using NN18 antibody show that p58 is abundant in unfertilized eggs and present throughout embryonic development of *Phallusia mammillata*, *Ascidia ceratodes*, and *Ciona intestinalis* (Swalla *et al*. 1991; Chenevert *et al*. 2013). In fixed embryos, NN18 strongly labels the myoplasm and muscle lineage blastomeres of *Phallusia mammillata*, *Ascidia ceratodes, Styela clava, Molgula oculata, Ciona savigny,* and *Ciona intestinalis* (Roegiers *et al*. 1999; Patalano *et al*. 2006; Paix *et al*. 2009; Swalla *et al*. 1991; Jeffery & Swalla 1992; Chiba *et al*. 1999; Marikawa 1995).

Swalla *et al.* (1991) also reported that p58 is necessary for restoration of larval features in *M. occulta* × *M. oculata* hybrids. The authors also proposed p58 as a cytoskeletal component (Jeffery & Swalla 1992). On the other hand, myoplasmin-C1 is one of the myoplasm-specific antigens recognized by monoclonal antibodies raised against isolated *Ciona* whole myoplasm, and is suggested to have a role in muscle differentiation (Nishikata *et al.* 1987). The myoplasmin-C1 has heptad repeats and is suggested to form homo- or hetero-oligomeric complexes *in vivo* through an alpha-helix

coiled-coil structure (Nishikata & Wada 1996). Actually, pull-down experiments suggest that myoplasmin-C1 forms a complex with p58. As the myoplasmin-C1 is detergent insoluble, the myoplasmin-C1 is suggested to bind to the cytoskeletal filaments (Nishikata & Wada 1996). The studies on the complex composed of myoplasmin-C1 and p58 is an interesting theme to understand the transport mechanisms of the myoplasmic cytoskeletal domain.

2.5 Purpose of this study

Since the ascidian myoplasmic reorganization is one of the most dynamic phenomena in intracellular transport systems, its molecular mechanism could be characteristic and novel. Therefore, the molecular mechanism might open a new paradigm of molecular transport and microtubule dynamics. However, because very few experimental tools have been available for the knockdown of maternal factors during ascidian oogenesis and there is no small chemical that inhibits the cytoplasmic and cortical reorganization except for cytoskeletal inhibitors, the molecular mechanisms of this cytoplasmic and cortical reorganization are not yet fully understood.

The purpose of this study is to investigate the mechanism of cytoplasmic and cortical reorganization and to propose a new insight into intracellular transport system. To this objects, I carried out the 2 experimental approaches.

First, the identity of the ascidian maternal factor p58 by using NN18 antibody was investigated and surprisingly revealed that the p58 is identical to the mitochondrial F_1-ATPase α-subunit. Since previous study also indicated that p58 is a cytoskeletal

protein and forms a complex with myoplasmin-C1, I built a bold hypothesis that the F_0F_1-ATPase ectopically exists to the cytosol in ascidian egg. To exam this hypothesis, the subcellular localization of the subunits of F_0F_1-ATPase was carefully analyzed by using immunological probes and finally demonstrated the appropriateness of my hypothesis **(Chapter 4.1 & 4.2)**.

Second, the chemical inhibitors that inhibit the cytoplasmic and cortical reorganization were screened. In this result, NaN_3 was obtained as the candidate inhibitor. Since NaN_3 is widely known as a mitochondrial respiratory inhibitor, the effects of NaN_3 and the other respiratory inhibitor, oligomycin, on ascidian early development were carefully compared. In addition to the effects of NaN_3 on the reorganization, it was figured out the further inhibitory effects on the spindle-midzone formation and the spindle orientation. All of these cellular processes are based on microtubules. Furthermore, similar effects of NaN_3 on the microtubule dynamics were observed in sea urchin embryo and human cultured cells. All these cellular processes, which were inhibited by the similar concentration of NaN_3, had similarity in the microtubule dynamics related to the cell cortex **(Chapter 4.3 & 4.4)**.

3 MATERIALS AND METHODS

3.1 Ascidian gonads and embryos

Wild type *Ciona intestinalis* adults were provided by Kyoto University and University of Tokyo through the National Bio-Resource Project of the Ministry of Culture, Sports, Science, Engineering and Technology (MEXT), Japan. The animals were kept at 18°C in laboratory tanks with a closed water circulation system. Gonads and eggs were obtained surgically. Eggs were obtained surgically and were inseminated with a diluted suspension of non-self sperm. The embryos were reared in Millipore-filtered seawater (MFSW) at 18°C. At this temperature, the first and the second phases of reorganization take place about 5 minutes post-fertilization (mpf) and 45 mpf, respectively. The first cleavage occurs at about 60 mpf and the larvae hatch about 18 hours post-fertilization (hpf).

3.2 Treatment with mitochondrial inhibitors

NaN_3 (Wako, Osaka, Japan) was dissolved in distilled water to a concentration of 5 M and stored as a stock solution at 4°C. Oligomycin (Sigma, St Louis, MO, USA) was dissolved in dimethylsulfoxide (DMSO) to a concentration of 1 mM and stored as a stock solution at -20°C. These stock solutions were diluted with MFSW immediately prior to use. For analyses of the effects of these inhibitors on cytoplasmic and cortical reorganization, embryos were treated with 5 mM NaN_3 or 1.5 μM oligomycin.

Untreated embryos were used for the control.

3.3 Antibody generation

Antibodies against *Ciona* F_1-ATPase α-subunit (anti-α), β-subunit (anti-β) were generated by MBL, Nagoya, Japan, and antibodies against γ-subunit (anti-ATPγ) and *Ciona* F_0 subunit b (anti-ATPb) were generated by Hokkaido System Science, Sapporo, Japan (anti-ATPγ and ATPb). Followings are the antigenic peptides for the antibody production designed from the *Ciona* genome database: CILDSIRNEGKITESTEA (KH.C10.579) for anti-α; CPIDERGPVDTEHFAGIH (KH.C3.87) for anti-β; SKASVYVPQLVQVRC and CPFFSVEVINQSPTI (KH.C14.125) for anti-ATPγ; RILFKAGRPVC and CVQKVDSQLAHGHMV (KH.C1.670) for anti-ATPb.

3.4 Immunohistochemistry

Ciona sperm was fixed on the cover slip with 100% methanol, followed by 100% ethanol. Gonads and embryos were fixed with 100% methanol, followed by 100% ethanol in the same way. For whole-mount specimens, unfertilized eggs were dechorionated. For sectioned specimens, fixed embryos were embedded in Polyester Wax (Steedman 1957; BDH, Poole, UK) and sectioned at 8 μm. Sectioned specimens were mounted onto coverslips and the Polyester Wax was removed using 100% ethanol. The whole-mount specimens or the sectioned specimens were washed with phosphate-buffered saline containing 0.05% Tween 20 (PBST) and were stained with appropriate sets of primary and secondary antibodies from the following: NN18 mouse

monoclonal antibody (anti-ATPα antibody; Sigma, St Louis, MO, USA, N5264; 1:200 dilution), anti-ATP5B chicken antisera (anti-ATPβ antibody; Sigma, GW22827; 1:1,000 dilution), anti-MnSOD rabbit antisera (StressMarq Biosciences, Victoria, Canada, SPC-117C/D; 1:40 dilution), anti-PDHE1α mouse monoclonal antibody (MitoScience, Eugene, OR, USA, MSP07; 1:50 dilution), anti-α-tubulin mouse monoclonal antibody (anti-microtubule antibody; Cedarlane Laboratories, Hornby, Ontario, Canada, CLT9002; 1:100 dilution), anti-aPKC rabbit antisera (Santa Cruz Biotechnology, Santa Cruz, CA, USA, sc-216; 1:200 dilution), anti-kinesin monoclonal antibody (BioMakor, Rehovot, Israel, 6508; 1:2,000 dilution), rabbit anti-chicken IgG (Sigma, C-6778; 1:200 dilution), rhodamine-conjugated goat anti-mouse IgG+M (BioSource International, Camarillo, CA, USA, AMI0706; 1:200 dilution), fluorescein isothiocyanate (FITC)-conjugated goat anti-rabbit IgG (American Qualex Antibodies, San Clemente, CA, USA, A102FS; 1:200 dilution), FITC-conjugated goat anti-mouse IgG+M (American Qualex Antibodies, A108FS; 1:200 dilution), Alexa Fluor 488-conjugated goat anti-mouse IgG (Molecular Probes, Eugene, OR, USA, A11001; 1:1000 dilution), Alexa Fluor 568-conjugated goat anti-chicken IgG (Molecular Probes, A11041; 1:2,000 dilution). DNA was visualized by staining with DAPI (4′6′-diamidino-2-phenylindole dihydrochloride). The stained specimens were observed using a BioRevo BZ-900 (Keyence, Osaka, Japan) or LSM700 confocal microscope (Carl Zeiss, Jena, Germany) or M205 FA stereomicroscope (Leica, Wetzlar, Germany).

3.5 Immunoscreening of cDNA library

Starting with RNA extracted from *Ciona* unfertilized eggs, an oligo-d(T)-primed cDNA library was constructed in Uni-ZAP XR and screened according to the manufacturer's method (Stratagene, La Jolla, CA, USA). About 50,000 plaques were plated, induced and probed with the NN18 monoclonal antibody, yielding 10 positive cDNA clones.

3.6 Immunoprecipitation

Ciona gonads were collected and frozen in liquid nitrogen, then pulverized with a mortar and a pestle without thawing and stored in aliquots at -80°C. Just before immunoprecipitation, frozen gonad material was lysed in 10 volumes of ice cold homogenization buffer (20 mM HEPES pH 7.5, 150 mM NaCl, 1 mM EDTA, 1% Triton X-100) containing 10 μg/ml leupeptin and 1 mM PMSF or protease inhibitor cocktail (P8340, Sigma-Aldrich) and homogenized for 10 strokes with a Potter-Elvehjem glass homogenizer fitted with a Teflon pestle. The homogenate was centrifuged at 5000 x g for 10 min and the supernatant was used immediately. NN18 antibody was bound to protein-G sepharose resin (Amersham Pharmacia Biotech) by incubating at 4°C for 1 hr. The gonad homogenate (soluble fraction) was pre-treated with protein-G sepharose for 1 hr at 4°C in order to reduce non-specific binding, and then incubated together with the NN18 bound protein-G sepharose for 24 hours at 4°C with gentle rocking. The resin pellet containing immunoprecipitated proteins was washed extensively with PBS, and soaked with SDS-sample buffer not containing 2-mercaptoethanol (0.0625 M Tris-HCl pH 6.8, 10% glycerol, 0.5 μM PMSF, 2.3%

SDS). Nondenaturing conditions were used during sample preparation and electrophoresis in order to separate the targeted protein (58 kD) from immunoglobulin heavy chain (55 kD), which also eluted from the sepharose. The products of immunoprecipitation were loaded onto SDS-PAGE gels without mercaptoethanol, which were either silver stained or blotted onto PVDF membrane (Immobilon; Millipore). The band corresponding to p58 was excised from a PVDF membrane stained with Coomasie Brilliant Blue and sequenced by the N-terminal Edman degradation method using a Model Procise 491 (Applied Biosystems) machine.

3.7 Subcellular fractionation of *Ciona* gonad homogenate

Gonads were washed several times with ice-cold homogenization solution (HS; 0.5 M sucrose, 50 mM Tris-HCl pH 7.5, 20 mM $MgCl_2$, 10 mM EGTA). This HS was modified from the previously described method (Fujiwara & Yasumasu 1997). The washed gonads were suspended in 10 volumes of ice-cold HS and homogenized with a Potter-Elvehjem glass homogenizer fitted with a Teflon pestle for 10 strokes. The homogenate was filtered through a nylon mesh (N-NO.270T; NBC, Tokyo, Japan) and centrifuged at 500 × g for 10 min. The homogenate was stratified into a pellet, a supernatant, and a fluffy layer. The pellet and the fluffy layer were designated the insoluble cytoplasmic mass (IC) fraction and fluffy layer (FL) fraction, respectively. The supernatant was centrifuged at 10,000 × g for 10 min and the resulting pellet and supernatant were designated the mitochondria-enriched (ME) fraction and soluble cytoplasmic (SC) fraction, respectively. The concentration of these protein samples was

determined by the Bicinchoninic Acid assay using Bicinchoninic Acid Solution (Sigma, B9643) and Copper (II) Sulfate Solution (Sigma, C2284). The same amount of the total protein was applied in each subsequent experiment.

3.8 Preparation of extracted eggs

The method for the preparation of extracted eggs was modified from the previously described method (Nishikata & Wada 1996). Unfertilized *Ciona* eggs were washed three times with Ca^{2+}-, Mg^{2+}-free seawater containing 1 mM EDTA. The washed eggs were treated with extraction buffer (20 mM $MgCl_2$, 10 mM KCl, 10 mM EGTA, 2% Triton X-100, 20% glycerol, 25 mM imidazole, pH6.9). The extracted eggs were collected by centrifugation and used for immunohistochemistry and Western blotting.

3.9 Measurement of the sperm motility

This analysis was described by Saito *et al*. (2012). Unfertilized eggs were inseminated with an excess number of sperms. The egg movement occurred by sperm motility was recorded by using a BioRevo BZ-900 (Keyence). The velocity (μm/second) of each egg was measured as the moving distance of the egg in the stacked image of an arbitrary one-second recording.

3.10 SDS-PAGE and Western blot

Protein samples were separated by SDS-PAGE, and blotted onto PVDF membrane (Immobilon, Millipore, Billerica, MA). Antibodies used in this study were as follows:

anti-ATPα antibody (1:2,000 dilution), anti-ATP5B chicken antisera (anti-ATPβ antibody; 1:16,000 dilution), anti-MnSOD rabbit antisera (1:800 dilution), anti-PDHE1α mouse monoclonal antibody (1:800 dilution), anti-GroEL rabbit antisera (Stressgen, Victoria, Canada, SPS-875; 1:800 dilution), anti-aPKC rabbit antisera (1:2,000 dilution), anti-ATPγ rabbit antisera (1:800 dilution), anti-ATPb rabbit antisera (1:800 dilution), anti-β-Tubulin mouse monoclonal antibody (Sigma, T5293; 1:500 dilution), rabbit anti-chicken IgG (Sigma, C-6778; 1:1,000 dilution), AP conjugated goat anti-mouse IgG+A+M (Zymed Laboratories, South San Francisco, CA, USA, 62-6422; 1:5,000 dilution), and AP conjugated goat anti-rabbit IgG (American Qualex Antibodies, A102AT; 1:5,000 dilution).

3.11 Phalloidin staining

Ciona embryos were fixed with 1.6% formaldehyde (Polysciences, Warrington, PA, USA) in MFSW. Fixed embryos were washed with PBST and stained with BODIPY 558/568 phalloidin (10 units/ml; Sigma). The stained specimens were observed using a LSM700 confocal microscope (Carl Zeiss).

3.12 Transmission electron microscope (TEM) observation

Ciona fertilized eggs were fixed in 2.0% paraformaldehyde, 3.0% glutaraldehyde and 3.0% NaCl in 0.2 M sodium phosphate buffer (pH 7.4) for 2 h at room temperature, followed by several rinses in buffer. The samples were postfixed in 1.0% osmium tetroxide in the same buffer for 30 min. Then, the samples were rinsed in distilled water

and stained with 1.0% uranyl acetate for 1h. After rinsing in distilled water, the samples were dehydrated in acetone and embedded in Spurr resin (Spurr 1969). Ultrathin sections were cut and stained with lead citrate for 10 min. The sections were observed under an electron microscope, JEM-1400 (JEOL, Tokyo, Japan). The numbers of mitochondria were counted manually from the photomicrographs.

3.13 Sea urchin embryos

Wild type *Anthocidaris crassispina* adults were collected around Kumihama-bay, Kyoto, Japan. Spawning was induced by intracoelomic injection of 0.5 M KCl and embryos were cultured in natural seawater at 23°C.

3.14 Immunostaining of sea urchin embryos

Anthocidaris embryos were fixed with 100% methanol, followed by 100% ethanol. Fixed embryos were embedded in Polyester Wax (Steedman 1957; BDH) and sectioned at 8 μm. Sectioned specimens were mounted onto coverslips and the Polyester Wax was removed using 100% ethanol. Sectioned specimens were washed with PBST and were stained with anti-α-tubulin mouse monoclonal antibody (anti-microtubule antibody; Cedarlane Laboratories, 1:100 dilution), followed by Alexa Fluor 488-conjugated goat anti-mouse IgG (Molecular Probes, A11001; 1:1000 dilution). The stained specimens were observed using a BioRevo BZ-900 (Keyence).

3.15 Cultured cells

HeLa cells were cultured in Eagle's MEM (Nissui, Tokyo, Japan) supplemented with 10% fetal bovine serum (Hyclone, Logan, UT, USA) in a humidified 10% CO_2-enriched atmosphere at 37°C.

3.16 Measurement of mitochondrial activity of cultured cells

Mitochondrial activity of HeLa cells was measured by MTT (3-(4,5-dimethyl-thiazole-2-yl)-2,5-diphenyl tetrazolium bromide) assay. A 1/10 volume of 0.5 % MTT solution (5 mg/ml MTT in PBS) was added to medium and incubated for 2 hr at 37˚C. Then, an equal volume of 2-propanol containing 0.04 M HCl was added to solubilize the MTT formazan. The difference between the peak absorbance at 570 nm and the bottom absorbance at 630 nm was measured. The cell number was counted under the phase contrast microscope (CK2, Olympus, Tokyo, Japan).

3.17 Immunostaining of cultured cells

HeLa cells on coverslips were fixed with 1.6% formaldehyde (Polysciences) in PBST, followed by 100% ethanol. These specimens were washed with PBST and were stained with anti-α-tubulin mouse monoclonal antibody (anti-microtubule antibody; Cedarlane Laboratories, 1:100 dilution) and anti-Aurora B antibody (Sigma, A5102; 1:100 dilution), followed by rhodamine-conjugated goat anti-mouse IgG+M (BioSource International, AMI0706; 1:200 dilution) and Alexa Fluor 488-conjugated goat anti-rabbit IgG (Molecular Probes, A11008; 1:1000 dilution). DNA was stained with 0.2

μg/ml DAPI. The stained specimens were observed using BioRevo BZ-900 (Keyence) or LSM700 confocal microscope (Carl Zeiss).

4 RESULTS

4.1 Identification of ascidian p58 as the F_1-ATPase subunit

4.1.1 Purification of p58 and identification as the F_1-ATPase subunit

The identification of p58 was accomplished by two independent methods: immuno-precipitation and immunoscreening. Sepharose resin coupled to NN18 antibody was incubated with a soluble fraction from *Ciona* gonad homogenate and bound proteins were separated on a non-reducing SDS-PAGE gel, so that the intact NN18 IgG would be migrated at a high molecular weight well separated from the target protein. p58 was successfully immunoprecipitated as determined by immunoblot (Fig. 4.1.1A, "western"), and a duplicate lane silver-stained for total protein (Fig. 4.1.1B, right) showed that it was highly purified and abundant enough to obtain N-terminal sequence. The resulting sequence of 27 amino acid residues (circled in Fig. 4.1.1B) is identical in 26 positions to residues 44–70 of the α-subunit of *Ciona* mitochondrial-type F_0F_1-ATPase. As this was an unexpected result, a *Ciona* cDNA expression library was screened with NN18 antibody. All positive clones encoded the same protein: F_1-ATPase α-subunit "CiATPsynA" ("Immunoscreen" line, Fig. 4.1.1B). The first 43 amino acids of *Ciona* F_1-ATPase α-subunit missing from the immunoprecipitated p58 correspond to

the transit signal peptide (boxed in Fig. 4.1.1B and Fig. 4.1.2), which targets proteins to mitochondria and is cleaved during the import process. Thus p58 protein recognized by the neurofilament NN18 antibody in the *Ciona* egg is the mature form of F_1-ATPase α-subunit. This protein along with F_1-ATPase β-subunit make up the intramitochondrial F_1-ATPase portion of the enzyme complex which is attached to the F_0 portion embedded in the mitochondrial membrane.

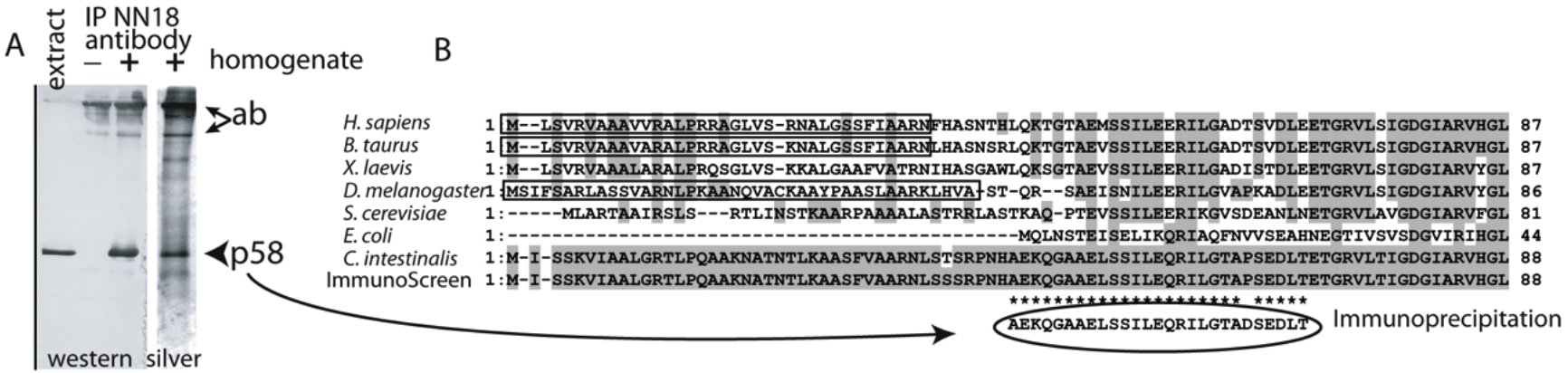

Figure 4.1.1 Purification of p58 by immunoprecipitation. (A) Beads to which the antibody NN18 was bound were incubated with (+) or without (−) *Ciona* oocyte homogenate and eluted proteins were subjected to immunoblot (left) or silver stain (right). The major proteins in the immunoprecipitate are p58 (arrow head) and the monoclonal antibody (arrows) which migrates as a large IgG because of the nondenaturing conditions of the gel (see text and methods). (B) N-terminal sequence of immunoprecipitated p58 (bottom line, circled) compared to F_1-ATPase α-subunit from diverse species; asterisks * indicate residues which are identical between p58 protein and *Ciona* F_1-ATPase α-subunit. Immunoprecipitated p58 lacks the first 43 amino acids of F_1-ATPase α-subunit, which correspond to reported mitochondrial signal peptides (boxed). The “ImmunoScreen” line is a translation of the cDNA clones (NP_001027729) obtained by screening an expression library with NN18 antibody, which is identical to the F_1-ATPase α-subunit gene model (KH.C10.579) annotated in the *Ciona* genome database, except in one position due to a polymorphism. See Figure 4.1.2. for the complete alignment and database accession numbers.

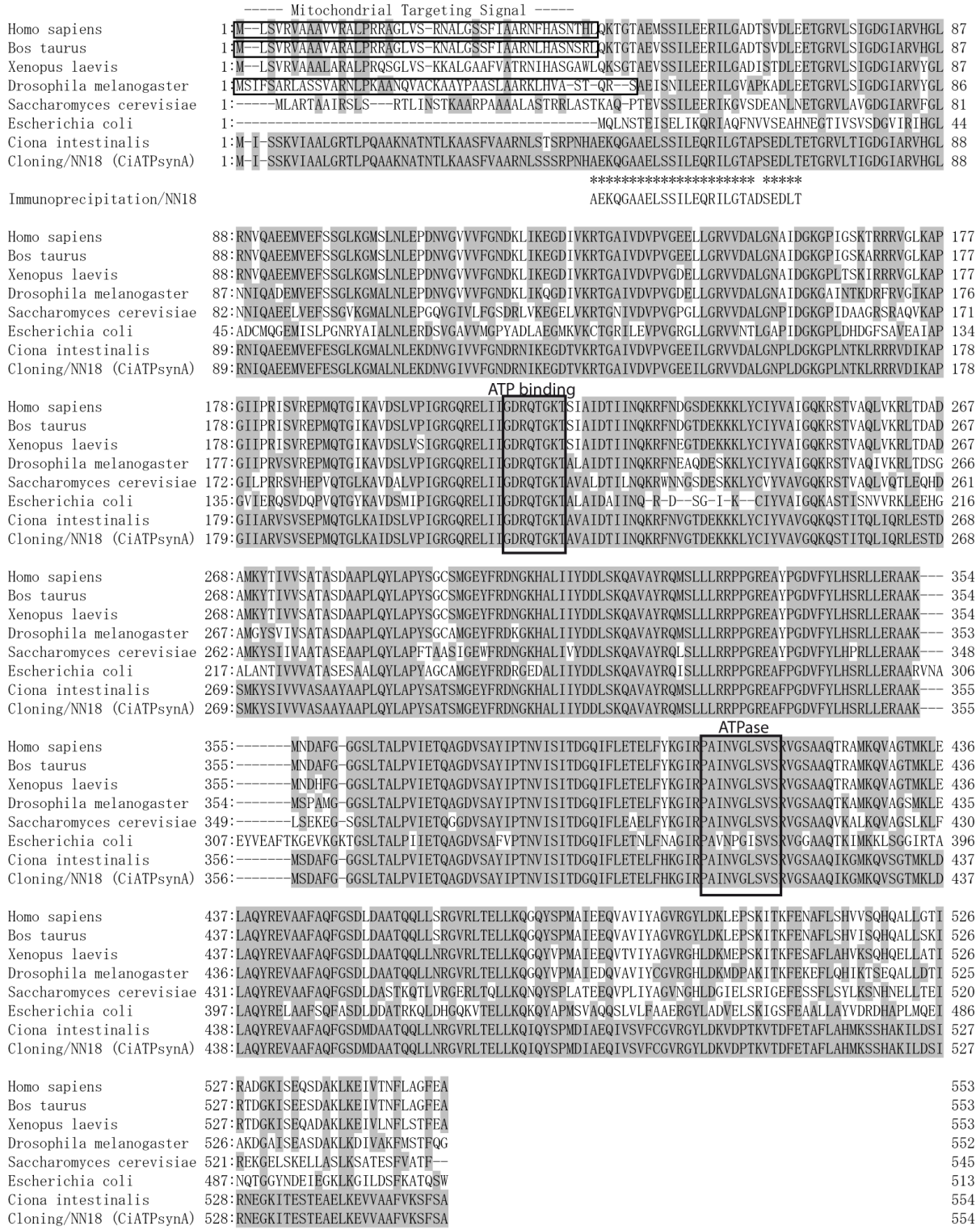
----- Mitochondrial Targeting Signal -----
Homo sapiens
Bos taurus
Xenopus laevis
Drosophila melanogaster
Saccharomyces cerevisiae
Escherichia coli
Ciona intestinalis
Cloning/NN18 (CiATPsynA)
Immunoprecipitation/NN18
ATP binding
ATPase

Figure 4.1.2 Alignment of amino acid sequences of F_1-ATPase α-subunit. Alignment of the complete sequences of F_1-ATPase α-subunit from *Homo sapiens* (NP_001001937), *Bos taurus* (NP_777109), *Xenopus laevis* (NP_001080447), *Drosophila melanogaster* (NP_726243), *Saccharomyces cerevisiae* (NP_009453), *Escherichia coli* (NP_418190), *Ciona intestinalis* (KH.C10.579.v1.A.SL1-1). "Cloning/NN18" is the complete sequence of the cDNA clone obtained by immunoscreening a *Ciona* expression library with NN18. "Immunoprecipitation/NN18" and "Mitochondrial Targeting Signal" are as described in Figure 4.1.1. The ATP binding (GDRQTGKT) and ATPase (PAINVGLSVS) sequences are also indicated.

4.2 Subcellular localization of F_1-ATPase subunits in ascidian myoplasm

4.2.1 Quest for the immunological probes for the Ciona *mitochondria*

First, immunological probes for ascidian mitochondria components were searched. Because mitochondria are specialized for their important roles in many biological events, such as apoptosis, aging, carcinogenesis, and disease pathogenesis (Svensson 2010), many kinds of mitochondrial probes have recently become commercially available. Some of these antibodies based on amino acid sequence homology between the immunogen used to generate the antibody and the equivalent protein in *Ciona* have been selected. In addition, some rabbit antisera against oligopeptides designed from the genomic sequence information of *Ciona* (Ghost database: http://ghost.zool.kyoto-u.ac.jp/cgi-bin/gb2/gbrowse/kh/) have been raised. These candidate antibodies were first screened by Western blotting against *Ciona*-gonad total protein. The antibodies available for probing the *Ciona* mitochondria are summarized in Table 4.1.1. These antibodies recognized the proteins as a single band of predicted-molecular weight of each immunogen in *Ciona* (data not shown).

Table 4.1.1 Available immunological probes for *Ciona* mitochondria

Name	Target molecule	Immunogen	From	Application†	M.W.‡	Localization	Source or Reference
anti-MnSOD	MnSOD (manganese superoxide dismutase)	rat MnSOD	rabbit antisera	WB, IC	24 kDa	matrix	StressMarq Biosciences, SPC-117C/D
anti-PDHE1α	PDHE1α (pyruvate dehydrogenase E1 component subunit alpha)	human PDHE1α	mouse monoclonal antibody	WB, IC	43 kDa	matrix	MitoScience, MSP07
anti-GroEL	HSP60 (60kDa heat shock protein)	*E. coli* GroEL	rabbit antisera	WB	61 kDa	matrix/cytosol	Stressgen, SPS-875
NN18 (anti-ATPα)	ATPα (F1-ATP synthase alpha-subunit)	porcine neurofilament 160	mouse monoclonal antibody	WB, IC, IP	60 kDa	inner membrane	Sigma, N5264
anti-α	ATPα	oligopeptides designed from *Ciona* ATPα sequence	rabbit antisera	WB	60 kDa	inner membrane	this study
anti-ATP5B (anti-ATPβ)	ATPβ (F1-ATP synthase beta-subunit)	human ATPβ	chickin antisera	WB, IC	56 kDa	inner membrane	Sigma-Aldrich, GW22827
anti-β	ATPβ	oligopeptides designed from *Ciona* ATPβ sequence	rabbit antisera	WB	56 kDa	inner membrane	this study
anti-ATPγ	ATPγ (F1-ATP synthase gamma-subunit)	oligopeptides designed from *Ciona* ATPγ sequence	rabbit antisera	WB	33 kDa	inner membrane	this study
anti-ATPb	ATPb (F0-ATP synthase subunit b)	oligopeptides designed from *Ciona* ATPb sequence	rabbit antisera	WB	30 kDa	inner membrane	this study

† Applicable experimental methods: WB, Western blotting; IC, immunohistochemistry; IP, immunoprecipitation.

‡ Molecular weight predicted from the *Ciona* genome sequence

For the second level of screening, immunofluorescent staining against *Ciona* sperm was used. *Ciona* sperm is a suitable material because each one has only a single mitochondrion adjacent to the sperm-head nucleus. Moreover, during penetration, sperm shows a characteristic behavior of the mitochondrion, the so-called sperm reaction (Lambert & Koch 1988). This process can occur *in vitro*, and sperm mitochondrion is translocated to the posterior tail tip and becomes spherical (Lambert & Epel 1979).

Fixed sperm were double-stained with anti-ATPα antibody and anti-ATPβ antibody or anti-MnSOD antibody, and counterstained with DAPI. A mitochondrion at the side of the sperm-head nucleus showed positive staining with these antibodies and these signals were nicely merged (Fig. 4.2.1). A mitochondrion was also identified in the tail of the sperm that induced the sperm reaction (Fig. 4.2.1H). Similar double staining was carried

out with anti-ATPβ and anti-PDHE1α antibodies. These antibodies also showed similar mitochondrion-specific staining (data not shown).

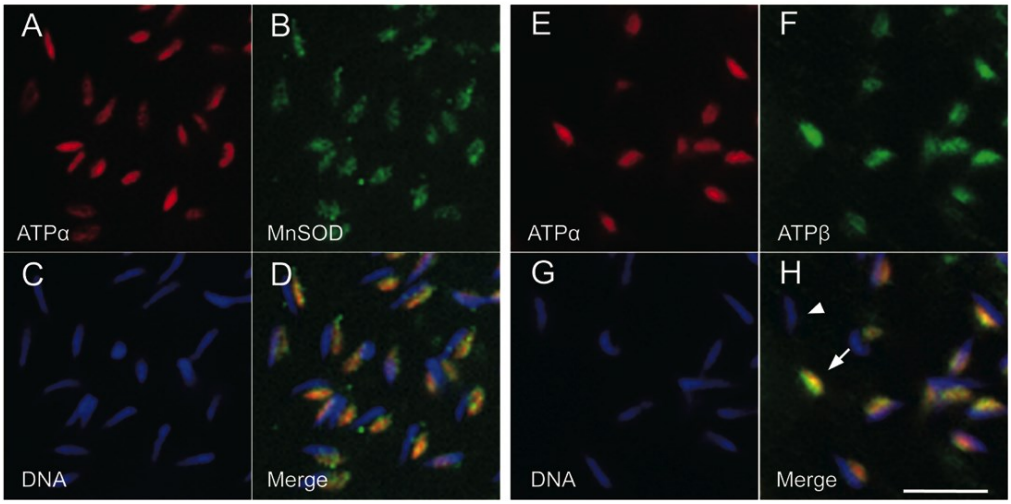

Figure 4.2.1 Antibody staining of *Ciona* mitochondria. *Ciona* sperm were fixed and double-stained with two different antibodies and counter stained with DAPI (C,G; DNA; blue). Merged images (Merge) were shown in D and H. (A-D) Comparison of anti-ATPα antibody (A; ATPα; Rhodamine, red) and anti-MnSOD antibody (B; MnSOD; FITC, green). (E-H) Comparison of anti-ATPα antibody (E; ATPα; Rhodamine, red) and anti-ATPβ antibody staining (F; ATPβ; FITC, green). Arrow and arrowhead indicate a single mitochondrion and a nucleus of sperm that induced the sperm reaction, respectively. All three antibodies recognize sperm mitochondria similarly. Scale bar, 5 μm.

4.2.2 Subcellular localization of F_0F_1-ATPase before and after fertilization

The behavior of mitochondria during cytoplasmic and cortical rearrangement has been described in detail (e.g. Sardet *et al*. 2007). In order to compare the localization patterns of exomitochondrial F_0F_1-ATPase and mitochondria, sectioned specimens of unfertilized eggs (Fig. 4.2.2A,B) and fertilized eggs at 5 min (Fig. 4.2.2C,D) and 45 min (Fig. 4.2.2E-G) after fertilization were double-stained with anti-ATPα as well as

anti-MnSOD, anti-ATPβ or anti-PDHE1α antibodies.

Throughout these stages, merged images of the double staining with anti-ATPα and anti-ATPβ antibodies showed a uniform yellowish pattern, suggesting the co-localization of these two antigens (Fig. 4.2.2B,D,F).

On the other hand, the double staining with anti-ATPα and anti-MnSOD antibodies showed a slight difference in staining pattern. In the unfertilized egg (Fig. 4.2.2A), both antibodies stained the mitochondria-rich cortical myoplasm. In the merged image, the cortical myoplasm showed a yellowish signal, but green- and red-colored small dot signals were found in the neighboring egg cytoplasm. In the egg 5 min after fertilization (Fig. 4.2.2C), although single color staining showed very similar staining patterns of the myoplasm, the merged image showed a clear difference. The thickness of 1 to 3 μm in the cortical myoplasm was intensely stained with anti-ATPα antibody, while weakly stained with anti-MnSOD antibody. In the egg 45 min after fertilization (Fig. 4.2.2E), different staining patterns for anti-ATPα and anti-MnSOD antibodies were obvious. The cortical region, which stained strongly for ATPα and weakly for MnSOD, was 2 to 6 μm in thickness. Double staining with anti-ATPβ and anti-PDHE1α antibodies yielded a very similar pattern as that with anti-ATPα and anti-MnSOD antibodies (Fig. 4.2.2G).

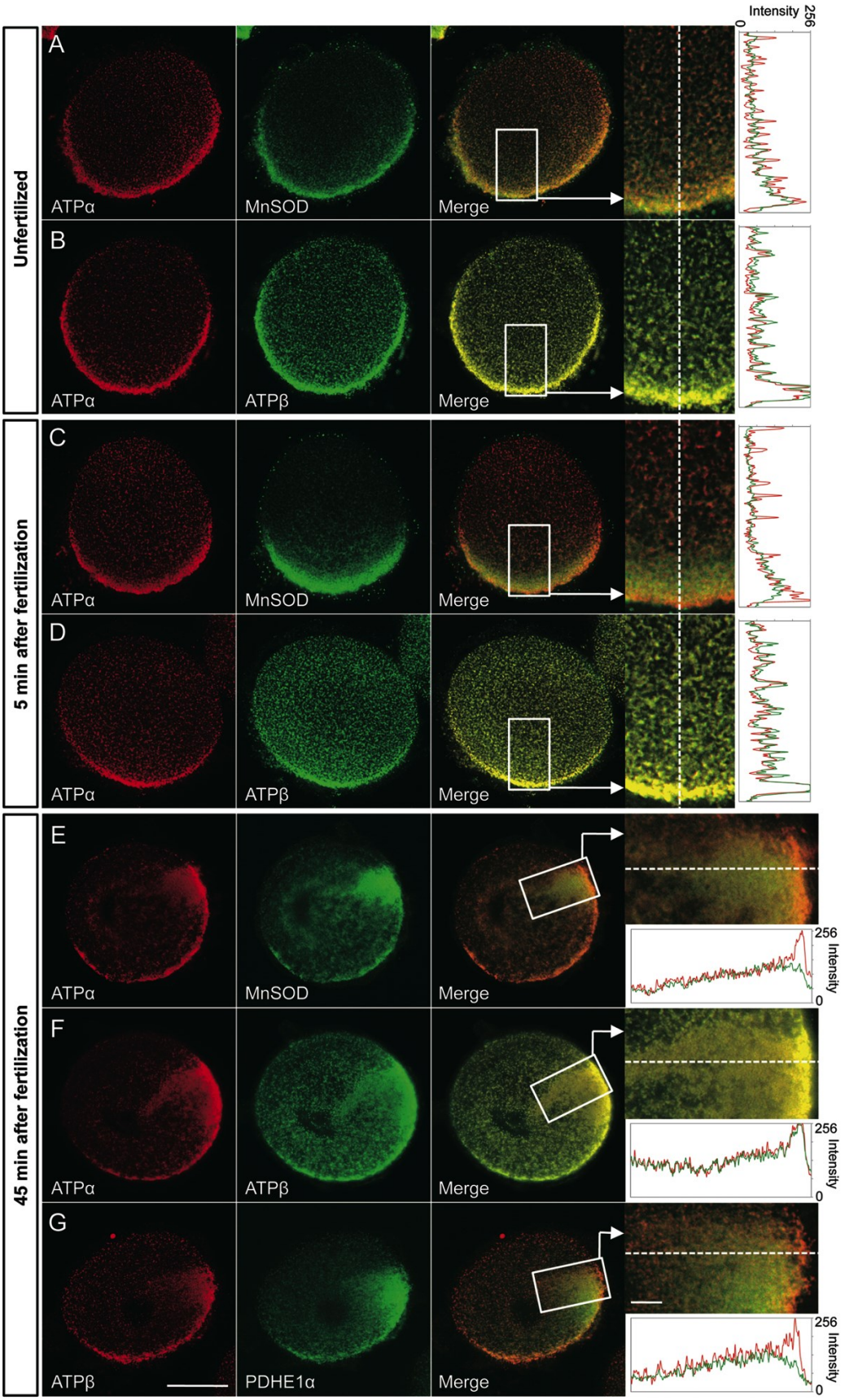
Unfertilized
5 min after fertilization
45 min after fertilization
A
B
C
D
E
F
G
ATPα
MnSOD
ATPβ
PDHE1α
Merge
Intensity
256
0

Figure 4.2.2 Subcellular localization of mitochondrial proteins in unfertilized and fertilized eggs. (A,B) Vertical section of unfertilized egg. (C,D) Vertical section of fertilized egg 5 min after fertilization. E-G; Sagittal section of fertilized egg 45 min after fertilization, the so-called crescent stage. Animal pole is up. A,C,E; Double staining with anti-ATPα antibody (ATPα; Rhodamine, red) and anti-MnSOD antibody (MnSOD; FITC, green). (B,D,F) Double staining with anti-ATPα antibody (ATPα; Rhodamine, red) and anti-ATPβ antibody (ATPβ; FITC, green). (G) Double staining with anti-ATPβ antibody (ATPβ; Alexa Fluor 568, red) and anti-PDHE1α antibody (PDHE1α; FITC, green). Merged image (Merge) of each set is also shown. The areas indicated by the white rectangle were enlarged and the line profiles of fluorescent intensity (red line, Rhodamine or Alexa Fluor 568; green line, FITC) along the indicated white dotted line are shown. Scale bar, 50 μm and 10 μm (enlarged view).

In order to clarify which antibody represented the mitochondria localization pattern, transmission electron microscopic (TEM) observation of the myoplasm at 45 min after fertilization was carried out. I found the mitochondria-less and ER-rich cortical region, which was about 2 to 6 μm in thickness beneath the plasma membrane (Fig. 4.2.3A,B). Then, the fluorescent-intensity of the immunofluorescent signal and the number of mitochondria from TEM observation were carefully compared. The number of mitochondria was counted in every 4 μm of the belt-like areas in the myoplasmic region along the anterior posterior axis (Fig. 4.2.3B). The data revealed that the cytoplasm of the first 4 μm in thickness beneath the plasma membrane had fewer amounts of mitochondria. Then, re-calculation of the fluorescent intensity was performed, averaged every 4 μm (Fig. 4.2.3C). The cortical most thickness of 4 μm showed intense anti-ATPα antibody staining and weak anti-MnSOD antibody staining. Comparing these results, it was concluded that the localization pattern of mitochondria was recapitulated by anti-MnSOD antibody staining. Moreover, the line profiles of double staining with

anti-ATPβ and anti-PDHE1α antibodies (Fig. 4.2.2G) were almost identical to the anti-ATPα and anti-MnSOD antibodies staining, supporting the congruence between localization patterns of mitochondria and those of mitochondrial matrix components. Hence, the mitochondria-less and ER-rich cortical region of the myoplasm corresponded closely to the F_0F_1-ATPase rich cortical region of the myoplasm.

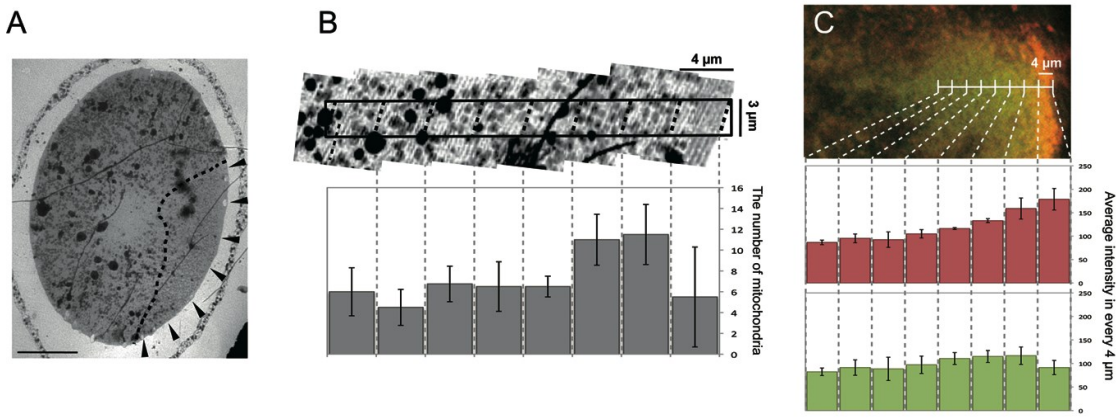

Figure 4.2.3 Comparison of TEM and immunofluorescent staining. (A) A low magnification of the sagittal section of a crescent stage embryo. Dotted line and arrowheads indicate the myoplasmic region. (B) A higher magnification of myoplasmic region indicated in A. The number of mitochondria within the 3 × 32-μm rectangle were counted in every 4-μm. The average of the data obtained from three different areas is indicated in the graph with standard deviation. (C) Same photo as in Figure 4.2.2E. Line profiles of red and green fluorescent intensity along the indicated white line was averaged every 4 μm. Scale bar, 20 μm in A.

4.2.3 Subcellular localization of F_0F_1-ATPase during oogenesis

The development of *Ciona* oocyte is classified into 5 stages by staining their accessory cells with DAPI (Shimai *et al*. 2010). In stage 1 oocytes (10-60 μm in diameter), several undifferentiated accessory cells are scattered around the oocyte. In stage 2 oocytes

(60-75 μm in diameter), accessory cells number is increased and they are stacked around the oocyte. In stage 3 oocytes (75-90 μm in diameter), the accessory cells have differentiated into test cells and the interspersed inner follicle cells and the chorion become obvious. In some cases, a perivitelline space is transiently observed. In stage 4 oocytes (90-100 μm in diameter), the cytoplasm of the oocyte has expanded and the clusters of test cells are buried in the oocyte cortex. This structure was designated the pocket structure by Shimai *et al*. (2010). In stage 5 oocytes (100-130 μm in diameter), the germinal vesicle has broken down, and the pocket structures have disappeared. The oocyte surface becomes smooth and an obvious perivitelline space has formed; this is the stage just before the unfertilized egg (Prodon *et al*. 2006).

In all stages of oogenesis, merged images of the double staining with anti-ATPα and anti-ATPβ antibodies essentially showed a uniform yellowish signal, suggesting that these two antigens are co-localized even in the gonad (Fig. 4.2.4I-M).

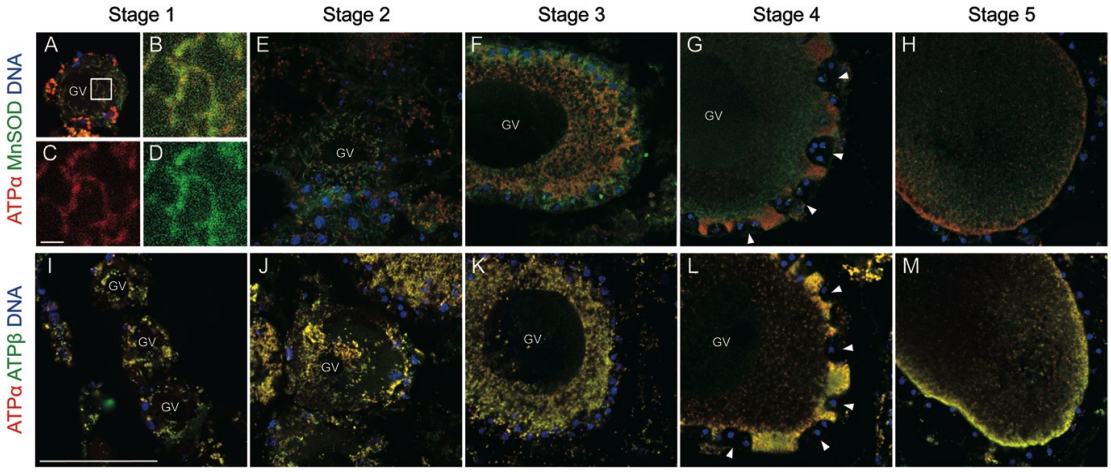

Figure 4.2.4 Subcellular localization of mitochondrial proteins during oogenesis. Histological sections of the stage 1 (A-D,I), stage 2 (E,J), stage 3 (F,K), stage 4 (G,L), and stage 5 (H,M) oocytes were double-stained with anti-MnSOD antibody (A, B, D-H; MnSOD; FITC, green) or anti-ATPα antibody (A-C,E-M; ATPα; Rhodamine, red), and anti-ATPβ antibody (I-M; ATPβ; FITC, green), counter stained with DAPI (A,E-M; DNA; blue). The area indicated by the white rectangle in A was enlarged and the staining patterns of anti-ATPα antibody (C) and anti-MnSOD antibody (D), and the merged image (B) are shown. Arrowheads show the pocket structure of the stage 4 oocytes (G, L). GV, germinal vesicle. Staging of oocyte was according to the criteria indicated by Shimai *et al*. (2010). Scale bars, 50 μm and 2 μm (enlarged view).

On the other hand, anti-ATPα and anti-MnSOD antibody-staining patterns were distinct. In stage 1 oocytes (Fig. 4.2.4A-D), both anti-ATPα and anti-MnSOD antibodies stained a string-like structure of mitochondria. However, the merged image was not uniformly yellow, suggesting that ATPα and MnSOD have a different distribution within the mitochondria. In stage 2 oocyte (Fig. 4.2.4E), the string-like staining of the previous stage developed to a more punctate pattern. This change was more obvious with the anti-ATPα antibody (Fig. 4.2.4J). In stage 3 oocytes (Fig. 4.2.4F), the cytoplasm was filled with intense punctate staining for the anti-ATPα antibody, while

the MnSOD staining became faint and its positive region was restricted to the relatively thick cortical area. In stage 4 oocytes (Fig. 4.2.4G), the staining region for the anti-ATPα antibody was restricted to the cortical region, which was adjacent to the pocket structure, and overlapped with the cortical staining of the anti-MnSOD antibody. However, the anti-MnSOD antibody signal grew faint, as the merged image shows, as if only ATPα signal was localized to the cortical area. The staining pattern of stage 5 oocytes was very close to that of unfertilized egg (Fig. 4.2.4H). Although the animal pole of unfertilized egg was free of mitochondria, the entire cortex of the stage 5 oocyte stained positive with both antibodies.

4.2.4 Subcellular localization of F_0F_1-ATPase during early development

During the cleavage stages, a unique structure called the CAB (centrosome-attracting body) is observed at the posterior pole (Hibino *et al*. 1998). It is suggested to have important roles for ascidian development such as in the asymmetric cleavages (Nishikata *et al*. 1999), embryonic axis formation (Negishi *et al*. 2007) and germ cell specification (Shirae-Kurabayashi *et al*. 2011; Kumano *et al*. 2011). TEM studies revealed that the CAB contains an electron-dense matrix, ER, and ribosomes, but no mitochondria (Iseto & Nishida 1999). Moreover, many postplasmic/PEM RNAs including *macho-1* (Prodon *et al*. 2007) and *vasa* homologue (Shirae-Kurabayashi *et al*. 2006), and some interesting proteins including PEM (Shirae-Kurabayashi *et al*. 2011) and aPKC (Patalano *et al*. 2006) are localized to the CAB.

In order to find out whether the CAB contains the exomitochondrial F_0F_1-ATPase, the 16-cell-stage embryos were double stained with anti-ATPα and anti-aPKC antibodies or with anti-ATPβ and anti-kinesin antibodies. The anti-aPKC and anti-kinesin antibodies positively stain the CAB during the cleavage stages (Patalano *et al*. 2006; Nishikata *et al*. 1999). As shown in Figure 4.2.5, anti-aPKC and anti-kinesin antibodies stained the CAB. On the other hand, the anti-ATPα and anti-ATPβ antibodies did not stain the CAB but stained the adjacent cytoplasmic region.

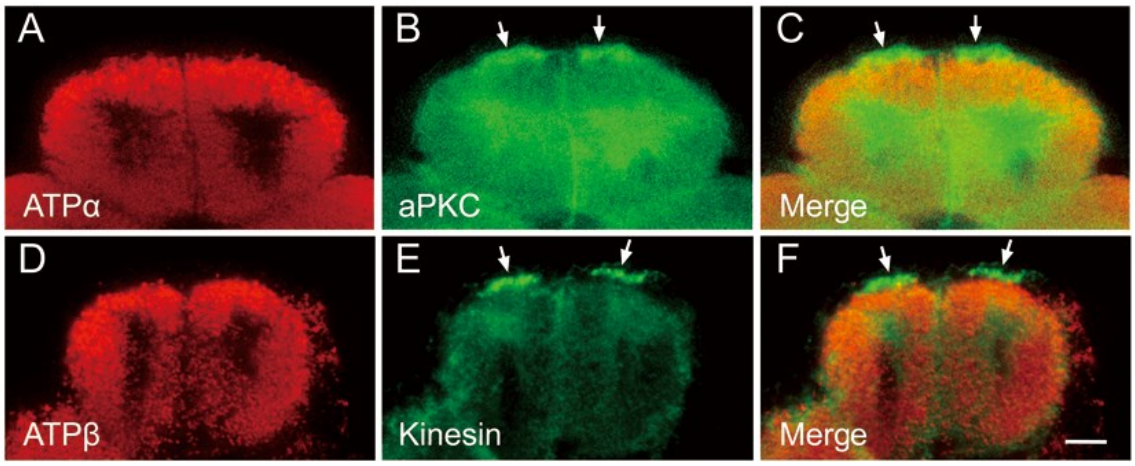

Figure 4.2.5 ATPα did not localize to the CAB at the 16-cell stage. Horizontal sections of the posterior pole region of a 16-cell stage embryo were double-stained with anti-ATPα antibody (A; ATPα; Rhodamine, red), and anti-aPKC antibody (B; aPKC; FITC, green) or with anti-ATPα antibody (D; ATPβ; Alexa Fluor 568, red), and anti-kinesin antibody (E; Kinesin; FITC, green). Merged images are also shown (C,F; Merge). Posterior is up. Arrows indicate the CAB. Scale bar, 10 μm.

During the tail-bud stage in the embryo, some tissues are differentiated, and the content of mitochondria varies according to the tissue type. Muscle cells and neural tissues are rich in mitochondria. As shown in Figure 4.2.6D-F, the merged images of the

double staining with anti-ATPα and anti-ATPβ antibodies reveal intense yellowish staining in muscle, mesenchyme, and brain, suggesting that these two antigens are co-localized even in the differentiated tissues. On the other hand, anti-ATPα and anti-MnSOD antibodies showed quite distinct staining patterns (Fig. 4.2.6A-C). The anti-MnSOD antibody stained the entire cytoplasm of muscle cells brightly as well as the small dots of epidermal cells, while anti-ATPα antibody stained muscle, mesenchyme, and brain cells. Even in the muscle cells, the merged image shows that the signal intensities of these two antibodies are different within the cell.

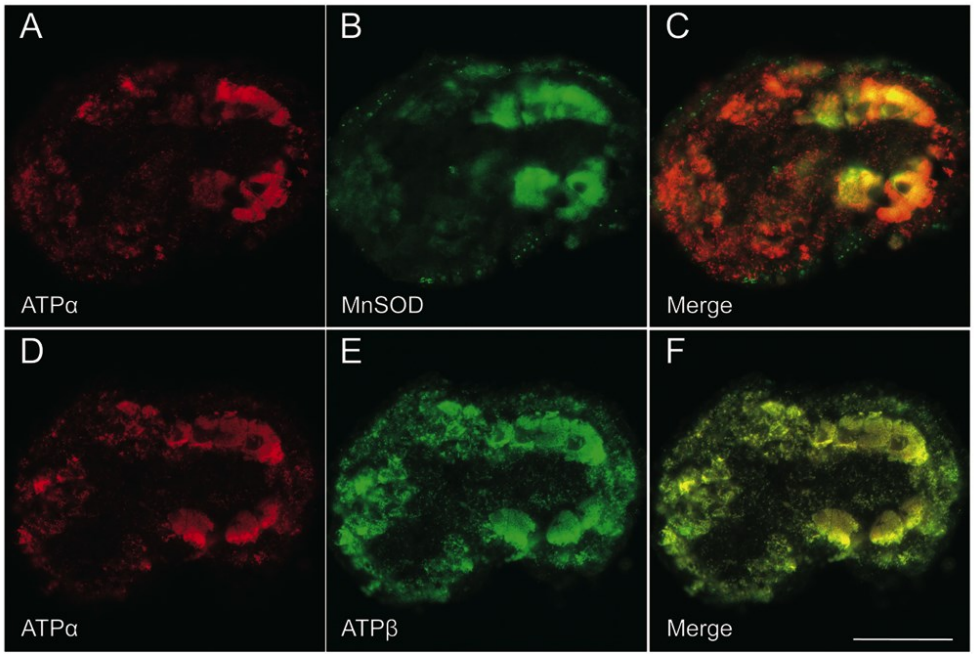

Figure 4.2.6 Subcellular localization of mitochondrial proteins at the tail-bud stage. Horizontal sections of the tail-bud stage embryo were double-stained with anti-ATPα antibody (A,D; ATPα; Rhodamine, red), and anti-MnSOD antibody (B; MnSOD; FITC, green) or anti-ATPβ antibody (E; ATPβ; FITC, green). Merged image of each set is also shown (C,F; Merge). Anterior is to the left. Scale bar, 50 μm.

4.2.5 Subcellular localization of F_0F_1-ATPase revealed by the fractionation method

The method of subcellular fractionation from *Ciona* gonad (Fig. 4.2.7A) was established. The gonad homogenate is first filtered through the nylon mesh to separate debris and undamaged oocytes. This gonad whole-lysate (W) was centrifuged at low speed (500 × *g*), and stratified into three layers: pellet, supernatant, and fluffy layer, from the centrifugal pole. The pellet and the fluffy layer were designated the insoluble cytoplasmic mass (IC) fraction and fluffy layer (FL) fraction, respectively. The supernatant was then centrifuged at high speed (10,000 × *g*) and the resulting pellet and supernatant were designated the mitochondria enriched (ME) fraction and soluble cytoplasmic (SC) fraction, respectively. The enrichment of mitochondria was always monitored by respiratory activity using the MTT (3-(4,5-dimethyl-thiazole-2-yl)-2,5-diphenyl tetrazolium bromide) assay. I used the fractions with an MTT value in the ME fraction that was at least two times higher than that of the whole lysate, IC and SC fractions.

As shown in Figure 4.2.7B, the FL fraction contained each of the proteins. It was assumed that the FL fraction was a fuzzy, lipid-containing fraction and contaminated with the supernatant of the first centrifugation, which contained ME and SC fractions. aPKC and most of the tubulin was segregated into the SC fraction indicating the effectiveness of this fractionation method to enrich the soluble proteins into the SC fraction. All of the mitochondrial components: ATPα, ATPβ, and ATPγ of the F_1-ATPase, ATPb of the F_0, PDHE1α, MnSOD, and HSP60 of the matrix component, were highly

enriched in the ME fraction. This data also confirmed the effective mitochondrial enrichment of the ME fraction by this method.

Finally, in the IC fraction, although faint bands were observed for the mitochondrial proteins, considerable amounts of ATPα and ATPβ were detected. As the same amount of protein from each fraction was loaded in each lane, and the total amount of protein in each fraction was measured, the recoveries of these protein bands in each fraction from gonad-whole lysate could be estimated from the band intensity. The recovery of MnSOD from whole-gonad homogenate was 49% ± 8.2% in the ME, but only 14% ± 7.0% in the IC. In the case of ATPα and ATPβ, the recovery in the ME was 33% ± 2.7% and 24% ± 1.6%, while the recovery in the IC was 35% ± 6.2% and 35% ± 11.5%, respectively. Assuming that the recovery of MnSOD reflects mitochondria content of each fraction, the high level of ATPα and ATPβ recovery to the IC fraction indicates that about 20% of the total amount of ATPα and ATPβ is located exomitochondrially.

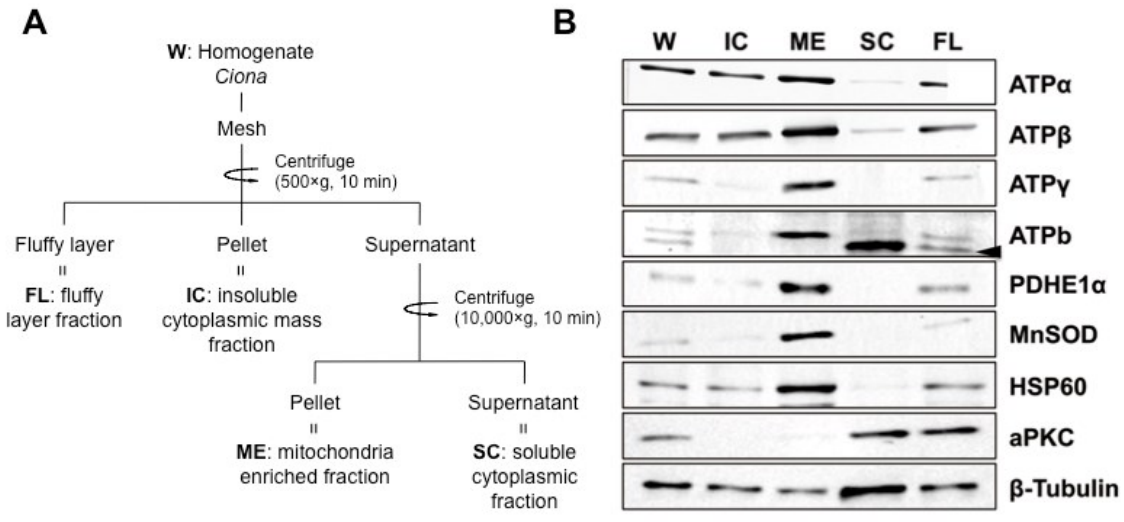

Figure 4.2.7 Subcellular localization of each subunit of F_0F_1-ATPase and mitochondrial marker proteins. (A) Schematic of fractionation methods. *Ciona* gonad whole lysates (W) were fractionated into 4 fractions; IC (insoluble cytoplasmic mass), ME (mitochondria enriched), SC (soluble cytoplasmic), and FL (fluffy layer) fractions. (B) In each lane, 2 μg of total protein from each fraction was loaded on a SDS-PAGE gel, and blotted onto PVDF membranes. The membranes were probed with anti-ATPα antibody (ATPα), anti-ATPβ antibody (ATPβ), anti-ATPγ antibody (ATPγ), anti-ATPb antibody (ATPb), anti-PDHE1α antibody (PDHE1α), anti-MnSOD antibody (MnSOD), anti-GroEL antibody (HSP60), anti-aPKC antibody (aPKC), and anti-β tubulin antibody (β-tubulin). Arrowhead indicates the bands of the different size, which were observed with the preimmune serum of the anti-ATPb antibody.

4.2.6 Interaction between F_1-ATPase subunits and the cytoskeleton

As p58 was suggested to be a cytoskeletal component (Jeffery & Swalla 1992; Nishikata & Wada 1996), the finding that exomitochondrial ATPα and ATPβ were fractionated into the IC fraction was not surprising. In order to confirm that the exomitochondrial ATPα bound to the cytoskeleton, the following experiment with the non-ionic detergent Triton X-100 was carried out. Many studies reported that ascidian eggs treated with Triton X-100 could well retain cytoskeletal components (e.g. Swalla *et al.* 1991; Nishikata & Wada 1996). On the other hand, many studies, in which the mammalian mitochondrial F_0F_1-ATPase could be solubilized with some kind of detergents, including Triton X-100, have been made (e.g. Linnett *et al.* 1975; Soper & Pedersen 1976). In particular, Ko *et al.* (2003) clearly showed that about 0.5% of Triton X-100 completely solubilizes the entire F_0F_1-ATPase from rat mitochondrial inner membrane.

Unfertilized eggs were extracted with 2% Triton X-100. Figure 4.2.8A shows a

Western blot of the total protein from whole eggs and detergent-extracted eggs. The same amount of total protein was loaded in each lane. While the most of the MnSOD was extracted from the egg, ATPα and ATPβ persisted within the egg. Similar to MnSOD, most of the PDHE1α, HSP60, ATPγ, and ATPb in the unfertilized egg were solubilized with Triton X-100 (data not shown). The same batch of whole and extracted unfertilized eggs was also immunohistochemically stained with anti-ATPα and anti-MnSOD antibodies (Fig. 4.2.8B-G). In the extracted egg, the remaining ATPα was stayed in the cortical region of the unfertilized egg. However, MnSOD was hardly detectable in the egg. On the basis of Ko's experiments (2003), ascidian mitochondrial ATPα would be solubilized in my condition. Moreover, the components insolublized in my condition would be cytoskeleton. So, these results suggested that the exomitochondrial ATPα was bound to the egg cytoskeleton.

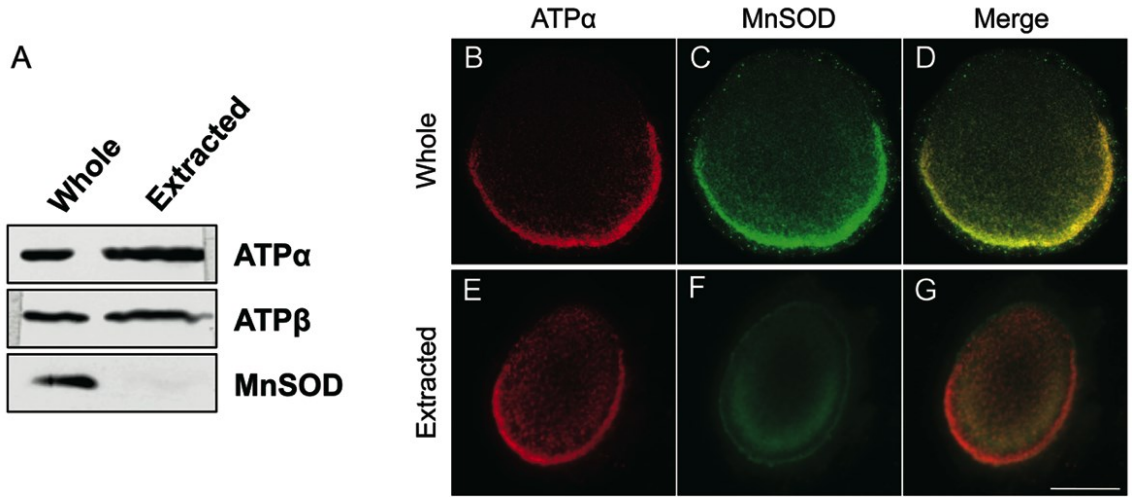

Figure 4.2.8 Different detergent solubility of mitochondrial proteins within the egg. The unfertilized eggs were treated with a non-ionic detergent, Triton X-100, as

described in materials and methods. A: The same amount (2 μg) of proteins from intact egg and extracted egg were loaded on an SDS-PAGE gel, and blotted onto PVDF membranes. The membranes were probed with anti-ATPα antibody (ATPα), anti-ATPβ antibody (ATPβ), and anti-MnSOD antibody (MnSOD). Most of the MnSOD protein was extracted from the egg. (B-G) Vertical sections of intact (B-D) and extracted (E-G) eggs were stained with anti-ATPα antibody (B,E; ATPα; Rhodamine, red) and anti-MnSOD antibody (C,F; MnSOD; FITC, green). Merged images are also shown (D,G; Merge). While most of the MnSOD protein was also extracted from the egg myoplasm, the ATPα protein remained in the myoplasm. Scale bar, 50 μm.

4.3 Inhibitory effects of mitochondrial inhibitors on cytoplasmic and cortical reorganization in ascidian embryo

4.3.1 Mitochondrial inhibitors inhibited the activity of sperm

Since the ascidian sperm has only one mitochondrion and little cytoplasm, sperm is a good target for mitochondrial inhibitors. According to the method described by Saito *et al.* (2012), the minimum concentrations of oligomycin and NaN_3, which inhibited *Ciona* sperm motility by measuring the velocity (μm/second) of the egg pushed by the sperm motility, were investigated. As shown in Figure 4.3.1, oligomycin and NaN_3 stopped the movement of the eggs in a concentration-dependent manner. Oligomycin and NaN_3 completely inhibited the sperm motility at minimum concentrations of 1.5 μM and 50 mM, respectively. Note that 5 mM NaN_3 exerted little effect on sperm motility, and the sperm still swam vigorously (75.7 ± 8.8% of the control motility), indicating the low toxicity of NaN_3 in sperm at this concentration.

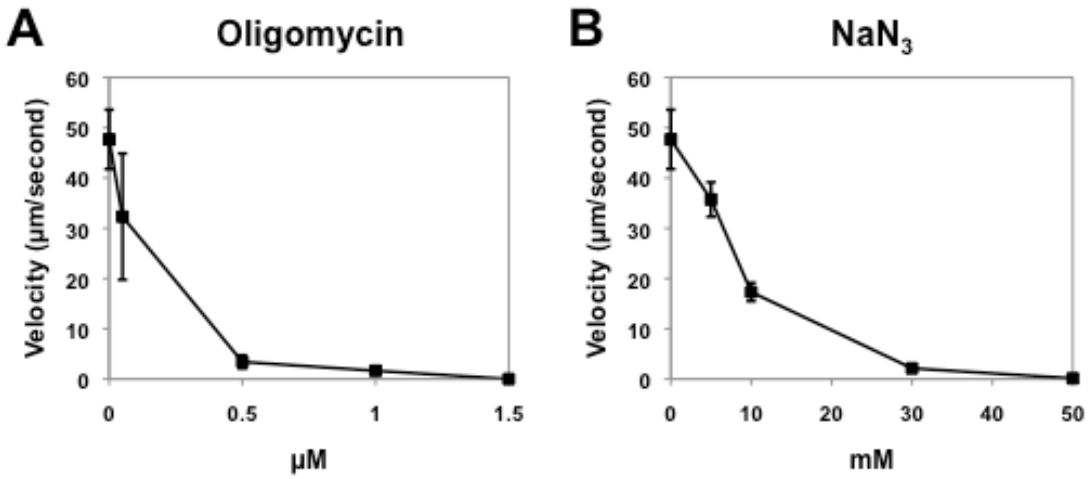

Figure 4.3.1 Effects of mitochondrial inhibitors on sperm motility. Sperm motility was assayed according to the method described by Saito *et al.* (2012). The vertical axis shows the velocity of the movement of the eggs after insemination. The egg movement was depended on the motility of the sperm, which attacked and pushed the egg. (A) Oligomycin-treated sperm. (B) NaN_3-treated sperm. Error bars represent standard deviations (SDs: n=3).

4.3.2 Cleavage was arrested by NaN_3 treatment at low concentration

Next, the effects of these inhibitors on the cleavage of *Ciona* embryos were investigated. Embryos were treated with oligomycin or NaN_3 from immediately after the first phase of reorganization (10 mpf; 1-cell stage) or the 2-cell stage (60 mpf), to the larval stage (18 hpf). All untreated embryos developed into the larval stage (Fig. 4.3.2A). In the case of oligomycin (Fig. 4.3.2B-E), at low concentration (0.05 μM) where sperms were motile (Fig. 4.3.1), almost all embryos treated with oligomycin developed into the larval stage. This showed 0.05 μM oligomycin had low toxicity in both sperm and embryo. At high concentrations (1.5 μM or 5 μM) that completely inhibited sperm motility (Fig.

4.3.1), both conditions gave rise to a similar result, in which embryos were arrested at 16- to 64-cell stage. On the other hand, NaN_3 (Fig. 4.3.2F-I) caused different results from that seen with oligomycin. At low concentration (5 mM), the embryos treated with NaN_3 could not develop to the larval stage and stopped at the 32- to 64-cell stage. At high concentrations (50 mM) that completely inhibited sperm motility, NaN_3-treated embryos were cleavage arrested by the 16-cell stage, which was earlier than that seen with 1.5 μM or 5 μM oligomycin. To summarize these results, toxicity of oligomycin was similar in both sperm motility and early cleavages, while, the toxicity of NaN_3 was different. The mechanism of inhibitory effect of NaN_3 in the early cleavage stages might be different from that in sperm motility.

In the case of oligomycin, regardless of its concentration, there was no obvious difference between the two start points of the treatment (Fig. 4.3.2B-E). But, in the case of NaN_3, when NaN_3 was added at the 2-cell stage, cleavage was stopped after several rounds of cleavage. However, when the NaN_3 treatment was started from the 1-cell stage, most of the embryos failed to cleave and stayed at 1-cell stage (Fig. 4.3.2F-I). Although the similarity between events inhibited by oligomycin and NaN_3 in the early cleavage stage was obscure, these results suggested the possibility that the events inhibited by NaN_3 were exist in both the 1-cell-stage embryo and in the early cleavage-stage embryo.

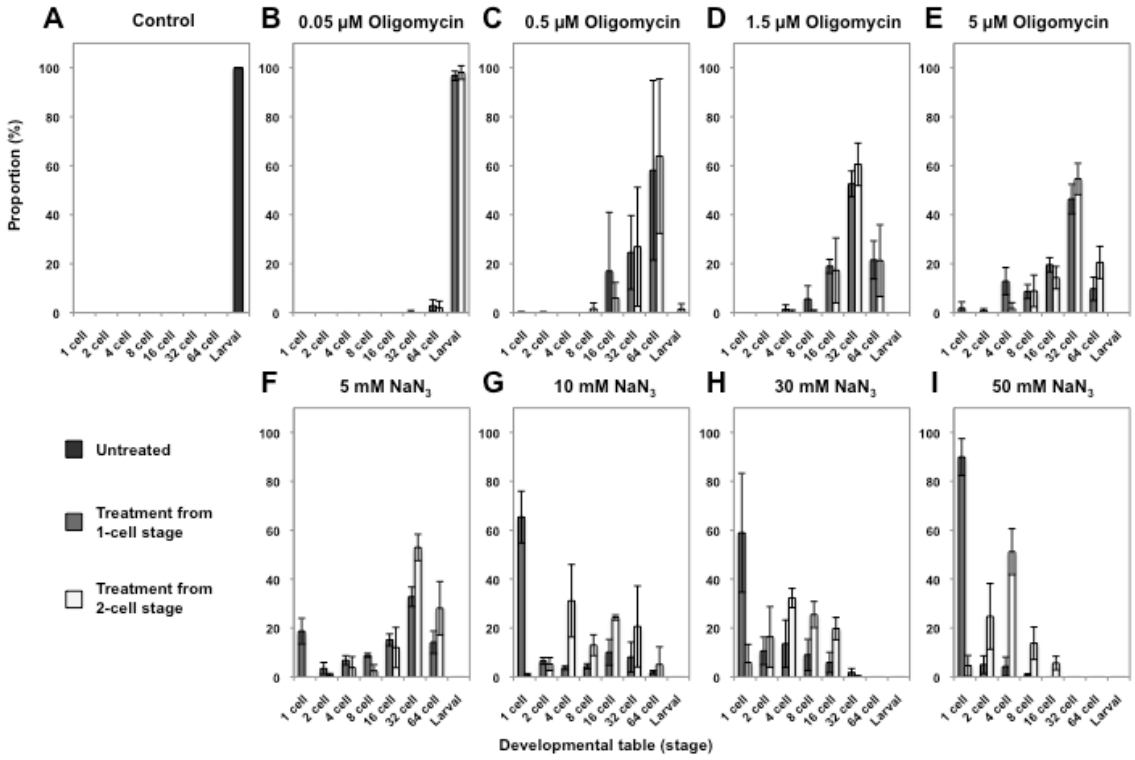

Figure 4.3.2 Effects of mitochondrial inhibitors on cleavage. *Ciona* embryos were treated with NaN_3 or oligomycin from the 1-cell stage (10 mpf; gray column) or 2-cell stage (60 mpf; white column) to the larval stage. The graphs show the proportion of the embryos, which stopped their development at each stage. These results were counted when control untreated embryos developed to the larval stage (18 hpf). (A) Control untreated embryos. (B-E) Oligomycin-treated embryos. (F-I) NaN_3-treated embryos. Error bars represent SDs (n=3).

4.3.3 NaN_3 inhibited the second phase of reorganization without hindering microtubule depolymerization

To reveal the cellular responses to oligomycin and NaN_3 in the 1-cell-stage embryo, embryos were treated with 1.5 μM oligomycin or 5 mM NaN_3. At these concentrations, oligomycin completely inhibited sperm motility but NaN_3 did not (Fig. 4.3.1). Embryos were treated with oligomycin or NaN_3 from immediately after the first phase of

reorganization (10 mpf) and fixed after the second phase of reorganization (45 mpf). Fixed embryos were stained for myoplasm and microtubules (Fig. 4.3.3). In the oligomycin-treated embryo (Fig. 4.3.3E-H), the myoplasm was reorganized posteriorly and formed a crescent, and the sperm aster was positioned at the center of the embryo and fully expanded. These reorganization patterns of the myoplasm and sperm aster were similar to those seen in control embryos (Fig. 4.3.3A-D). The proportions of these normally reorganized embryos were 90.5 ± 6.8% and 89.2 ± 6.6% in control and oligomycin-treated embryos, respectively. No significant difference was found between these two cases (P = 0.850, t-test). These reorganized embryos showed microtubule bundles localized at the cortical region of the myoplasm (Fig. 4.3.3B,F, arrows). On the other hand, in the case of NaN_3, posteriorly segregated myoplasm was observed only in 3.3 ± 0.3% of the treated embryos. In the other embryos (96.7 ± 0.3%), although the sperm aster was expanded at the center of embryo, the myoplasm remained at the egg cortex of the vegetal hemisphere (Fig. 4.3.3I-L). Interestingly, microtubule bundles were not localized at the cortex; however, I could detect the fuzzy staining of tubulin inside the egg (Fig. 4.3.3J, arrowhead). These results indicated that NaN_3 inhibited the movement of myoplasm during the second phase of reorganization, but did not inhibit the polymerization of microtubule. This is the first report of inhibition of ascidian cytoplasmic and cortical reorganization by a reagent that is not a cytoskeletal inhibitor.

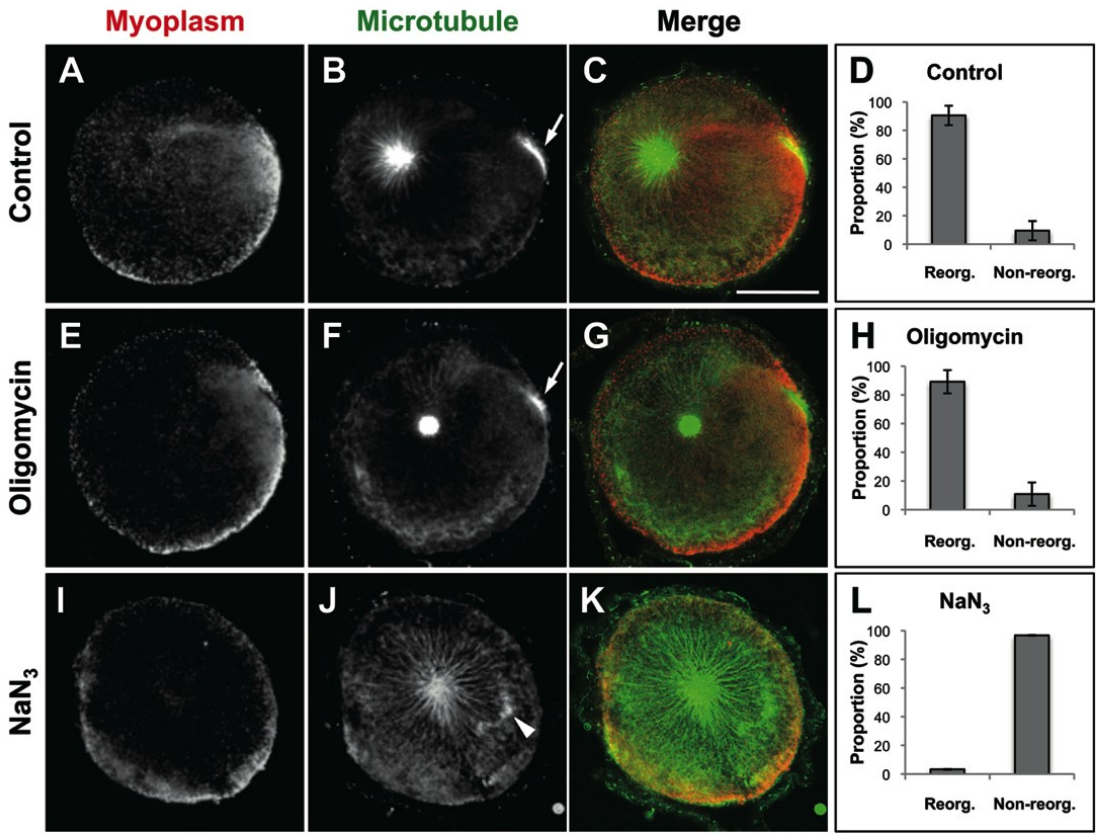

Figure 4.3.3 NaN_3 inhibits the movement of myoplasm in the second phase of reorganization. Vertical sections of *Ciona* 1-cell-stage embryos after second phase of reorganization (45 mpf) were stained for myoplasm (A,E,I) and microtubules (B,F,J). Merged images are shown in panels C,G,K (red; myoplasm, green; microtubule). The animal pole is up. Posterior is to the right. (D,H,L) Graphs show the proportion of embryos that underwent the second phase of reorganization (Reorg.) or not (Non-reorg.). (A-D) Control untreated embryos. (E-H) Oligomycin-treated embryos. (I-L) NaN_3-treated embryos. NaN_3 inhibited myoplasmic reorganization without depolymerization of microtubules. Error bars represent SDs (n=3). Scale bar, 50 μm.

4.3.4 NaN_3 altered the sperm-aster migration pathway during the second phase of reorganization

To investigate the effects of oligomycin and NaN_3 on the migration pathway of the sperm aster, 1-cell-stage embryos were treated with these inhibitors from 10 mpf and fixed at several time points during the second phase of reorganization. The positions of the sperm aster were measured from five different sagittal sections and normalized to coordinates relative to the center of the embryo. In the case of control (Fig. 4.3.4A-E) and oligomycin-treated (Fig. 4.3.4F-J) embryos, the sperm asters migrated posteriorly along the egg cortex, and then turned anteriorly and were positioned at the center of the egg. During this migration, at around 35 mpf, some microtubules of the sperm aster were expanded and elongated along the posterior cortex forming parallel bundles (Fig. 4.3.4C,H), which is suggested to be important for myoplasmic reorganization (Chiba *et al*. 1999). In the case of NaN_3 (Fig. 4.3.4K-O), the sperm aster left the vegetal cortex faster than that of the control embryo and directly migrated to the center of the embryos with wobbling. This wobbling is clearly represented by the relatively long error bars at each time-point. Moreover, although the sperm aster was observed in the center of the egg, the cytoplasmic or the background staining with anti-α-tubulin antibody was relatively high and cortical microtubule bundles were not detected at 45 mpf. These results suggest that the target molecules of NaN_3 are important for attracting the sperm aster to the cortex and for the reorganization of the myoplasm posteriorly.

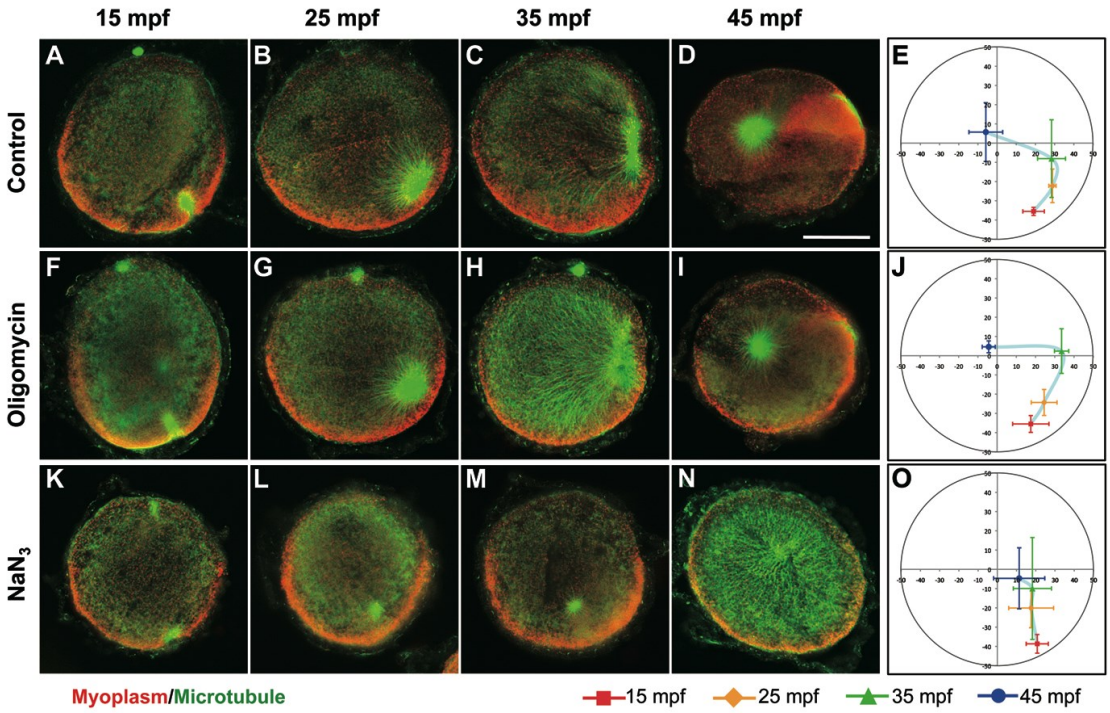

Figure 4.3.4 Migration pathway of the sperm aster during the second phase of reorganization. Vertical sections of *Ciona* 1-cell-stage embryos during second phase of reorganization were stained for myoplasm (red) and microtubules (green). (A,F,K) 15 mpf. (B,G,L) 25 mpf. (C,H,M) 35 mpf. (D,I,N) 45 mpf. (A-E) Control untreated embryos. (F-J) Oligomycin-treated embryos. (K-O) NaN_3-treated embryos. (E,J,O) The positions of the sperm aster were measured from five different sections and normalized to coordinates relative to the center of the embryo. Error bars show SDs (n=5). The x-axis and y-axis show the anteroposterior axis and animal-vegetal axis, respectively. The animal pole is up. Posterior is to the right. Sperm asters treated with NaN_3 directly migrated to the center of the embryos with a wobbling motion. Scale bar, 50 μm.

4.3.5 The first phase of reorganization was not inhibited by treatment with NaN_3

To examine the effects of NaN_3 on the first phase of reorganization, unfertilized eggs were pretreated with 5 mM NaN_3 for 30 min and then inseminated in the presence of NaN_3. The unfertilized egg and the fertilized egg after the first phase of reorganization

(5 mpf) were stained for myoplasm and microfilaments (Fig. 4.3.5). In the unfertilized egg, myoplasm was localized to the periphery of the vegetal pole and microfilaments were evenly localized to the entire cortex except for the animal pole (Fig. 4.3.5A,C; Roegiers *et al.* 1995; Chiba *et al.* 1999). In the fertilized egg, myoplasm was brought to the vegetal pole region and microfilaments were detected in the cortex of the vegetal hemisphere (Fig. 4.3.5B,D). In this stage of the fertilized egg, a small bulge, the so-called contraction pole, was observed at the vegetal region (Roegiers *et al.* 1995). The cortex of the contraction pole was stained relatively strongly (Fig. 4.3.5B,D). These results were consistent with previous studies (Roegiers *et al.* 1995; Chiba *et al*. 1999), and suggested that NaN_3 does not affect cortical microfilaments nor the first phase of myoplasmic reorganization.

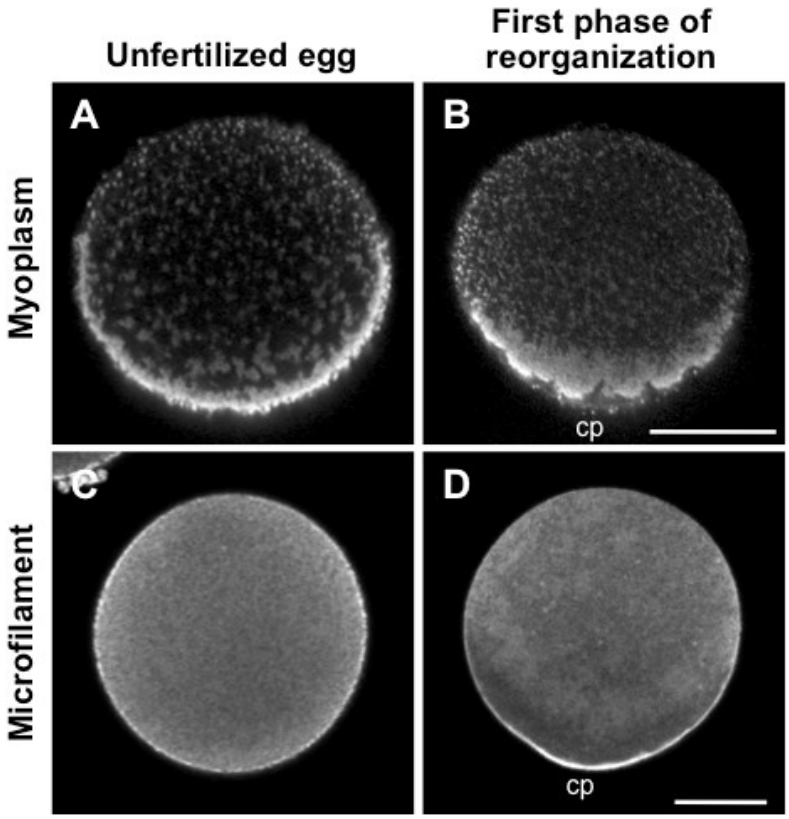

Figure 4.3.5 Distribution of myoplasm and microfilaments during the first phase of reorganization in embryos treated with NaN_3. *Ciona* unfertilized eggs were treated with NaN_3 for 30 min and were inseminated in the presence of NaN_3. Whole-mount specimen of unfertilized eggs and 1-cell-stage embryos during the first phase of reorganization (5 mpf) were stained for myoplasm and microfilaments. (A,C) Optical section of unfertilized egg. (B,D) Optical section of 1-cell-stage embryos during the first phase of reorganization. Myoplasm was segregated to the vegetal pole and microfilaments enriched in the contraction pole (cp). The animal pole is up. Scale bars, 50 μm.

4.3.6 Distribution of the myoplasm was disturbed in NaN_3-treated embryos at the cleavage stage

In my next experiments, it was asked whether disrupted cytoplasmic and cortical reorganization affected the establishment of the anteroposterior axis. The embryos were pulse treated with NaN_3 from 10 to 45 mpf, washed with MFSW, and were reared until the desired stage.

First, it was focused on the distribution of the myoplasm at the cleavage stage. In the control embryo at the 4-cell stage, the myoplasm was segregated posteriorly and localized to the B3-blastomere pair (Fig. 4.3.6A-C; Sardet *et al*. 2007). On the other hand, in the NaN_3-treated embryo, although the two rounds of cleavage occurred somewhat normally, the myoplasm stayed at the vegetal pole region of every blastomere and did not localize to the posterior pole (Fig. 4.3.6D-F). This suggests that the distribution of the myoplasm during the cleavage stage was not restored after NaN_3 pulse-treatment and thus, the anteroposterior axis of the embryo was disrupted at the cleavage stage.

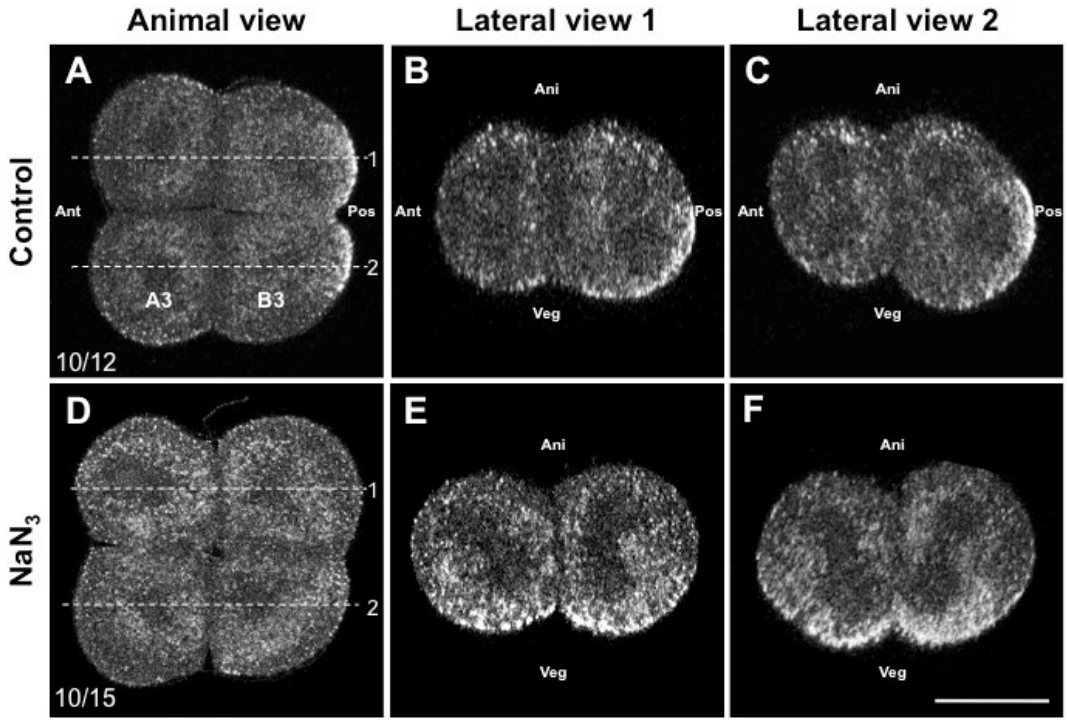

Figure 4.3.6 Distribution of the myoplasm in embryos pulse-treated with NaN_3. *Ciona* embryos were pulse-treated with NaN_3 during the second phase of reorganization (from 10 to 45 mpf). Whole-mount specimens of 4-cell-stage embryos were stained for myoplasm. (A-C) Optical section of control untreated embryo. (D-F) Optical section of NaN_3-pulse-treated embryo. (A,D) Animal views. (B,C,E,F) Lateral views at the positions of the dotted lines in A and D. Numbers (bottom left in A and D) indicate the proportion of embryos represented by the images. Scale bar, 50 μm.

4.3.7 Establishment of the anteroposterior axis was failed by the NaN_3 pulse-treatment

The cleavage pattern of ascidian embryos is bilaterally symmetrical and three rounds of unequal cleavage occur at the posterior pole of the vegetal hemisphere (Conklin 1905a,b; Satoh 1979). The centrosome-attracting body (CAB) plays an important role in not only for producing unequal cleavages, but also for the localization of cytoplasmic

information at the posterior pole (Nishikata *et al.* 1999; Sardet *et al.* 2007; Negishi *et al.* 2007). To investigate the establishment of the anteroposterior axis in the NaN_3-pulse-treated embryo, the cleavage pattern (Fig. 4.3.7) and CAB formation (Fig. 4.3.8) were analyzed in 16-cell-stage embryos.

As shown in Figure 4.3.7, most of the NaN_3-pulse-treated embryos were able to cleave and reach the 16-cell stage, but their configurations were abnormal. Thus, the embryos were divided into three categories based on the abnormalities in their cleavage patterns. The "Unequal" category included embryos that had two obviously small blastomeres, and thus about the half of them showed a bilaterally symmetrical normal pattern (Fig. 4.3.7A). The "Equal" category included embryos that did not possess an obviously small blastomere; most of these embryos looked like morulae and showed no obvious embryonic axis (Fig. 4.3.7B). "Uncleaved" embryos were those that failed to cleave or fused their blastomeres after several rounds of cleavage, and they appeared similar to 1-cell-stage embryos (Fig. 4.3.7C). Among the control embryos, most (97.0 ± 4.3%) underwent unequal cleavage and showed normal cleavage patterns (Fig. 4.2.7D). In NaN_3-pulse-treated embryos, only 15.1 ± 3.7% of the embryos underwent unequal cleavage and the other embryos showed equal cleavage (54.2 ± 25.1%) or remained uncleaved (31.9 ± 21.9%). The loss of unequal cleavage represented a disturbance in the establishment of the anteroposterior axis.

Moreover, CAB formation was investigated at the 16-cell stage (Fig. 4.3.8). At this stage, CAB was observed in 93.6 ± 4.4% of the control embryos (Fig. 4.3.8A,B) but only in 27.1 ± 11.2% of the NaN_3-pulse-treated embryos (Fig. 4.3.8C,D). This result

also suggests that NaN_3 inhibits the establishment of anteroposterior axis.

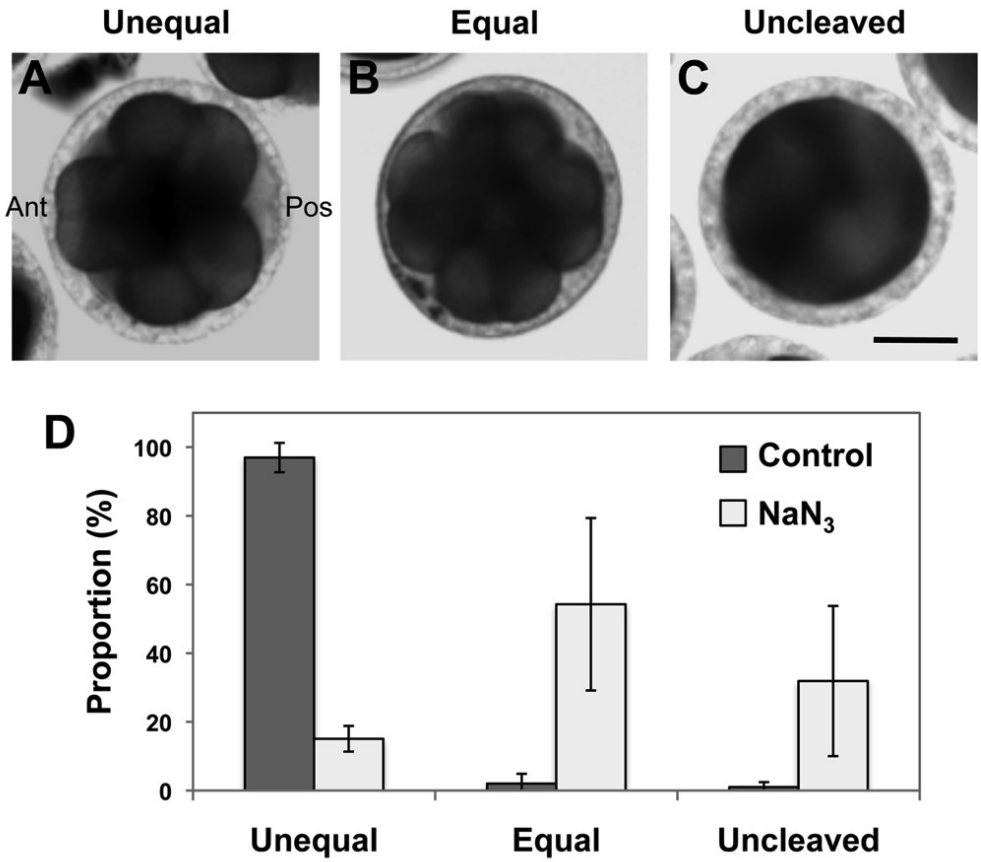

Figure 4.3.7 Anteroposterior axes of embryos were not established upon pulse-treatment with NaN_3. *Ciona* embryos were pulse-treated with NaN_3 during the second phase of reorganization (from 10 to 45 mpf). The cleavage abnormalities of 16-cell-stage embryos were divided into three categories. (A-C) A typical example of each category is shown. Details are in the text. Scale bar, 50 μm. (D) The graphs show the proportion of the categorized embryos among control untreated embryos (gray column) and NaN_3-pulse-treated embryos (white column). Error bars represent SDs (n=3-4).

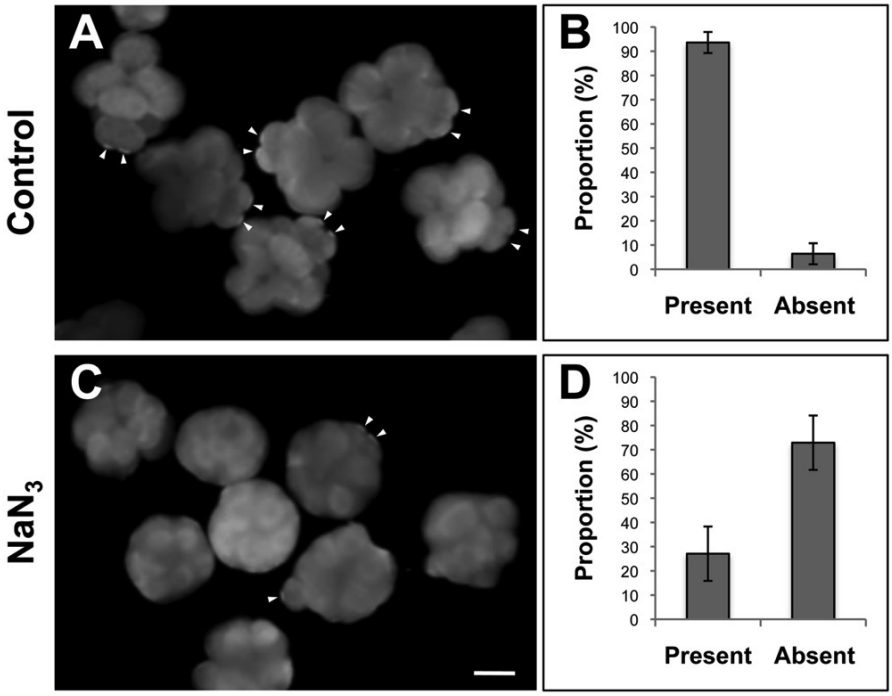

Figure 4.3.8 NaN_3 inhibited the formation of the centrosome-attracting body (CAB). *Ciona* embryos were pulse-treated with NaN_3 during the second phase of reorganization (from 10 to 45 mpf). Whole-mount specimens of the 16-cell-stage embryo were stained for CAB (arrow heads). (A) Control untreated embryo. (C) NaN_3-pulse-treated embryo. (B,D) The graphs show the proportion of embryos in which the CABs were present or absent, among control untreated embryos (B) or NaN_3-pulse-treated embryos (D). Error bars represent SDs (n=3). Scale bar, 50 μm.

Finally, the establishment of the anteroposterior axis was analyzed at the larval stage of NaN_3-pulse-treated embryos. The resulting embryos were divided into three categories. The category "Distinct head and tail" included embryos that had obvious head and/or tail structures (Fig. 4.3.9B), and thus included the normal larvae (Fig. 4.3.9A). The category "No distinct head and tail" included embryos in which head or tail structures could not be distinguished, and thus appeared to be cell masses (Fig. 4.3.9C). The category "Uncleaved" included embryos that failed to cleave or fused their

blastomeres after several rounds of cleavage, and these appeared similar to 1-cell-stage embryos (Fig. 4.3.9D). Corresponding to the results shown in Figures 4.3.7 and 4.3.8, most of the NaN_3-pulse-treated embryos developed into the "No distinct head and tail" category (Fig. 4.3.9E). This result clearly shows that NaN_3 pulse-treatment inhibited anteroposterior-axis formation and this did not recover during development. All these results with NaN_3-pulse-treated embryos strongly suggest that the posterior movement of the myoplasm in the second phase of cytoplasmic and cortical rearrangement in the 1-cell-stage embryo was solely responsible for the establishment of the anteroposterior axis, and the disturbance of this rearrangement was very difficult to recover. This clearly shows the importance of cytoplasmic and cortical reorganization on the mosaic mode of ascidian embryogenesis.

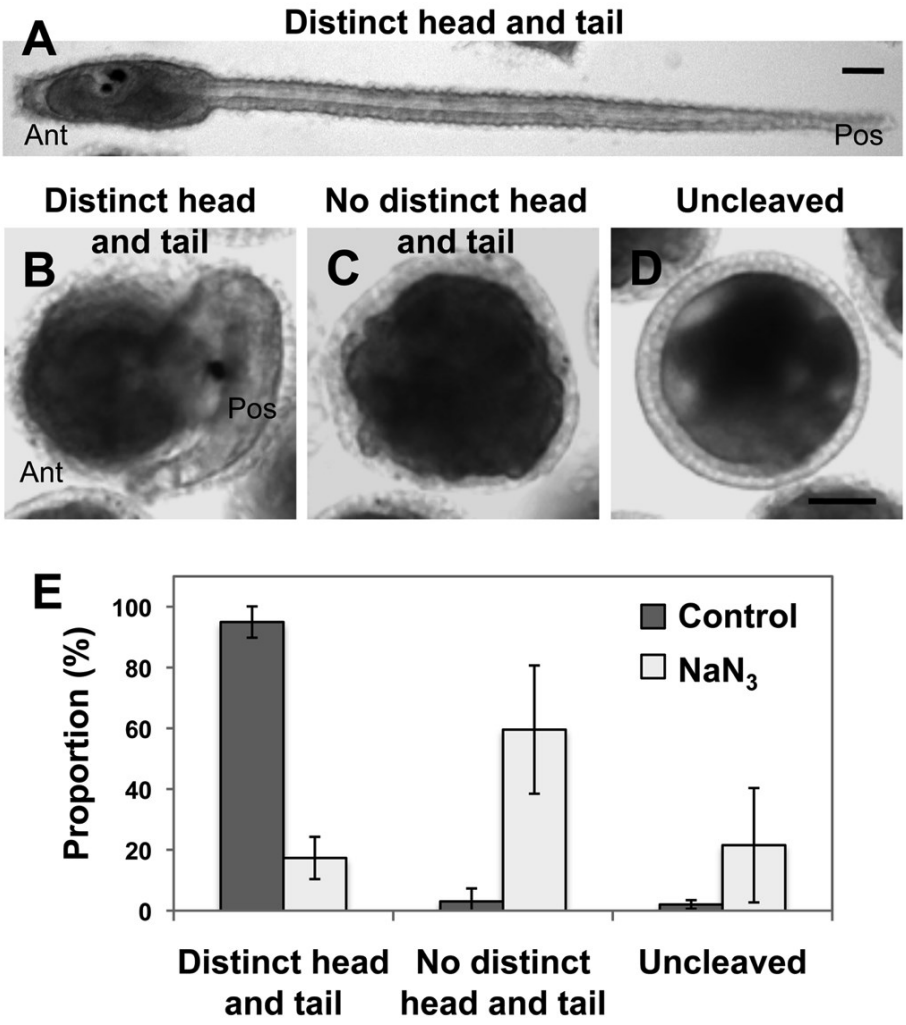

Figure 4.3.9 NaN_3-pulse-treated embryos developed into larvae that had no distinct head and tail. *Ciona* embryos were treated with NaN_3 during the second phase of reorganization (from 10 to 45 mpf). The morphological abnormalities of larval-stage embryos were divided into three categories. (A-D) A typical example of each category is shown. Details are in the text. Scale bar, 50 μm. (E) The graphs show the proportion of the categorized embryos among control untreated embryos (gray column) or NaN_3-pulse-treated embryos (white column). Error bars represent SDs (n=3-4).

4.4 Comparison of the inhibitory effects of NaN_3 on microtubule dynamics in ascidian, sea urchin, and human

4.4.1 NaN_3 inhibited the spindle formation during cleavage

In previous chapter, it was showed that NaN_3 inhibited the movement of myoplasm and the migration pathway of sperm aster during the second phase of reorganization. Since the reorganization is microtubule dependent manner, there is a possibility that NaN_3 inhibits the other cellular process depending on microtubules.

The effects of NaN_3 on spindle microtubule dynamics during ascidian early development were investigated. During the first cleavage, in control-untreated embryo, the spindles elongated along with the longitudinal axis (Fig. 4.4.1A). The astral microtubules were elongated from two centrosomes and formed a bipolar spindle. The plus ends of these two astral microtubules were crossed each other at the equatorial plate, and cleavage furrow was nicely formed on this cleavage plane. The spindle midzone was strongly stained with this antibody suggesting the relatively thick microtubule bundles in the midzone (Fig. 4.4.1A,A'). On the other hand, in NaN_3-pulse-treated embryo, although the position of the cleavage furrow and the radially elongated astral microtubules seemed normal, the centrosome was shifted from the center of each aster and two astral microtubules did not cross at the equatorial plate. Bipolar spindle was an irregular shape and was tilted from the normal position, which was perpendicular to the equatorial plane defined by the cleavage furrow. Moreover,

bright obscure staining between dividing chromosomes, which was thought to be a remnant of the spindle midzone, was observed. In addition, dividing chromosomes were scattered (Fig. 4.4.1B,B'). These results suggested that NaN_3 inhibited the formation of microtubule bundles at the midzone and the establishment of proper bipolar spindle in proper orientation.

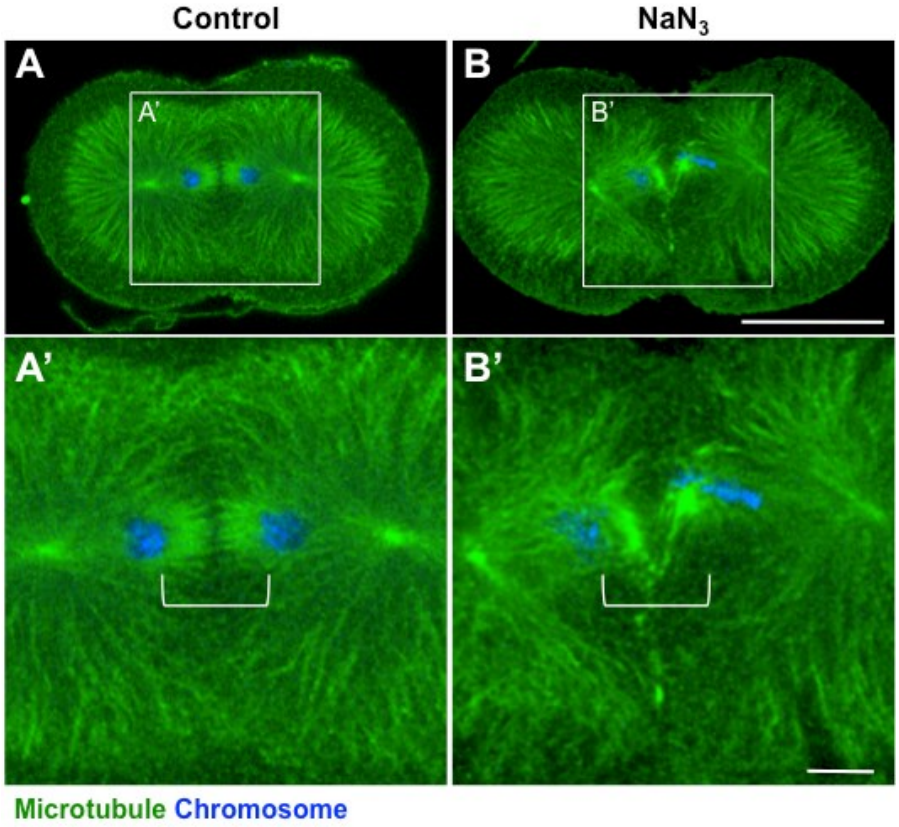

Figure 4.4.1 Abnormal spindle formation by the NaN_3 treatment. *Ciona* embryos were pulse-treated with NaN_3 during the second phase of reorganization (from 10 to 45 mpf). Whole-mount specimens of embryos during the first cleavage were stained for microtubule (green) and chromosome (blue). (A,A') Optical section of control untreated embryo. (B,B') Optical section of NaN_3-treated embryo. Thick microtubule bundles at midzone (square blankets) became abnormal by NaN_3-treatment. Scale bar, 50 μm (A,B) and 10 μm (A',B').

4.4.2 Effects of NaN_3 on spindle orientation in ascidian embryo

In ascidian 4-cell stage embryos, every spindle has its characteristic position and orientation, because the next 8-cell stage has a characteristic configuration (Conklin 1905). In B3-blastomere pair (posterior side), centrosome-attracting body (CAB) is formed at the posterior-vegetal cortex; the spindles are attracted and oriented to the CABs (Hibino *et al.* 1998; Nishikata *et al.* 1999; Sardet *et al.* 2007; Negishi *et al.* 2007).

To investigate the further effects of NaN_3 on spindle orientation, the control untreated and NaN_3-treated embryos at 4-cell stage were analyzed with 3D (three dimensions)-rendering models. The 3D models were rendered from the confocal images of 4-cell stage embryos stained for myoplasm, microtubule, and chromosome (Fig. 4.4.2A-D). In animal view, the spindles of control untreated embryos were arranged in bilaterally symmetric pattern in both A3 and B3 blastomeres from animal view (Fig. 4.4.2A), however, those of NaN_3-treated embryos were more randomized (Fig. 4.4.2C,D).

Because the anteroposterior and left-right axes were not obvious in the NaN_3-treated embryo (Ishii *et al.* 2014), the comparison of the spindle orientation between control untreated and NaN_3-treated embryo was difficult in animal view. Thus, the largest angles between spindles and animal-vegetal axis (designated as spindle angle; $\leq 90^\circ$) were measured in lateral view (Fig. 4.4.2E-G). In control untreated embryos, all of the spindle angles of anterior (A3) blastomeres were between 0° and 15°. So, the spindle of

A3 seemed to elongate almost parallel to the animal-vegetal axis. The spindle angles of posterior (B3) blastomeres were between 10˚ and 50˚ and more than half of them were between 25˚ and 35˚. In NaN_3-treated embryos, however, the spindle angles were widely distributed between 0˚ and 75˚ and the distribution pattern was totally different from that of control untreated embryo. Statistical analysis indicates that these distributions of spindle orientations in control untreated and NaN_3-treated embryos were highly significant (P = 0.0049, t-test; Fig. 4.4.2G). These results indicated that the spindle orientations of the embryo treated with NaN_3 were randomized and the spindles were oriented in various directions. NaN_3 might inhibit the molecule, which was important for spindle orientation.

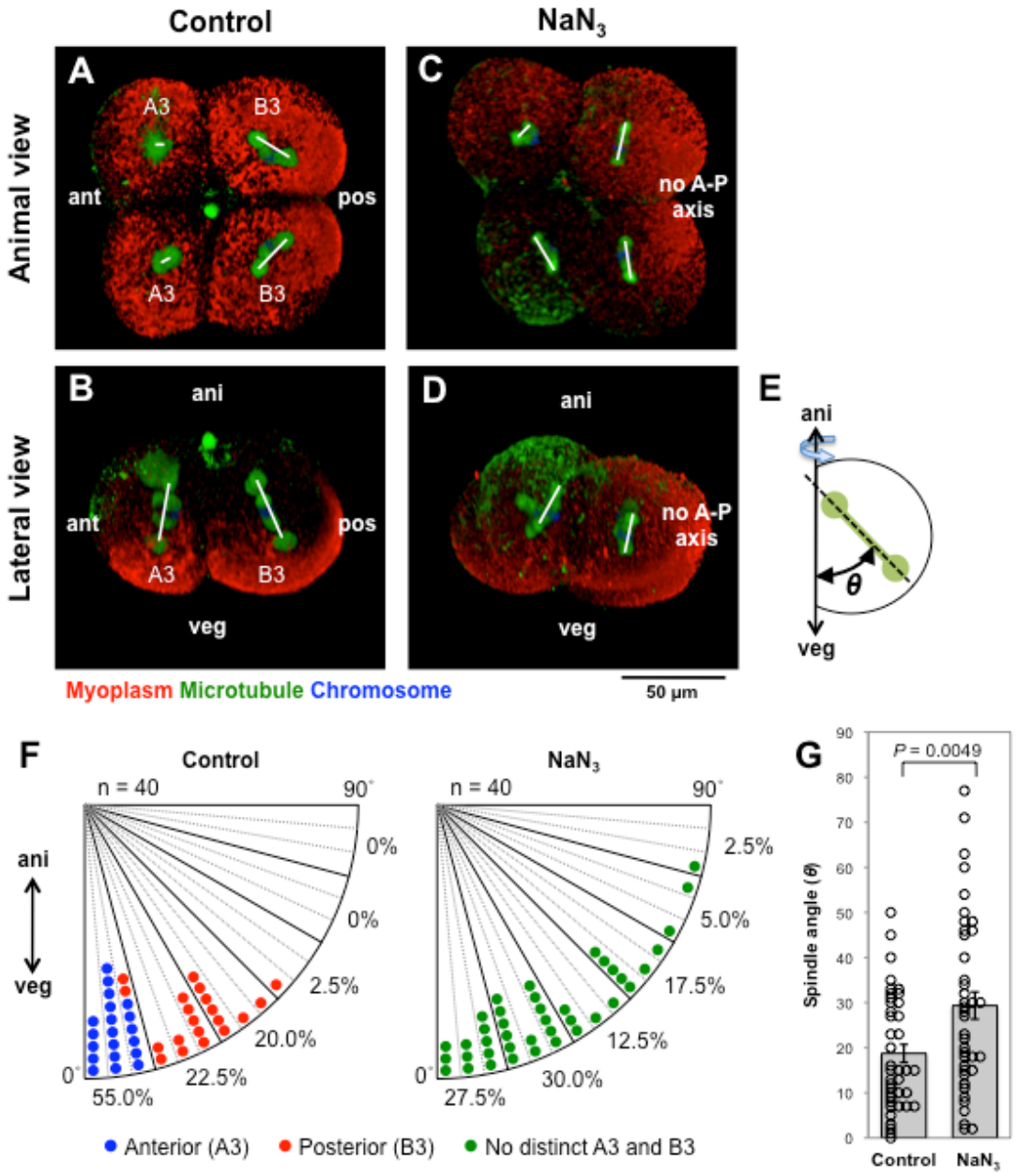

Figure 4.4.2 Spindle orientation in ascidian embryo. (A-D) *Ciona* embryos were pulse-treated with NaN_3 during the second phase of reorganization (from 10 to 45 mpf). Whole-mount specimens of 4-cell-stage embryos were stained for myoplasm (red), microtubule (green), and chromosome (blue). The 3D models were rendered from the confocal images. (A,C) Animal view. (B,D) Lateral view. Scale bar, 50 μm. (E) Schematic diagram represents the measurement of spindle angles from lateral view. The largest angle (≤90˚) between the spindle and the animal-vegetal (A-V) axis was measured. (F) Distribution of spindle orientation in each blastomeres from control untreated embryos and NaN_3-treated embryos. (G) Statistic analysis of the distribution of spindle orientation. Columns with error bars represent mean ± s.e.m (n = 40).

4.4.3 Effects of NaN_3 on spindle orientation in sea urchin embryo

The different model animal, the sea urchin *Anthocidaris crassispina*, was further used to examine the consequence of effects of NaN_3 on spindle orientation. *Anthocidaris* embryos were treated with NaN_3 from 1-cell stage (15 mpf) to morula stage (7 hpf). All untreated embryos developed into the morula stage and NaN_3-treated embryos were cleavage-arrested in concentration-dependent manner (Fig. 4.4.3A). Most of embryos treated with 10 mM NaN_3 were failed to cleave at 1-cell stage, however, 46.8 ± 9.1% of embryos treated with 5 mM NaN_3 were allowed to cleave up to 4-cell stage. Interestingly, at 4-cell stage, the blastomere of control embryos were arranged on the same plane (Fig. 4.4.3B), however, NaN_3-treated embryos showed tetrahedral shape (Fig. 4.4.3C). In 2-cell stage embryos, normal spindle pair was lined in parallel (Fig. 4.4.3D), while the spindles treated with 5 mM NaN_3 were orthogonal to each other (Fig. 4.4.3E), suggesting that the abnormal spindle orientation caused the abnormal cleavage patterns.

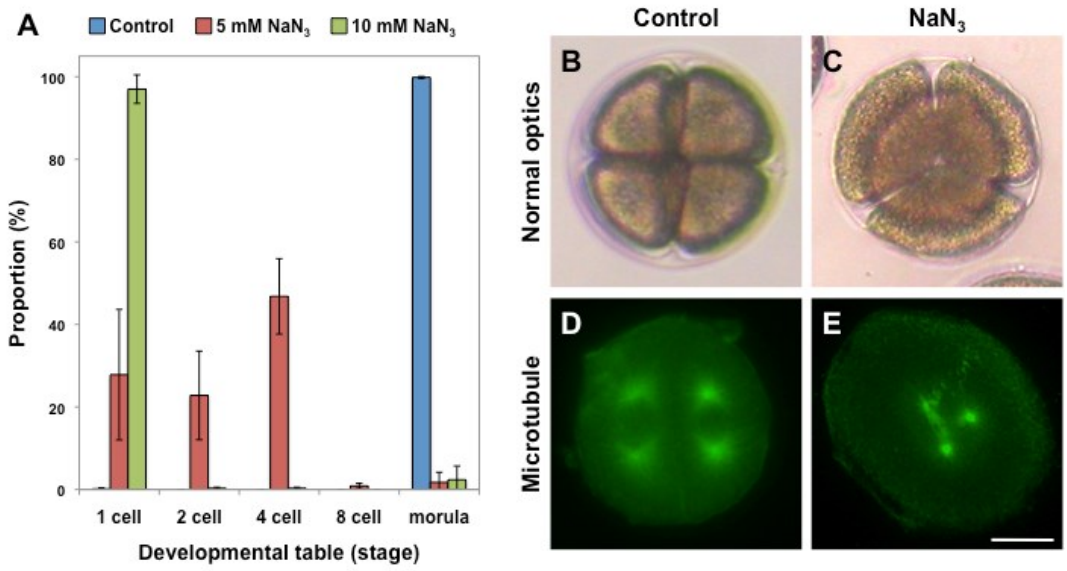

Figure 4.4.3 Effects of NaN_3 on cleavage pattern and spindle orientation in sea urchin embryos. (A) Sea urchin embryos were treated with NaN_3 from 15 mpf to the morula stage. The graphs show the proportion of the embryos, which stopped their development at each stage. These results were counted when control untreated embryos developed to the morula stage. Error bars represent SDs (n=3). (B,D) 4-cell stage. (C,E) 2-cell stage stained for microtubule. (B,C) Control-untreated embryo. (D,E) NaN_3-treated embryo. NaN_3-treated embryos showed tetrahedral cleavage pattern and orthogonal spindle orientation. Scale bar, 25 μm.

4.4.4 NaN_3 inhibited midzone formation and spindle orientation in HeLa cell

To reveal further effects of NaN_3 on spindle microtubule dynamics, HeLa cells were used and treated with NaN_3 for 24 hr. After treatment, the cell numbers and MTT values of NaN_3-treated cells were decreased in concentration-dependent manner (Fig. 4.4.4A). The numbers of cells treated with 15 mM or 30 mM NaN_3 was 20.4 ± 2.2% and 11.0 ± 1.0% of control-untreated cells, respectively. This cytotoxic effect might suggest the inhibitory effect of NaN_3 on the respiration. On the other hand, in 5 mM NaN_3 treatment,

cell number was 57.3 ± 7.4% of control-untreated cells, and no obvious cell death was observed. If there were some effects on HeLa cells under 5 mM NaN_3 treatment, the target molecule of NaN_3 could be different from that of cytotoxic effect. Thus, HeLa cells were treated with NaN_3 at 5 mM. In order to describe the effects of NaN_3 during interphase, HeLa cells were double stained for microtubule and chromosome. As shown in Figure 4.4.4B,C, this treatment caused a failure in mitosis and produced multinucleated cells. Then, to describe the effect of NaN_3 on the mitotic cell division, HeLa cells were triple-stained for microtubule, chromosome, and aurora B, which was a midzone marker protein and important for chromosome alignment (Fig. 4.4.5). At metaphase, in control-untreated cells, cells became round-shape, microtubules formed a ball-shape bipolar spindle, aurora B was localized to the kinetochore, and chromosomes were arranged on the equatorial plate (Fig. 4.4.5A-D). On the other hand, in NaN_3-treated cells, cells became ovoid-shape, the distorted-bipolar spindle was tilted from the longitudinal axis. Moreover, aurora B was diffused from midzone and the chromosome was scattered (Fig. 4.4.5E-H). These results indicated that NaN_3 inhibited midzone formation and spindle orientation in HeLa cell. This result was consistent with those in ascidian and sea urchin embryos.

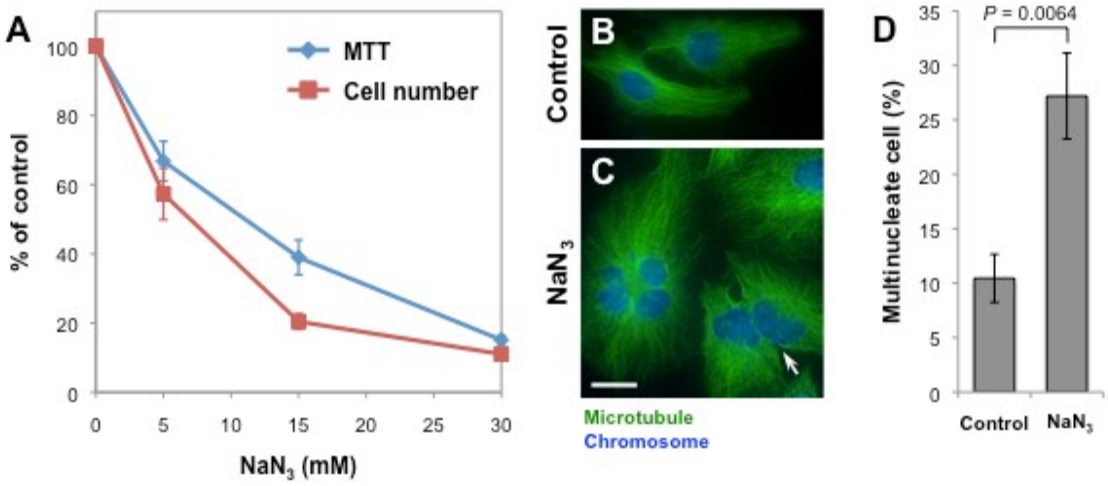

Figure 4.4.4 Effects of NaN_3 on growth and mitosis in HeLa cells. (A-J) HeLa cells were treated with NaN_3 at designated concentrations (5, 15, 30 mM in A; 5 mM in B-D) for 24 hr. (A) Cell numbers and measurements of mitochondrial respiratory activity using MTT assay of HeLa cells were manually counted. (B,C) HeLa cells were fixed and stained for microtubule (green) and DNA (blue). NaN_3-treatment caused a failure in cytokinesis and formation of multinucleated cells (arrow). Scale bar, 10 μm. (D) The graph shows the proportion of the multinucleated cells among control-untreated cells and NaN_3-treated cells. Error bars represent SDs (n=3).

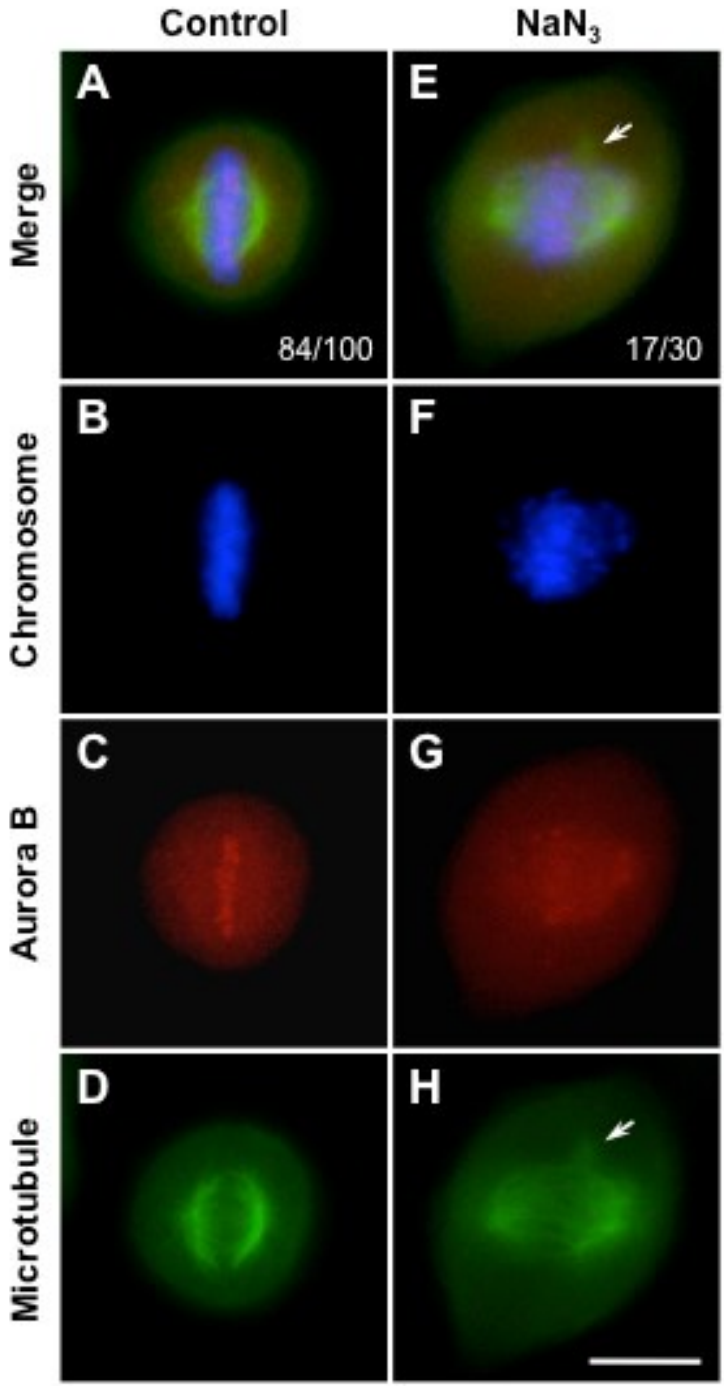

Figure 4.4.5 Effects of NaN_3 on spindle midzone formation and the orientation in HeLa cells. HeLa cells on the mitotic cell division were stained for microtubule (green), Aurora B (red), and chromosome (blue). Numbers (bottom right in A,E) indicate the proportion of cells represented by the images. NaN_3 caused misalignment of chromosomes. Arrows indicate the abnormal midzone microtubules. (A-D) Control-untreated cells. (E-H) NaN_3-treated cells. Scale bar, 10 μm.

5 DISCUSSIONS

5.1 p58 was identical to the F_1-ATPase α-subunit

In this study, the application of biochemical methods to ascidian eggs allowed to identify the protein recognized by the standard myoplasm-marker antibody NN18. Unexpectedly, it was F_1-ATPase α-subunit. Somewhat alarmingly, it was unrelated to the original antigenic protein. While the cause of this cross-reaction is unknown, the occurrence may be representative of general situations, which lead to mistaken identity, some of which have been documented (Bordeaux *et al.* 2010; Schnell *et al*. 2012; Willingham 1999; Michel *et al.* 2009). For instance a secondary affinity for an abundant protein may be revealed when the presumed antigen is not present in the tissue of interest, as is the case for the NN18 antibody. The *Ciona* genome encodes 5 intermediate filament genes (Karabinos *et al.* 2004) but no homolog to the neurofilamant (type IV) class which antibody NN18 recognizes in vertebrates. F_0F_1-ATPase is one of the most abundant proteins in eggs as determined by analysis of the *Ciona* proteome (http://cipro.ibio.jp/2.5/expression profile KH.C10.579; Nomura *et al.* 2009). As the F_0F_1-ATPase transcript is abundant in the egg and decreases during cleavage stages, the constant level of F_0F_1-ATPase throughout embryonic development likely reflects stable maternal protein (Swalla *et al*. 1991; Chenevert *et al*. 2013). It is like a pattern that of the transcript encoding ascidian ATP translocase (Miya *et al.* 1994). It is worth pointing out that since p58 (F_1-ATPase α-subunit) is so stable and

well-characterized, the commercially available NN18 monoclonal can be used by the ascidian community as a reliable standard to compare protein amount among samples.

5.2 Comparison of subcellular localizations between mitochondrial proteins

By using comprehensive immunohistochemical staining, two staining patterns were categorized: staining with anti-ATPα and anti-ATPβ antibodies: and staining with anti-MnSOD and anti-PDHE1α antibodies. The former are mitochondrial inner membrane proteins and the latter are mitochondrial matrix proteins. The differences observed in the staining patterns might be due to this intramitochondrial localization pattern. As the exact localization pattern of mitochondria and these staining patterns could not be compared, it was unclear which pattern represents the mitochondrial localization pattern. As MnSOD is an anti-oxidant enzyme and its expression is thought to be regulated according to the cell conditions (e.g. Andreyev *et al.* 2005; Aiken *et al*. 2008), its localization pattern may not always represent the mitochondria localization pattern. However, in this study, at least at the crescent stage, TEM clearly distinguished a 2- to 6-μm-thick mitochondria-less cortical region from a mitochondria-rich internal region. The latter was congruent with the immunofluorescent staining with anti-MnSOD antibodies. The mitochondria-less cortical region was pointed out by previous studies to be an ER-rich domain (e.g. Speksnijder *et al.* 1993; Roegiers *et al.* 1999). As this region is also known as the site for the postplasmic maternal RNAs localization (Yoshida *et al.* 1996), Sardet *et al.* (2007) called this region the cortical endoplasmic reticulum and

maternal postplasmic/PEM RNAs domain (cER-mRNA domain). From these points of view, at least at the crescent stage, the distribution of MnSOD represents the mitochondria localization pattern and, hence, the intense staining of this cER-mRNA domain with anti-ATPα and anti-ATPβ antibodies was not due to the mitochondrial F_0F_1-ATPase, but arose from the exomitochondrial F_1-ATPase subunits.

In previous studies, anti-ATPα antibody (NN18) was used as a marker for the myoplasm (e.g. Swalla *et al.* 1991; Chiba *et al.* 1999), and sometimes it was used as a marker for the mitochondria, which localize to the myoplasm (e.g. Prodon *et al.* 2006; Prodon *et al.* 2007). These studies did not pay much attention to the intense staining in the cER-mRNA domain. In the current study, double staining with anti-ATPα and anti-MnSOD antibodies first clearly highlighted the cER-mRNA domain as the ATPα-enriched and MnSOD-less cortical region. However, the relationship between exomitochondrial F_1-ATPase subunits and the cortical ER and postplasmic RNAs has yet to be analyzed.

5.3 Localization analyses by the subcellular fractionation method

The subcellular fractionation method used in this study was reliable. Although the FL fraction was contaminated with the ME and SC fractions, the constituent molecules in the IC, ME, and SC fractions were clearly distinct. This reliability was confirmed by the monitoring of mitochondrial respiratory activity. Using this reliable method, it was found that only ATPα and ATPβ were recovered in both IC and ME fractions. The other

mitochondrial components, three matrix proteins, one subunit of F_0, and even one subunit of F_1-ATPase, were mostly recovered in the ME fraction. This result strongly suggests that only ATPα and ATPβ are localized exomitochondrially.

In order to obtain more convincing evidence for the exomitochondrial localization of these proteins, immunoelectron microscopic observations are necessary. In addition, subcellular fractionation of crescent stage embryos and immunoprecipitation experiments with anti-ATPα and anti-ATPβ antibodies will offer very insightful data. Such immunoprecipitation experiments will lead us closer to identifying the binding partner of these exomitochondrial F_1-ATPase subunits, which will offer a clue to understanding their function.

5.4 Association of cytosolic F_1-ATPase subunits with the cytoskeleton

As p58 is believed to be a cytoskeletal protein (Jeffery & Swalla 1992) and to bind to the myoplasmin-C1 (Nishikata & Wada 1996), the exomitochondrial F_1-ATPase subunits were necessarily thought to associate with the cytoskeleton. In the current study, the difference in solubility in detergent between ATPα and MnSOD in the living unfertilized egg was distinguished; however, the results could be due to differences in the molecular nature of the inner membrane protein and the matrix protein. Although this possibility cannot be excluded, the long research history of the mammalian F_0F_1-ATPase testifies to the solubility of mitochondrial F_0F_1-ATPase even in 0.5% Triton X-100-containing buffers (Ko *et al*. 2003). So, the finding in the current study

that any of the ATPα was insoluble in the buffers containing a relatively high concentration (2%) of Triton X-100 was unexpected. My extraction experiments showed that exomitochondrial ATPα in the ascidian egg was bound to the cytoskeleton. This result also supported the existence of the exomitochondrial ATPα.

Swalla *et al*. (1991) reported that p58 is necessary for restoration of larval features in *Molgula occulta* × *Molgula oculata* hybrids. They also proposed p58 as a cytoskeletal component (Jeffery & Swalla 1992). On the other hand, myoplasmin-C1 was one of the myoplasm-specific antigens recognized by monoclonal antibodies raised against isolated *Ciona* whole myoplasm, and was suggested to have a role in muscle differentiation (Nishikata *et al*. 1987). The myoplasmin-C1 has heptad repeats and is suggested to form homo- or hetero-oligomeric complexes *in vivo* through an alpha-helix coiled-coil structure (Nishikata & Wada 1996). Actually, myoplasmin-C1 is detergent insoluble and pull-down experiments suggested direct binding to p58 (Nishikata & Wada 1996). The functions of these proteins and the importance of the internal region of the myoplasm have yet to be elucidated. However, in this study, it was found that p58 is identical to the F_1-ATPase α-subunit. F_1-ATPase α-subunit is completely co-localized with the β-subunit in both mitochondria and cytosol, suggesting F_1-ATPase α- and β-subunits, and myoplasmin-C1 might form a novel complex in the cytosol. This complex was designated as “exo-ATPα/β”. Although, much more research is required to further define the molecular nature of exo-ATPα/β, mitochondrial involvement in ascidian early development becomes an interesting theme.

5.5 Novelty of the ascidian exomitochondrial F_1-ATPase subunits

Exomitochondrial F_0F_1-ATPase has been reported in mammalian cells. In human umbilical vein endothelial cells (HUVEC), exomitochondrial F_0F_1-ATPase was located on the plasma membrane and functioned as an angiostatin receptor (Moser *et al.* 2001; Veitonmaki *et al.* 2004). In the human hepatocellular liver carcinoma cell line (HepG2) and normal human liver cells, exomitochondrial F_0F_1-ATPase was located on the plasma membrane and functioned as an apolipoprotein A-1 (apoA-1) receptor (Martinez *et al.* 2003; Manguiullo *et al.* 2008). Also, in some human tumor cells, exomitochondrial F_0F_1-ATPase was located on the plasma membrane and lowered the surrounding pH (Kenan & Wahl 2005). All of these F_0F_1-ATPases were the complete form of the enzyme complex and, additionally, their ATP hydrolyzing enzyme activities were experimentally proven (Moser *et al.* 2001; Manguiullo *et al.* 2008).

My results are totally new from the viewpoints of the completeness of the enzyme complex and intracellular localization. In this study, it is suggested that only a part of the F_0F_1-ATPase, subunit α and β, is exomitochondrially localized in the cytosol and form a novel complex "exo-ATPα/β". Moreover, this localized region is the cortical ER-rich region of the myoplasm, at least at the crescent stage. However, the function of the exo-ATPα/β in the ascidian embryo is still obscure. The localized region, which was the cER-mRNA domain, suggests its involvement in the versatile functions of the myoplasm such as, muscle development (e.g. Nishida & Sawada 2001), embryonic axis formation (e.g. Negishi *et al.* 2011) and germ cell specification (e.g. Shirae-Kurabayashi

et al. 2011) and cytoplasmic and cortical reorganization (Chiba *et al*. 1999; Ishii *et al*. 2012; Ishii *et al.* 2014).

5.6 NaN_3 inhibited cytoplasmic and cortical reorganization

Since oligomycin and NaN_3 are well-known mitochondrial inhibitors, the effects of these inhibitors on ascidian early development were expected to be similar. However, their effects were distinct. At high concentrations that completely inhibited sperm motility (NaN_3: ≥50 mM, oligomycin: ≥1.5 μM), both inhibitors interfered with cleavage, however, NaN_3 exerting more severe effects. NaN_3 stopped cleavage when treated at the 1-cell stage, but oligomycin allowed eggs to reach up to 64-cell stage. At low concentrations that allowed sperm motile (NaN_3: ≤5 mM, oligomycin: ≤0.05 μM), NaN_3 did not allow embryos to develop beyond the 64-cell stage, while oligomycin allowed to reach the larval stage. In this condition (5mM), NaN_3 inhibited the movement of the myoplasm to the posterior region and altered the migration pathway of the sperm aster during the second phase of the cytoplasmic and cortical reorganization. Oligomycin, even at high concentration, did not affect the myoplasmic movement nor the sperm aster migration during the reorganization. Although the embryos pulse treated with 5 mM NaN_3 were disrupted the reorganization, they continued development after the treatment. Remarkably, the NaN_3-pulse-treated embryos did not show the unequal cleavage, the CAB formation, nor the formation of distinct head and tail, indicating the loss of anteroposterior axis.

Microtubule inhibitors also inhibited the movement of the myoplasm and the

migration of the sperm aster (Sawada & Schatten 1989; Chiba *et al.* 1999); however, NaN_3 inhibited the myoplasmic reorganization without the microtubule depolymerization and altered the pathway of the sperm aster migration. In NaN_3-treated embryos, the sperm aster detached from the vegetal cortex following the start of the treatment and migrated to the center of the egg with a wobbling motion. This suggests the existence of an unknown molecule that could attract or attach the sperm aster to the egg cortex during the second phase of reorganization (Fig. 5.1). This attachment plays an important role in the movement of the myoplasm.

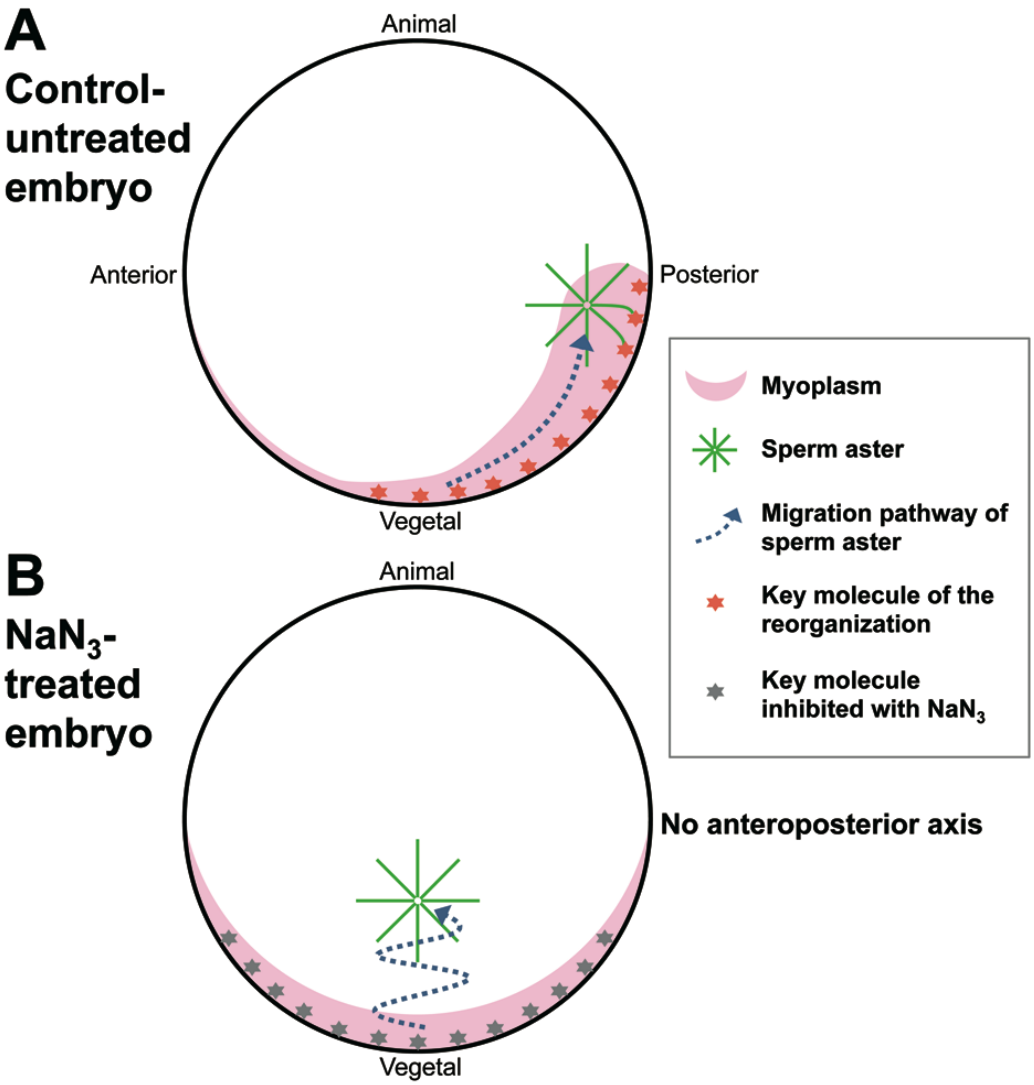

Figure 5.1 Model of NaN_3 effects on the second phase of reorganization. (A) Control untreated embryo. Myoplasm moves to the future-posterior region along with sperm aster migration. During this migration, the sperm aster is attracted or attached to the cortex by the key molecule of the reorganization (orange asterisk). (B) NaN_3-treated embryo. As the key molecule is inhibited by NaN_3 (gray asterisk), the movement of the myoplasm and the attachment of the sperm aster to the cortex are inhibited. Moreover, sperm asters treated with NaN_3 wobbled to the center of the embryos.

5.7 Establishment of the anteroposterior axis was inhibited in NaN_3-pulse-treated embryos

The centrosome-attracting body (CAB) is important for the unequal cleavages in 8- to 32-cell-stage embryos (Hibino *et al.* 1998). The components of the CAB are already localized to the cortical region of the myoplasm in 1-cell-stage embryos, and the formation of the CAB begins from the 2-cell stage (Hibino *et al.* 1998; Nishikata *et al*. 1999; Sardet *et al.* 2007; Negishi *et al.* 2007). When the posterior-vegetal cytoplasm (PVC), including the cortical region of the myoplasm, is surgically removed, CAB formation and unequal cleavages do not occur (Nishida 1994; Nishikata *et al.* 1999). In addition, the anteroposterior axis is not established and the embryo develops into a larva with no distinct head and tail, and no muscle-cell differentiation (Nishida 1994). Moreover, when the PVC is transplanted to the anterior-vegetal position of PVC-removed embryos, the CAB is formed in the former anterior side and the developed larvae have a reverse anteroposterior polarity (Nishida 1994; Nishikata *et al*. 1999).

In the present study, it was able to prepare abnormal embryos with an anteroposterior disorder by pulse-treatment with NaN_3. The abnormal localization of the myoplasm in the NaN_3-pulse-treated embryo was not restored after the washing-out of NaN_3. The myoplasm did not move to the posterior region and remained at the vegetal pole during cleavages. At the 16-cell stage, NaN_3-pulse-treated embryos failed to establish the anteroposterior axis, similar to the PVC-removed embryo. Although the PVC was not removed in this experiment, CAB formation failed in most cases in

NaN_3-treated embryos. This suggests that the normal reorganization of the myoplasm is important for the mechanism of CAB formation, which should occur within the PVC. The failure of anteroposterior axis establishment in the NaN_3-pulse-treated embryo strongly supports the idea that the determination of the posterior pole is initiated by cytoplasmic and cortical reorganization.

5.8 Target molecules of NaN_3 involved in cytoplasmic and cortical reorganization

In this study, it was showed that oligomycin did not affect cytoplasmic and cortical reorganization. This result was consistent with the general knowledge that oligomycin is an inhibitor of mitochondrial respiration. Target molecule of oligomycin is the ring of subunit c in the F_0 complex of the F_0F_1-ATPase (Hong & Pedersen 2008; Symersky *et al.* 2012).

NaN_3 is also known as an inhibitor of mitochondrial respiration. The main target molecule in this respiratory inhibition is the respiratory chain complex IV, cytochrome *c* oxidase (Yoshikawa *et al*. 1998). The azide anion of NaN_3 binds to the metal sites, heme a3 and Cu_B, that form the oxygen reduction site of cytochrome *c* oxidase (Yoshikawa *et al*. 1998; Fei *et al*. 2000). In addition, many other metalloproteins can be inhibited by azide binding to their metal sites in a similar manner. They include peroxidase (Ortiz *et al.* 1988; Tuisel *et al.* 1991; Harris *et al.* 1991; DePillis *et al.* 1990; Samokyszyn & Ortiz *et al.* 1991), cytochrome p450 (Hollenberg 1992), and hemoglobin (Sjostrand 1953).

NaN_3 also inhibits the ATP-hydrolase activity of F_1-ATPase from mitochondria, bacteria, and chloroplasts but not ATP synthesis (Bowler *et al*. 2006; Hong & Pedersen 2008). The binding of azide requires the prior binding of both ADP and Mg^{2+}. Azide binds to the catalytic site in the β-subunit and interacts with the β-phosphate of ADP, mimicking the nonbridging oxygen atom of the γ-phosphate. The binding of azide in the catalytic site is very tight and azide is closely associated via hydrogen bonds with β-Lys-162 in the p-loop domain and α-Arg-373 (Bowler *et al.* 2006; Hong & Pedersen 2008). The tight interaction between azide and the side chains prevents the conversion of the subunit to the open conformation and the release of ADP. In a similar manner, NaN_3 inhibits several ATPases that have the p-loop domain in the phosphate-binding site, such as the ABC transporter (Dallas *et al.* 2003, Jha *et al.* 2003), the preprotein translocase SecA (Miller *et al.* 2002; Oliver *et al*. 1990), and DNA topoisomerase IIα (Ju *et al.* 2001). On the other hand, while vesicular ATPase and archaeal ATPases from *Sulfolobus* also have the p-loop domain in the ATP binding pocket, NaN_3 does not inhibit them (Hirata *et al.* 2003; Uchida *et al.* 1985; Vasilyeva & Forgac 1998; Schafer & Meyering-Vos 1992). This indicates that NaN_3 does not inhibit all ATPases that have a p-loop domain (Bowler *et al.* 2006).

Because a number of NaN_3 target molecules have been reported as written above, it is difficult to narrow down the candidates of NaN_3 target molecules in the ascidian egg. Meanwhile, a number of metalloproteins and ATPase are maternally expressed in the ascidian egg (Nishikata *et al*. 2001), it is also difficult to identify real target of NaN_3 involved in cytoplasmic and cortical reorganization. Primarily expected candidates are

motor proteins, for example, myosin, dynein, and kinesin, which have ATPase activities. However, it is unclear whether NaN_3 inhibits these motor proteins. Treatment with NaN_3 at low concentration used in this study did not significantly inhibit the movement of the sperm motility nor the constriction of the actin network during the first phase of reorganization, suggesting that the motor proteins working in these systems were not the NaN_3 target molecules.

Previously, it was revealed that the α- and β-subunits of F_1-ATPase are exomitochondrially localized to the cortical region of the myoplasm in the ascidian egg (Ishii *et al.* 2012, Chenevert *et al.* 2013). Interestingly, exomitochondrial F_1-ATPase subunits have been proven to bind to some cytoskeletal filaments and myoplasmin-C1 (Nishikata & Wada 1996) and are thought to form a novel complex without F_0 subunits. This complex was designated as exo-ATPα/β. The function of this novel complex is unclear, however, exo-ATPα/β should be one of the candidates of NaN_3 target molecules involved in cytoplasmic and cortical reorganization.

Vasilyeva & Forgac (1998) reported that NaN_3 inhibited ATP-dependent proton transport via vesicular ATPase without ATP hydrolysis. Thus, NaN_3 could affect the intracellular pH indirectly. This postulated change of intracellular pH may inhibit the ascidian cytoplasmic and cortical rearrangement, but it will be a future problem. Regardless of whether the effect of the NaN_3 was direct or indirect, the investigation of the inhibitory effects of NaN_3 may lead us to the future discovery that may be important for understanding the cytoplasmic and cortical reorganization in the ascidian development.

5.9 Similar effects of NaN_3 on spindle dynamics among ascidian, sea urchin, and human

In addition to the effect on the cytoplasmic and cortical reorganization, the same concentration of NaN_3 affected the spindle dynamics, midzone formation and its orientation, in the ascidian embryo. These cellular processes, including cytoplasmic and cortical reorganization, are related to the microtubules. Furthermore, similar effects of NaN_3 on the spindle dynamics were observed in sea urchin embryo and HeLa cell.

A number of molecules involved in spindle midzone formation and spindle orientation are reported (Kallio *et al.* 2002; Petronczki *et al*. 2008; Zimniak *et al.* 2009; Carmena *et al*. 2009; Abe *et al*. 2010; Tamura & Draviam 2012; Lu & Johnston 2013). Interestingly, several molecules play key roles in both spindle midzone formation and spindle orientation; for example, aurora, end binding 1 (EB1), and polo-like kinase 1 (Plk1). These molecules are highly conserved among yeast to human. NaN_3 might inhibit one of these molecules.

In ascidian embryo, at cleavage stage, centrosome-attracting body (CAB) is required for not only the unequal cleavage but also the spindle orientation, which is important for the correct cleavage planes. Interestingly, Plk1 is localized to the spindle midzone and also the CAB (Negishi *et al.* 2011). In the CAB, Plk1 binds to the other CAB component, posterior end mark (PEM), and contributes to the spindle orientation. On the other hand, at 1-cell stage, most of the CAB components are localized to the cortical region of myoplasm. The localization of plk1 is unclear, however, at least the binding

partner PEM is localized to the cortical region of the myoplasm (Shirae-Kurabayashi *et al*. 2011). It is suggested that the cortical region of the myoplasm is important for the transport system of maternal factors, cytoplasmic and cortical reorganization, where microtubules are localized (Chiba *et al*. 1999; Ishii *et al.* 2012). NaN_3 might bind to the component(s) localized to both cortical region and spindle midzone, and finally, inhibit the microtubule-dependent cellular processes including intracellular transport system and mitosis. Moreover, these component(s) might be conserved at least in ascidian, sea urchin, and human; those are deuterostomes. In addition to reveal the intracellular transport mechanism of ascidian maternal factors, identification of the target molecules of NaN_3 will be a clue to understanding the mechanism underlying the microtubule-dependent cellular processes, which conserved within wide variety of cells.

6 PERSPECTIVES

6.1 Perspective of studies on the ascidian exomitochondrial F_1-ATPase subunits

In the fields of cell biology, it is well known that identical proteins are found in more than one subcellular compartment. It is called “dual targeting” or “dual distribution” of the protein (e.g. Karniely & Pines 2005; Herrmann 2009). For example, the mature form of fumarase (Stein *et al.* 1994; Soltys & Gupta 1999) and aconitase (Regev-Rudzki *et al.* 2005) are distributed within both mitochondria and cytosol. In these two examples, the dual targeting mechanism is achieved by the specific folding properties of the C-terminal region, which distinguishes import into the matrix or release back into the cytosol (Knox *et al.* 1998). In this study, one of the exomitochondrial subunits, F_1-ATPase α-subunit, was immunoprecipitated by the NN18 antibody and the N-terminal amino acid sequence was determined. The sequence was lacked the tentative mitochondria-targeting signal sequence and was thought to represent a matured form. Therefore, F_1-ATPase α-subunit has a possibility to achieve its dual distribution by the same mechanism as fumarase. In this context, a novel dual-targeting protein within the ascidian egg was showed. The large size of the egg facilitates the discrimination between mitochondria and cytosol. Moreover, the processes of oogenesis and early development, including the cytoplasmic and cortical reorganization, have been well described. This model could provide a unique and powerful experimental system to

analyze the dual targeting mechanism.

On the other hand, in the fields of developmental biology and evolutionary biology, ascidian exomitochondrial F_1-ATPase subunits are novel examples of gene cooption. Gene cooption is a kind of evolutionary innovation by appropriating pre-existing genes for new functions with or without gene duplication (Harlin-Cognato *et al.* 2006). As the exomitochondrial F_1-ATPase subunits do not constitute a complete complex of F_0F_1-ATPase, they might have a function different from that in F_0F_1-ATPase. In particular, the gene coopted between the mitochondria and the cytosol is unique, and might be related to the transfer of genes from the original endosymbiont to the nuclear genome of the host (Gray *et al*. 1999). Analyses of how and why the nuclear-encoded mitochondrial protein used in the cytosol may provide a hint for understanding the origin of the eukaryotic cell (Andersson *et al.* 2003).

6.2 Perspective for understanding the target molecules of NaN_3 involved in cytoplasmic and cortical reorganization

The finding that NaN_3 could inhibit cytoplasmic and cortical reorganization is a good clue for analyzing the molecular mechanism underlying the correct localization of maternal factors in mosaic eggs. The quest for the molecular target of NaN_3 offers a good experimental system for analyzing cytoplasmic and cortical reorganization at the molecular level. However, very few experimental tools are available for studying the molecular mechanisms of ascidian maternal factors. Inhibition of maternal proteins by the microinjection of antibodies (e.g. Nishikata *et al.* 1987), and knockdown of maternal

mRNAs by antisense-oligonucleotides within the unfertilized egg (e.g. Nishida & Sawada 2001) are examples of such experiments. However, recently, a transgenic technique has been developed in the ascidian and can be used to knockdown specific maternal genes (Sasakura *et al.* 2010; Kawai *et al.* 2012). Listing all p-loop-containing ATPases, metalloproteins, and components of exo-ATPα/β that are expressed during oogenesis, and knocking down each gene, is a promising way to identify candidate molecules and to prove their functions in cytoplasmic and cortical reorganization. Because myoplasmic reorganization is one of the most dynamic phenomena in intracellular transport systems, the molecular mechanism could be characteristic and novel. The molecular mechanism, which is inhibited by NaN_3, will open a new paradigm of molecular transport.

6.3 Perspective for understanding the target molecules of NaN_3 involved in microtubule dynamics

In ascidian development, it was revealed the effects of NaN_3 on the microtubule dynamics, such as the spindle midzone formation and spindle orientation, in a similar concentration where those affected the cytoplasmic reorganization. This suggested that the target molecule of NaN_3 could be similar in both cytoplasmic reorganization and cleavage. Both cellular processes are microtubule dependent (Chiba *et al.* 1999; Alberts *et al.* 2009). So, it could be possible that the NaN_3 inhibited the conserved mechanism in controlling the microtubule dynamics.

Moreover, it was further revealed that the effects of NaN_3 on the microtubule

dynamics were conserved within ascidian embryo, sea urchin embryo and human cultured cell. This might suggest that NaN_3 bound to and inhibited the key molecule(s) involved in the microtubule dynamics conserved at least in deuterostomes. Thus, it was suggest the aurora, end binding 1 (EB1), and polo-like kinase 1 (Plk1) as candidates for the NaN_3 target, because they are reported to have roles in both midzone formation and spindle orientation (Kallio *et al.* 2002; Petronczki *et al*. 2008; Zimniak *et al.* 2009; Carmena *et al*. 2009; Abe *et al*. 2010; Tamura & Draviam 2012; Lu & Johnston 2013) and are highly conserved among yeast to human including sea urchin and ascidian. Recently, these molecules are receiving increased attention as important molecules for controlling the mitosis (Kallio *et al.* 2002; Carmena *et al*. 2009; Abe *et al*. 2010; Tamura & Draviam 2012; Petronczki *et al*. 2008). The experimental system using the NaN_3 could be helpful to reveal the basic mechanism underlying the mitosis.

6.4 Perspective for the relationship between intracellular transport system and microtubule dynamics

The spindle orientation relative to cell polarity axes regulates the cell division plane. The orientation is achieved through signaling pathways that provide a molecular link between the cell cortex and astral microtubules (Lu & Johnston 2013). Moreover, the relationship between nuclear division and cytokinesis in mitosis has not been settled since Rappaport and Rappaport (1974, 1985, 1993) extensively studied using sea urchin embryo. They revealed that the mitotic apparatus determines furrow placement in the cell cortex (Rappaport 1961). In ascidian embryo, as the sperm aster and the cortical

region of the myoplasm are important for the cytoplasmic and cortical reorganization, the interaction between sperm aster and the egg cortex might play a key role in the reorganization (Chiba *et al.* 1999). In this context, the relationship between microtubules and cortical region of cell might have pivotal role in many cellular processes including mitosis and intracellular transport.

If the target molecule of NaN_3 is located in the cortical region of the cell and controlled the microtubule dynamics including ascidian cytoplasmic reorganization, it might have a fundamental role for linking between microtubules and cell cortex. Moreover, if the target molecule of NaN_3 was identical to all the microtubule-dependent cellular process, quest for the target molecules of NaN_3 will be a clue to understanding the unknown mechanism of microtubules including mitosis and intracellular transport.

Acknowledgements

I would like to sincerely thank my research advisor, Professor Takahito Nishikata, for his continuous support in my works. He taught me the essentials of how to do and plan the experiments, how to analyze the data, and how to write papers. I also thank Mr. Takuma Shirai, Ms. Chisato Makino, Ms. Shiori Kunihiro, and all members of Dr. Nishikata's Lab for technical supports and discussions.

I would like to appreciate to Professor Junji Kawakami and Professor Satoshi Fujii for critical reading of this thesis and their valuable suggestions.

I would also like to thank Dr. Janet Chenevert at Université Pierre et Marie Curie and CNRS for the collaborative works described in Chapter 4.1.

I wish to thank Dr. Kyoko Hatano and Mr. Manabu Tanaka at Kyoto University for the collaborative works and initial technical guidance on electron microscopy as described in Chapter 4.2.

Adult *C. intestinalis* were provided by Kyoto University and University of Tokyo with support from the National Bio-Resource Project (NBRP) of the MEXT, Japan. I thank Dr A. Kijima and all the members of the Onagawa Field Science Center, Tohoku University; Dr M. Furusho of the Faculty of Maritime Sciences, Kobe University; Dr T. G. Kusakabe of the Faculty of Science and Engineering, Konan University; and Dr Y. Satou and Ms K. Hirayama of Kyoto University for their kind help in collecting animals.

This work was supported in part by the Sasakawa Scientific Research Grant from

the Japan Science Society (2010-2012).

References

Abe, Y., Okumura, E., Hosoya, T., Hirota, T. and Kishimoto, T. (2010). A single starfish Aurora kinase performs the combined functions of Aurora-A and Aurora-B in human cells. *J. Cell Sci.* **123**, 3978–3988.

Aiken, K. J., Bickford, J. S., Kilberg, M. S. and Nick, H. S. (2008). Metabolic regulation of manganese superoxide dismutase expression via essential amino acid deprivation. *J. Biol .Chem.* **283**, 10252–10263.

Alberts, B., Johnson, A., Lewis, J., Raff M., Roberts, K. and Walter, P. (2007). *Molecular Biology of the Cell,* Garland Science, New York, 5th ed.

Amikura, R., Sato, K. and Kobayashi, S. (2005). Role of mitochondrial ribosome-dependent translation in germline formation in Drosophila embryos. *Mech. Dev.* **122**, 1087–1093.

Andersson, S. G., Karlberg, O., Canback, B. and Kurland, C. G. (2003). On the origin of mitochondria: a genomics perspective. *Philos. Trans. R. Soc. Lond. B. Biol. Sci.* **358**, 165–177. discussion 177–179.

Andreyev, A. Y., Kushnareva, Y. E. and Starkov, A. A. (2005). Mitochondrial metabolism of reactive oxygen species. *Biochemistry Mosc.* **70**, 200–214.

Arboleda, D., Forostyak, S., Jendelova, P., Marekova, D., Amemori, T., Pivonkova, H., Masinova, K. and Sykova, E. (2011). Transplantation of predifferentiated adipose-derived stromal cells for the treatment of spinal cord injury. Cell Mol. Neurobiol. **31**, 1113–1122.

Aridor, M. and Hannan, L. A. (2000). Traffic jam: a compendium of human diseases that affect intracellular transport processes. *Traffic*. **1**, 836–851.

Balaratnasingam, C., Morgan, W. H., Bass, L., Kang, M., Cringle, S. J. and Yu, D. Y. (2011) Axotomy-induced cytoskeleton changes in unmyelinated mammalian central nervous system axons. Neuroscience **177**, 269–282.

Berg, W. E. and Humphreys, W. J. (1960). Electron microscopy of four-cell stages of the ascidians Ciona and Styela. *Dev.Biol.* **2**, 42–60.

Bordeaux, J., Welsh, A., Agarwal, S., Killiam, E., Baquero, M., Hanna, J., Anagnostou, V. and Rimm, D. (2010). Antibody validation. *Biotechniques* **48**, 197–209.

Bowler, M. W., Montgomery, M. G., Leslie, A. G. and Walker, J. E. (2006). How azide inhibits ATP hydrolysis by the F-ATPases. *Proc. Natl. Acad. Sci. USA* **103**,

8646–8649.

Brown, E. J., Albers, M. W., Shin, T. B., Ichikawa, K., Keith, C. T., Lane, W. S. and Schreiber, S. L. (1994). A mammalian protein targeted by G1-arresting rapamycin-receptor complex. *Nature* **369**, 756–758.

Cafferkey, R., Young, P. R., McLaughlin, M. M., Bergsma, D. J., Koltin, Y., Sathe, G. M., Faucette, L., Eng, W.K., Johnson, R.K. and Livi, G.P. (1993). Dominant missense mutations in a novel yeast protein related to mammalian phosphatidylinositol 3-kinase and VPS34 abrogate rapamycin cytotoxicity. *Mol. Cell. Biol.* **13**, 6012–6023.

Carmena, M., Ruchaud, S. and Earnshaw, W. C. (2009). Making the Auroras glow: regulation of Aurora A and B kinase function by interacting proteins. *Curr. Opin. Cell Biol.* **21**, 796–805.

Chenevert, J., Pruliere, G., Ishii, H., Sardet, C. and Nishikata, T. (2013). Purification of Mitochondrial Proteins HSP60 and ATP Synthase from Ascidian Eggs: Implications for Antibody Specificity. *PLoS ONE* **8**, e52996.

Chiba, S., Miki, Y., Ashida, K., Wada, M. R., Tanaka, K. J., Shibata, Y., Nakamori, R. and Nishikata, T. (1999). Interactions between cytoskeletal components during myoplasm rearrangement in ascidian eggs. *Dev. Growth Differ.* **41**, 265–272.

Conklin, E. G. (1905a). Mosaic development in ascidian eggs. *J. Exp. Zool.* **2**, 145–223.

Conklin, E. G. (1905b). The organization and cell lineage of the ascidian egg. *J. Acad. Nat. Sci. Phila.* **13**, 1–119.

Corrêa, C. L., da Silva, S. F., Lowe, J., Tortelote, G. G., Einicker-Lamas, M., Martinez, A. M. and Allodi, S. (2004). Identification of a neurofilament-like protein in the protocerebral tract of the crab Ucides cordatus. *Cell Tissue Res.* **318**, 609–615.

Dallas, S., Zhu, X., Baruchel, S., Schlichter, L. and Bendayan, R. (2003). Functional expression of the multidrug resistance protein 1 in microglia. *J. Pharmacol. Exp. Ther.* **307**, 282–290.

Delsuc, F., Brinkmann, H., Chourrout, D. and Philippe, H. (2006). Tunicates and not cephalochordates are the closest living relatives of vertebrates. *Nature* **439**, 965–968.

DePillis. G. D., Wariishi. H., Gold. M. H. and Ortiz de Montellano, P. R. (1990). Inactivation of lignin peroxidase by phenylhydrazine and sodium azide. *Arch. Biochem. Biophys.* **280**, 217–223.

Dumollard, R., Duchen, M. and Sardet, C. (2006). Calcium signals and mitochondria at fertilisation. *Semin. Cell Dev. Biol.* **17**, 314–323.

Fei, M. J., Yamashita, E., Inoue, N., Yao, M., Yamaguchi, H., Tsukihara, T., Shinzawa-Itoh, K., Nakashima, R. and Yoshikawa, S. (2000). X-ray structure of azide-bound fully oxidized cytochrome c oxidase from bovine heart at 2.9 A resolution. *Acta. Crystallogr D. Biol. Crystallogr* **56**, 529–535.

Fenteany, G., Standaert, R. F., Lane, W. S., Choi, S., Corey, E.J. and Schreiber. S.L. (1995). Inhibition of proteasome activities and subunit-specific amino-terminal threonine modification by lactacystin. *Science* **268**, 726–731.

Franke, F. E., Schachenmayr, W., Osborn, M. and Altmannsberger, M. (1991) Unexpected immunoreactivities of intermediate filament antibodies in human brain and brain tumors. *Am. J. Pathol.* **139**, 67–79.

Franker, M. A. and Hoogenraad, C. C. (2013). Microtubule-based transport–basic mechanisms, traffic rules and role in neurological pathogenesis. *J. cell sci.* **126**, 2319–2329.

Fujiwara, A. and Yasumasu, I. (1997). Does the respiratory rate in sea urchin embryos increase during early development without proliferation of mitochondria? *Dev. Growth Differ.* **39**, 179–189.

Fuller, B. G., Lampson, M. A., Foley, E. A., Rosasco-Nitcher, S., Le, K. V., Tobelmann, P., Brautigan, D. L., Stukenberg, P. T. and Kapoor, T. M. (2008). Midzone activation of aurora B in anaphase produces an intracellular phosphorylation gradient. *Nature* **453**, 1132–1136.

Gilbert, S. F. (2010). *Early Development in Selected Invertebrates*. Developmental Biology. 237–241.

Glotzer, M. (2005). The molecular requirements for cytokinesis. *Science* **307**, 1735–1739.

Gualtieri, R. and Sardet, C. (1989). The endoplasmic reticulum network in the ascidian egg: localization and calcium content. *Biol. Cell* **65**, 301–304.

Gray, M. W., Burger, G. and Lang, B. F. (1999). Mitochondrial evolution. *Science* **283**, 1476–1481.

Harlin-Cognato, A., Hoffman, E. A. and Jones, A. G. (2006). Gene cooption without duplication during the evolution of a male-pregnancy gene in pipefish. *Proc. Natl. Acad. Sci. USA* **103**, 19407–19412.

Harris, R. Z., Wariishi, H., Gold, M. H. and Ortiz de Montellano, P. R. (1991). The catalytic site of manganese peroxidase. Regiospecific addition of sodium azide and

alkylhydrazines to the heme group. *J. Biol. Chem.* **266**, 8751–8758.

Herrmann, J. M. (2009). Putting a break on protein translocation: Metabolic regulation of mitochondrial protein import: MicroCommentary. *Mol. Microbiol.* **72**, 275–278.

Hibino, T., Nishikata, T. and Nishida H. (1998). Centrosome-attracting body: a novel structure closely related to unequal cleavages in the ascidian embryo. *Dev. Growth Differ.* **40**, 85–95.

Hirata, T., Iwamoto-Kihara, A., Sun-Wada, G. H., Okajima, T., Wada, Y. and Futai, M. (2003). Subunit rotation of vacuolar-type proton pumping ATPase: relative rotation of the G and C subunits. *J. Biol. Chem.* **278**, 23714–23719.

Hirokawa, N., Noda, Y., Tanaka, Y. and Niwa, S. (2009). Kinesin superfamily motor proteins and intracellular transport. *Nat. Rev. Mol. Cell Biol.* **10**, 682–696.

Hirokawa, N. (2011). From electron microscopy to molecular cell biology, molecular genetics and structural biology: intracellular transport and kinesin superfamily proteins, KIFs: genes, structure, dynamics and functions. *J. Electron Microsc. (Tokyo)* **60**, S63–92.

Hollenberg, P. F. (1992). Mechanisms of cytochrome P450 and peroxidase-catalyzed xenobiotic metabolism. *FASEB J*. **6**, 686–694.

Hong, S. and Pedersen, P. L. (2008). ATP synthase and the actions of inhibitors utilized to study its roles in human health, disease, and other scientific areas. *Microbiol. Mol. Biol. Rev.* **72**, 590–641.

Iseto, T. and Nishida, H. (1999). Ultrastructural studies on the centrosome-attracting body: electron-dense matrix and its role in unequal cleavages in ascidian embryos. *Dev. Growth Differ.* **41**, 601–109.

Ishii, H., Kunihiro, S., Tanaka, M., Hatano, K. and Nishikata, T. (2012). Cytosolic subunits of ATP synthase are localized to the cortical endoplasmic reticulumrich domain of the ascidian egg myoplasm. *Dev. Growth Differ.* **54**, 753–766.

Ishii, H., Shirai, T. Makino, C. and Nishikata, T. (2014). Mitochondrial inhibitor sodium azide inhibits the reorganization of mitochondria-rich cytoplasm and the establishment of the anteroposterior axis in ascidian embryo. *Dev. Growth Differ.* **56**, 175–188.

Jeffery, W. R. and Meier, S. (1983). A yellow crescent cytoskeletal domain in ascidian eggs and its role in early development. *Dev. Biol.* **96**, 125–143.

Jeffery, W. R. (1985). Identification of proteins and mRNAs in isolated yellow crescents of ascidian eggs. J. *Embryol. Exp. Morphol.* **89**, 275–287.

Jeffery, W. R. and Swalla, B. J. (1992). Factors necessary for restoring an evolutionary change in an anural ascidian embryo. *Dev. Biol.* **153**, 194–205.

Jeffery, W. R. (1995). Development and evolution of an egg cytoskeletal domain in ascidians. *Curr. Top. Dev. Biol.* **31**, 243–276.

Jha, S., Karnani, N., Dhar, S. K., Mukhopadhayay, K., Shukla, S., Saini, P., Mukhopadhayay, G. and Prasad, R. (2003). Purification and characterization of the N-terminal nucleotide binding domain of an ABC drug transporter of Candida albicans: uncommon cysteine 193 of Walker A is critical for ATP hydrolysis. *Biochemistry* **42**, 10822–10832.

Ju, R., Mao, Y., Glick, M. J., Muller, M. T. and Snyder, R. D. (2001). Catalytic inhibition of DNA topoisomerase IIalpha by sodium azide. *Toxicol. Lett.* **121**, 119–126.

Kallio, M. J., McCleland, M. L., Stukenberg, P. T. and Gorbsky, G. J. (2002). Inhibition of aurora B kinase blocks chromosome segregation, overrides the spindle checkpoint, and perturbs microtubule dynamics in mitosis. *Curr. Biol.* **12**, 900–905.

Karabinos, A., Zimek, A. and Weber, K. (2004). The genome of the early chordate Ciona intestinalis encodes only five cytoplasmic intermediate filament proteins including a single type I and type II keratin and a unique IF-annexin fusion protein. *Gene* **326**, 123–129.

Karniely, S. and Pines, O. (2005). Single translation--dual destination: mechanisms of dual protein targeting in eukaryotes. *EMBO Rep*. **6**, 420–425.

Kawai, N., Ochiai, H., Sakuma, T., Yamada, L., Sawada, H., Yamamoto, T. and Sasakura, Y. (2012). Efficient targeted mutagenesis of the chordate Ciona intestinalis genome with zinc-finger nucleases. *Dev. Growth Differ.* **54**, 535–545.

Kenan, D .J. and Wahl, M. L. (2005). Ectopic localization of mitochondrial ATP synthase: A target for anti-angiogenesis intervention? *J. Bioenerg. Biomembr*. **37**, 461–465.

Kloc, M., Bilinski, S. and Etkin, L. D. (2004). The Balbiani body and germ cell determinants: 150 years later. *Curr Top Dev. Biol.* **59**, 1–36.

Knox, C., Sass, E., Neupert, W. and Pines, O. (1998). Import into mitochondria, folding and retrograde movement of fumarase in yeast. *J. Biol. Chem.* **273**, 25587–25593

Ko, Y. H., Delannoy, M., Hullihen, J., Chiu, W. and Pedersen, P. L. (2003). Mitochondrial ATP synthasome. Cristae-enriched membranes and a multiwell detergent screening assay yield dispersed single complexes containing the ATP synthase and carriers for Pi and ADP/ATP. *J. Biol. Chem.* **278**, 12305–12309.

Kumano, G., Takatori, N., Negishi, T., Takada, T. and Nishida, H. (2011). A maternal factor unique to ascidians silences the germline via binding to P-TEFb and RNAP II regulation. *Curr Biol*. **21**, 1308–1313.

Kunz, J., Henriquez, R., Schneider, U., Deuter-Reinhard, M., Movva, N. R. and Hall, M. N. (1993). Target of rapamycin in yeast, TOR2, is an essential phosphatidylinositol kinase homolog required for G1 progression. *Cell* **73**, 585–596.

Lambert, C. C. and Epel, D. (1979). Calcium-mediated mitochondrial movement in ascidian sperm during fertilization. *Dev. Biol.* **69**, 296–304.

Lambert, C. C. and Koch, R. A. (1988). Sperm Binding and Penetration during Ascidian Fertilization. *Dev. Growth Differ.* **30**, 325–336.

Lemaire, P., Smith, W. C. and Nishida, H. (2008). Ascidians and the plasticity of the chordate developmental program. *Curr. Biol.* **18**, R620–631.

Linnett, P. E., Mitchell, A. D. and Beechey, R. B. (1975). Changes in inhibitor sensitivity of the mitochondrial ATPase activity after detergent solubilisation. *FEBS Lett.* **53**, 180–183.

Lu, M. S., and Johnston, C. A. (2013). Molecular pathways regulating mitotic spindle orientation in animal cells. *Development* **140**, 1843–1856.

Makabe, K. W., Kawashima, T., Kawashima, S., Minokawa, T., Adachi, A., Kawamura, H., Ishikawa, H., Yasuda, R., Yamamoto, H., Kondoh, K., Arioka, S., Sasakura, Y., Kobayashi, A., Yagi, K., Shojima, K., Kondoh, Y., Kido, S., Tsujinami, M., Nishimura, N., Takahashi, M., Nakamura, T., Kanehisa, M., Ogasawara, M., Nishikata, T. and Nishida, H. (2001). Large-scale cDNA analysis of the maternal genetic information in the egg of Halocynthia roretzi for a gene expression catalog of ascidian development. *Development* **128**, 2555–2567.

Mandal, S., Guptan, P., Owusu-Ansah, E. and Banerjee, U. (2005). Mitochondrial regulation of cell cycle progression during development as revealed by the tenured mutation in Drosophila. *Dev. Cell* **9**, 843–854.

Mangiullo, R., Gnoni, A., Leone, A., Gnoni, G. V., Papa, S. and Zanotti, F. (2008). Structural and functional characterization of F(o)F(1)-ATP synthase on the extracellular surface of rat hepatocytes. *Biochim. Biophys. Acta.* **1777**, 1326–1335.

Marikawa (1995) Distribution of myoplasmic cytoskeletal domains among egg fragments of the ascidian Ciona savignyi: the concentration of the deep filament lattice in the fragment enriched in muscle determinants. *J. Exp. Zool.* **271**, 348–355.

Martel, R. R., Klicius, J. and Galet, S. (1977). Inhibition of the immune response by rapamycin, a new antifungal antibiotic. *Can. J. Physiol. Pharmacol.* **55**, 48–51.

Martinez, L. O., Jacquet, S., Esteve, J. P., Rolland, C., Cabezón, E., Champagne, E., Pineau, T., Georgeaud, V., Walker, J. E., Tercé, F., Collet, X., Perret, B. and Barbaras, R. (2003). Ectopic β-chain of ATP synthase is an apolipoprotein A-I receptor in hepatic HDL endocytosis. *Nature* **421**, 75–79.

Michel, M. C., Wieland, T. and Tsujimoto, G. (2009). How reliable are G-protein-coupled receptor antibodies? *Naunyn. Schmiedebergs Arch. Pharmacol* **379**, 385–388.

Miller, A., Wang, L. and Kendall, D. A. (2002). SecB modulates the nucleotide-bound state of SecA and stimulates ATPase activity. *Biochemistry* **41**, 5325–5332.

Mitra, K., Wunder, C., Roysam, B., Lin, G. and Lippincott-Schwartz, J. (2009). A hyperfused mitochondrial state achieved at G1-S regulates cyclin E buildup and entry into S phase. *Proc. Natl. Acad. Sci. USA* **106**, 11960–11965.

Miya, T., Makabe, K. and Satoh, N. (1994). Expression of a gene for major mitochondrial protein, ADP/ATP tranlocase, during embryogenesis in the ascidian Halocynthia roretzi. *Dev. Growth Differ.* **36**, 39–48.

Moser, T. L., Kenan, D. J., Ashley, T. A., Roy, J. A., Goodman, M. D., Misra, U. K., Cheek, D. J. and Pizzo, S. V. (2001). Endothelial cell surface F1-FO ATP synthase is active in ATP synthesis and is inhibited by angiostatin. *Proc. Natl. Acad. Sci. USA* **98**, 6656–6661.

Nakajima, K., Yin, X., Takei, Y., Seog, D. H., Homma, N. and Hirokawa, N. (2012). Molecular motor KIF5A is essential for GABA(A) receptor transport, and KIF5A deletion causes epilepsy. *Neuron* **76**, 945–961.

Negishi, T., Takada, T., Kawai, N. and Nishida, H. (2007). Localized PEM mRNA and protein are involved in cleavage-plane orientation and unequal cell divisions in ascidians. *Curr. Biol.* **17**, 1014–1025.

Negishi, T., Kumano, G. and Nishida, H. (2011). Polo-like kinase 1 is required for localization of Posterior End Mark protein to the centrosome-attracting body and unequal cleavages in ascidian embryos. *Dev. Growth Differ.* **53**, 76–87.

Nishida, H. (1994). Localization of determinants for formation of the anterior-posterior axis in eggs of the ascidian Halocynthia roretzi. *Development* **120**, 3093–3104.

Nishida, H. and Sawada, K. (2001). macho-1 encodes a localized mRNA in ascidian eggs that specifies muscle fate during embryogenesis. *Nature* **409**, 724–729.

Nishida, H. (2005). Specification of embryonic axis and mosaic development in

ascidians. *Dev. Dyn.* **233**, 1177–1193.

Nishikata, T., Mita-Miyazawa, I., Deno, T. and Satoh, N. (1987). Monoclonal antibodies against components of the myoplasm of eggs of the ascidian Ciona intestinalis partially block the development of muscle-specific acetylcholinesterase. *Development* **100**, 577–586.

Nishikata, T. and Wada, M. (1996). Molecular characterization of myoplasmin-C1: a cytoskeletal component localized in the myoplasm of the ascidian egg. *Dev. Genes. Evol.* **206**, 72–79.

Nishikata, T., Hibino, T. and Nishida, H. (1999). The centrosome-attracting body, microtubule system, and posterior egg cytoplasm are involved in positioning of cleavage planes in the ascidian embryo. *Dev. Biol.* **209**, 72–85.

Nishikata, T., Yamada, L., Mochizuki, Y., Satou, Y., Shin-i, T., Kohara, Y. and Satoh, N. (2001). Profiles of maternally expressed genes in fertilized eggs of Ciona intestinalis. *Dev. Biol.* **238**, 315–331.

Nomura, M., Nakajima, A. and Inaba, K. (2009). Proteomic profiles of embryonic development in the ascidian Ciona intestinalis. *Dev. Biol.* **325**, 468–481.

Oliver, D. B., Cabelli, R. J., Dolan, K. M. and Jarosik, G. P. (1990). Azide-resistant mutants of Escherichia coli alter the SecA protein, an azide-sensitive component of the protein export machinery. *Proc. Natl. Acad. Sci. USA* **87**, 8227–8231.

Omura, S., Fujimoto, T., Otoguro, K., Matsuzaki, K., Moriguchi, R., Tanaka, H. and Sasaki, Y. (1991). Lactacystin, a novel microbial metabolite, induces neuritogenesis of neuroblastoma cells. *J. Antibiot. (Tokyo)* **44**, 113–116.

Ortiz de Montellano, P. R., David, S. K., Ator, M. A. and Tew, D. (1988). Mechanism-based inactivation of horseradish peroxidase by sodium azide. Formation of meso-azidoprotoporphyrin IX. *Biochemistry* **27**, 5470–5476.

Paix, A., Yamada, L., Dru, P., Lecordier, H., Pruliere, G., Chenevert, J., Satoh, N. and Sardet, C. (2009). Cortical anchorages and cell type segregations of maternal postplasmic/PEM RNAs in ascidians. *Dev. Biol.* **336**, 96–111

Patalano, S., Prulière, G., Prodon, F., Paix, A., Dru, P., Sardet, C. and Chenevert J. (2006). The aPKC-PAR-6-PAR-3 cell polarity complex localizes to the centrosome attracting body, a macroscopic cortical structure responsible for asymmetric divisions in the early ascidian embryo. *J. Cell Sci.* **119**, 1592–1603.

Petronczki, M., Lénárt, P. and Peters, J. M. (2008). Polo on the Rise-from Mitotic Entry to Cytokinesis with Plk1. *Dev. Cell* **14**, 646–659.

Prodon, F., Dru, P., Roegiers, F. and Sardet, C. (2005). Polarity of the ascidian egg

cortex and relocalization of cER and mRNAs in the early embryo. *J. Cell Sci.* **118**, 2393–2404.

Prodon, F., Chenevert, J. and Sardet, C. (2006). Establishment of animal-vegetal polarity during maturation in ascidian oocytes. *Dev. Biol.* **290**, 297–311.

Prodon, F., Yamada, L., Shirae-Kurabayashi, M., Nakamura, Y. and Sasakura, Y. (2007). Postplasmic/PEM RNAs: a class of localized maternal mRNAs with multiple roles in cell polarity and development in ascidian embryos. *Dev. Dyn.* **236**, 1698–1715.

Rappaport, R. (1961). Experiments concerning the cleavage stimulus in sand dollar eggs. *J. Exp. Zool.* 148, 81–89

Rappaport, R. (1985). Repeated furrow formation from a single mitotic apparatus in cylindrical sand dollar eggs. *J. Exp. Zool.* **234**, 167–171.

Rappaport, R. and Rappaport, B. N. (1974). Establishment of cleavage furrows by the mitotic spindle. *J. Exp. Zool.* 189, 189–196.

Rappaport, R. and Rappaport, B. N. (1993). Duration of division-related events in cleaving sand dollar eggs. *Dev. Biol.* **158**, 265–273.

Regev-Rudzki, N., Karniely, S., Ben-Haim, N. N. and Pines, O. (2005). Yeast aconitase in two locations and two metabolic pathways: seeing small amounts is believing. *Mol. Biol. Cell*. **16**, 4163–4171.

Reverberi, G. (1975). On some effects of cytochalasin B on the eggs and tadpoles of the ascidians. *Acta. Embryol. Exp.* **2**, 137–158.

Roegiers, F., McDougall, A. and Sardet, C. (1995). The sperm entry point defines the orientation of the calcium-induced contraction wave that directs the first phase of cytoplasmic reorganization in the ascidian egg. *Development* **121**, 3457–3466.

Roegiers, F., Djediat, C., Dumollard, R., Rouvière, C. and Sardet, C. (1999). Phases of cytoplasmic and cortical reorganizations of the ascidian zygote between fertilization and first division. *Development* **126**, 3101–3117.

Ruchaud, S., Carmena, M. and Earnshaw, W. C. (2007). Chromosomal passengers:conducting cell division. *Nat. Rev. Mol. Cell Biol.* **8**, 798–812.

Sabatini, D. M., Erdjument-Bromage, H., Lui, M., Tempst, P. and Snyder, S. H. (1994) RAFT1: a mammalian protein that binds to FKBP12 in a rapamycin-dependent fashion and is homologous to yeast TORs. *Cell* **78**, 35–43.

Sabers, C. J., Martin, M. M., Brunn, G. J., Williams, J. M., Dumont, F. J., Wiederrecht, G. and Abraham, R. T. (1995). Isolation of a protein target of the FKBP12-rapamycin complex in mammalian cells. *J. Biol. Chem.* **270**, 815–822.

Saito, T., Shiba, K., Inaba, K., Yamada, L. and Sawada, H. (2012). Self-incompatibility response induced by calcium increase in sperm of the ascidian Ciona intestinalis. *Proc. Natl. Acad. Sci. USA* **109**, 4158–4162.

Samokyszyn, V. M. and Ortiz de Montellano, P. R. (1991). Topology of the chloroperoxidase active site: regiospecificity of heme modification by phenylhydrazine and sodium azide. *Biochemistry* **30**, 11646–11653.

Sardet, C., Speksnijder, J., Inoue, S. and Jaffe, L. (1989). Fertilization and ooplasmic movements in the ascidian egg. *Development* **105**, 237–249.

Sardet, C., Speksnijder, J., Terasaki, M. and Chang, P. (1992). Polarity of the ascidian egg cortex before fertilization. *Development* **115**, 221–237.

Sardet, C., Nishida, H., Prodon, F. and Sawada, K. (2003). Maternal mRNAs of PEM and macho 1, the ascidian muscle determinant, associate and move with a rough endoplasmic reticulum network in the egg cortex. *Development* **130**, 5839–5849.

Sardet, C., Dru, P. and Prodon, F. (2005). Maternal determinants and mRNAs in the cortex of ascidian oocytes, zygotes and embryos. *Biol. Cell* **97**, 35–49.

Sardet, C., Paix, A., Prodon, F., Dru, P. and Chenevert, J. (2007). From oocyte to 16-cell stage: cytoplasmic and cortical reorganizations that pattern the ascidian embryo. *Dev. Dyn.* **236**, 1716–1731.

Sasakura, Y., Suzuki, M. M., Hozumi, A., Inaba, K. and Satoh, N. (2010). Maternal factor-mediated epigenetic gene silencing in the ascidian Ciona intestinalis. *Mol. Genet. Genomics* **283**, 99–110.

Satoh, N. (1979). On the 'clock' mechanism determining the time of tissue-specific enzyme development during ascidian embryogenesis. I. Acetylcholinesterase development in cleavage-arrested embryos. *J. Embryol. Exp. Morphol.* **54**, 131–139.

Satoh, N., Deno, T., Nishida, H., Nishikata, T. and Makabe, K. W. (1990). Cellular and molecular mechanisms of muscle cell differentiation in ascidian embryos. *Int. Rev. Cytol.* **122**, 221–258.

Satoh, N. (1994). *Developmental Biology of Ascidians.* Cambridge, Cambridge University Press, Cambrige.

Satoh, N. (2003). The ascidian tadpole larva: comparative molecular development and genomics. *Nat. Rev. Genet.* **4**, 285–295.

Sawada, T. and Schatten, G. (1988). Microtubules in ascidian eggs during meiosis, fertilization, and mitosis. *Cell Motil. Cytoskeleton* **9**, 219–230.

Sawada, T. and Schatten, G. (1989). Effects of cytoskeletal inhibitors on ooplasmic

segregation and microtubule organization during fertilization and early development in the ascidian Molgula occidentalis. *Dev. Biol.* **132**, 331–342.

Schäfer, G. and Meyering-Vos, M. (1992). The plasma membrane ATPase of archaebacteria. A chimeric energy converter. *Ann. N. Y. Acad. Sci.* **671**, 293–309.

Schnell, U., Dijk, F., Sjollema, K. A. and Giepmans, B. N. G. (2012). Immunolabeling artifacts and the need for live-cell imaging. *Nat. Methods* **9**, 152–158.

Schreiber, S. L. (1991). Chemistry and biology of the immunophilins and their immunosuppressive ligands. *Science* **251**, 283–287.

Schreiber, S. L. (1993). Chemical genetics. *Chem. Eng. News* **81**, 51–61.

Sciacovelli, M., Guzzo, G., Morello, V., Frezza, C., Zheng, L., Nannini, N., Calabrese, F., Laudiero, G., Esposito, F., Landriscina, M., Defilippi, P., Bernardi, P. and Rasola, A. (2013). The mitochondrial chaperone TRAP1 promotes neoplastic growth by inhibiting succinate dehydrogenase. *Cell Metab.* **17**, 988–999.

Sharif, B., Na, J., Lykke-Hartmann, K., McLaughlin, S. H., Laue, E., Glover, D. M. and Zernicka-Goetz, M. (2010). The chromosome passenger complex is required for fidelity of chromosome transmission and cytokinesis in meiosis of mouse oocytes. *J. Cell Sci.* **123**, 4292–4300.

Shimai, K., Ishii, H. and Nishikata. T. (2010). Interaction between Oocyte and Accessory Cells during Ascidian Oogenesis. *Mem. Konan Univ., Sci. Eng. Ser.* **6**, 31–41.

Shirae-Kurabayashi, M., Nishikata, T., Takamura, K., Tanaka, K. J., Nakamoto, C. and Nakamura, A. (2006). Dynamic redistribution of vasa homolog and exclusion of somatic cell determinants during germ cell specification in Ciona intestinalis. *Development* **133**, 2683–2693.

Shirae-Kurabayashi, M., Matsuda, K. and Nakamura, A. (2011). Ci-Pem-1 localizes to the nucleus and represses somatic gene transcription in the germline of Ciona intestinalis embryos. *Development* **138**, 2871–2881.

Sharif, B., Na, J., Lykke-Hartmann, K., McLaughlin, S. H., Laue, E., Glover, D. M. and Zernicka-Goetz, M. (2010). The chromosome passenger complex is required for fidelity of chromosome transmission and cytokinesis in meiosis of mouse oocytes. *J. Cell Sci.* **123**, 4292–4300.

Sjostrand, T. (1953). The oxidation of haemoglobin in the presence of NaN_3. *Acta. Physiol. Scand.* **28**, 244–254.

Soltys, B. J. and Gupta, R. S. (1999). Mitochondrial-matrix proteins at unexpected locations: are they exported? *Trends Biochem. Sci.* **24**,174–177.

Soper, J. W. and Pedersen, P. L. (1976). Adenosine triphosphatase of rat liver mitochondria: detergent solubilization of an oligomycin- and dicyclohexylcarbodiimide-sensitive form of the enzyme. *Biochemistry* **15**, 2682–2690.

Speksnijder, J. E., Terasaki, M., Hage, W. J., Jaffe, L. F. and Sardet, C. (1993). Polarity and reorganization of the endoplasmic reticulum during fertilization and ooplasmic segregation in the ascidian egg. *J. Cell Biol.* **120**, 1337–1346.

Steedman, H. F. (1957). Polyester wax; a new ribboning embedding medium for histology. *Nature* **179**, 1345.

Stein, I., Peleg, Y., Even-Ram, S. and Pines, O. (1994). The single translation product of the FUM1 gene (fumarase) is processed in mitochondria before being distributed between the cytosol and mitochondria in Saccharomyces cerevisiae. *Mol. Cell. Biol.* **14**, 4770–4778.

Suen, D. F., Norris, K. L. and Youle, R. J. (2008). Mitochondrial dynamics and apoptosis. *Genes Dev.* **22**, 1577–1590.

Spurr, A. R. (1969). A low-viscosity epoxy resin embedding medium for electron microscopy. *J. Ultrastruct. Res.* **26**, 31–43.

Swalla, B. J., Badgett, M. R. and Jeffery, W. R. (1991). Identification of a cytoskeleton protein localized in the myoplasm of ascidian eggs: Localization is modifed during anural development. *Development* **111**, 425–436.

Symersky, J., Osowski, D., Walters, D. E. and Mueller, D. M. (2012). Oligomycin frames a common drug-binding site in the ATP synthase. *Proc. Natl. Acad. Sci. USA* **109**, 13961–13965.

Tamura, N. and Draviam, V. M. (2012). Microtubule plus-ends within a mitotic cell are 'moving platforms' with anchoring, signalling and force-coupling roles. *Open Biol.* **2**, 120132.

Tuisel, H., Grover, T. A., Lancaster, J. R. Jr., Bumpus, J. A. and Aust, S. D. (1991). Inhibition of lignin peroxidase H2 by sodium azide. *Arch. Biochem. Biophys.* **288**, 456–462.

Uchida, E., Ohsumi, Y. and Anraku, Y. (1985). Purification and properties of H+-translocating, Mg2+-adenosine triphosphatase from vacuolar membranes of Saccharomyces cerevisiae. *J. Biol. Chem.* **260**, 1090–1095.

Vader, G., Medema, R. H. and Lens, S. M. (2006). The chromosomal passenger complex: guiding Aurora-B through mitosis. *J. Cell Biol.* **173**, 833–837.

Vale, R. D. (2003). The molecular motor toolbox for intracellular transport. *Cell* **112**,

467–480.

Vasilyeva, E. and Forgac, M. (1998). Interaction of the clathrin-coated vesicle V-ATPase with ADP and sodium azide. *J. Biol. Chem.* **273**, 23823–23829.

Veitonmäki, N., Cao, R., Wu, L. H., Moser, T. L., Li, B., Pizzo, S. V., Zhivotovsky, B. and Cao, Y. (2004). Endothelial cell surface ATP synthase-triggered caspase-apoptotic pathway is essential for K1-5-induced antiangiogenesis. *Cancer Res.* **64**, 3679–3686.

Willingham, M. C. (1999). Conditional epitopes. is your antibody always specific? *J. Histochem. Cytochem.* **47**, 1233–1236.

Yoshida, S, Marikawa, Y. and Satoh, N. (1996). Posterior end mark, a novel maternal gene encoding a localized factor in the ascidian embryo. *Development* **122**, 2005–2012.

Yoshikawa, S., Shinzawa-Itoh, K., Nakashima, R., Yaono, R., Yamashita, E., Inoue, N., Yao, M., Fei, M. J., Libeu, C. P., Mizushima, T., Yamaguchi, H., Tomizaki, T. and Tsukihara, T. (1998). Redox-coupled crystal structural changes in bovine heart cytochrome c oxidase. *Science* **280**, 1723–1729.

Zhou, R. R., Wang, B., Wang, J., Schatten, H. and Zhang, Y. Z. (2010). Is the mitochondrial cloud the selection machinery for preferentially transmitting wild-type mtDNA between generations? Rewinding Müller's ratchet efficiently. *Curr. Genet.* **56**, 101–107.

Zimniak, T., Stengl, K., Mechtler, K. and Westermann, S. (2009). Phosphoregulation of the budding yeast EB1 homologue Bim1p by Aurora/Ipl1p. *J. Cell Biol.* **186**, 379–391.

Publication list

Original articles

Main papers

1. Ishii, H., Kunihiro, S., Tanaka, M., Hatano, K. and Nishikata, T. (2012). Cytosolic subunits of ATP synthase are localized to the cortical endoplasmic reticulum-rich domain of the ascidian egg myoplasm. *Dev. Growth Differ.* **54**, 753–766.
2. Chenevert, J., Pruliere, G., Ishii, H., Sardet, C. and Nishikata, T. (2013). Purification of Mitochondrial Proteins HSP60 and ATP Synthase from Ascidian Eggs: Implications for Antibody Specificity. *PLoS ONE* **8**, e52996.
3. Ishii, H., Shirai, T. Makino, C. and Nishikata, T. (2014). Mitochondrial inhibitor sodium azide inhibits the reorganization of mitochondria-rich cytoplasm and the establishment of the anteroposterior axis in ascidian embryo. *Dev. Growth Differ.* **56**, 175–188.

Related paper

1. Shimai, K., Ishii, H. and Nishikata, T. (2009). Interaction between Oocyte and Accessory Cells during Ascidian Oogenesis. *Mem. Konan Univ., Sci. Eng. Ser.* **56**, 31–41 (in Japanese with English abstract).

Proceedings

1. 石井宏和, 鷺池将朗, 西方敬人. (2010). ホヤ卵 ATP 合成酵素 α サブユニットおよび β サブユニットは細胞質中に局在する. *生命機能研究会プロシーディングス* **1**, 19–20.

2. 石井宏和, 西方敬人. (2011). ホヤ卵マイオプラズムにはミトコンドリア型 ATP 合成酵素が異所的に局在する. *生命機能研究会プロシーディングス* **2**, 17–18.
3. 石井宏和, 牧野千里, 西方敬人. (2012). ホヤ卵細胞質再配置におけるミトコンドリア阻害剤の影響. *生命機能研究会プロシーディングス* **3**, IVT–1.

Presentations

International meetings

1. Shimai, K., Ishii H., Tamari, Y., Kitaura, Y. and Nishikata, T. The promoter analysis of the ascidian neural tube specific gene. 5th International Tunicate Meeting, Okinawa (June, 2009).
2. Nishikata, T., Shimai, K. and Ishii, H. Ascidian ATP synthase alpha-subunit is localized within the egg cytoplasm. 5th International Tunicate Meeting, Okinawa (June, 2009).
3. Ishii, H. and Nishikata, T. Ectopic ATP synthase was localized to the sub-cortical region of the ascidian egg myoplasm. 6th International Tunicate Meeting, Montreal, Canada (July, 2011).
4. Ishii, H. A new and advantageous experimental system for analyzing the dual targeting mechanism of mitochondrial protein. FIBER International Symposium, Kobe, Japan (November, 2011).
5. Ishii, H., Makino, C. and Nishikata, T. Effects of mitochondrial inhibitors on ascidian ooplasmic segregation. Asia-Pacific Developmental Biology Conference APDBC2012, Taipei, Taiwan (October, 2012).
6. Kunihiro, S., Ishii, H., Tanigawa, A., Inoue, T., and Nishikata, T. The difference between oocyte maturations in and out of the ovary during Ciona oogenesis. 7th international tunicate meeting, Naples, Italy (July, 2013).
7. Ishii, H., Shirai, T., Makino, C. and Nishikata, T. Sodium azide inhibited

ooplasmic segregation in the ascidian embryo. 7th international tunicate meeting, Naples, Italy (July, 2013).

Domestic meetings

1. Ishii, H. and Nishikata T. ATP synthase α-subunit is localized to the egg cytoplasm in the ascidian Ciona intestinalis. FIBER Forum 2008, Kobe (December, 2008).
2. 石井宏和, 島井光太郎, 西方敬人. ホヤ卵内における ATP 合成酵素α鎖の局在と細胞骨格ドメイン. 研究者の集い 2009, 神戸 (2009 年, 9 月).
3. Shimai, K., Ishii, H. and Nishikata, T. Interaction between oocyte and accessory cells during ascidian oogenesis. FIBER Forum 2009, Kobe (December, 2009).
4. Ishii, H., Sagiike, S. and Nishikata, T. Ascidian ATP synthase alpha- and beta-subunit are localized within egg cytoplasm. 第 33 回日本分子生物学会年会・第 83 回日本生化学会大会合同大会, 神戸 (2010 年, 12 月).
5. Ishii, H., Sagiike, S. and Nishikata, T. Ascidian ATP synthase alpha- and beta-subunit are localized within egg cytoplasm. FIBER Forum 2010, Kobe (December, 2010).
6. 石井宏和, 鷺池将朗, 西方敬人. ホヤ卵 ATP 合成酵素αサブユニットおよびβサブユニットは細胞質中に局在する. 第一回生命機能研究会, 神戸 (2010 年、12 月).
7. 石井宏和, 西方敬人. ホヤ卵マイオプラズムにおける ATP 合成酵素の異所的な局在. 日本動物学会近畿支部研究発表会, 京都 (2011 年, 5 月).
8. Ishii, H., Sagiike, S. and Nishikata, T. Ectopic localization of mitochondrial ATP synthase within ascidian egg myoplasm. 第 44 回日本発生生物学会年会, 沖縄 (2011 年, 5 月).
9. 石井宏和, 西方敬人. ホヤ卵マイオプラズムにはミトコンドリア型 ATP 合成酵素が異所的に局在する. 第二回生命機能研究会, 神戸 (2011 年, 8 月).

10. 石井宏和, 国広潮里, 西方敬人. 異所的 ATP 合成酵素 α および β サブユニットはホヤ卵マイオプラズムの表層領域に局在する. 第 34 回日本分子生物学会年会, 横浜 (2011 年, 12 月).
11. 谷川亜里紗, 野島尚俊, 石井宏和, 西方敬人. ホヤ脊索鞘特異的モノクローナル抗体の作製. 日本動物学会近畿支部研究発表会, 京都 (2012 年, 5 月).
12. Ishii, H., Tanaka, M., Hatano, K. and Nishikata, T. Immunoelectron microscopic studies of the ectopic β-subunit of ATP synthase in the ascidian egg. 第 45 回日本発生生物学会大会, 神戸 (2012 年, 5 月).
13. 石井宏和. 異所的 ATP 合成酵素 α および β サブユニットはホヤ卵マイオプラズムの表層領域に局在する. ホヤ研究会 2012, 京都 (2012 年, 6 月).
14. 石井宏和, 牧野千里, 西方敬人. ホヤ卵細胞質再配置におけるミトコンドリア阻害剤の影響. 第三回生命機能研究会, 神戸 (2012 年, 9 月).
15. 石井宏和, 西方敬人. Exo-ATPα/β 複合体はホヤ卵マイオプラズム表層領域に局在する. 日本動物学会第 83 回大阪大会, 大阪 (2012 年, 9 月).
16. Ishii, H., Makino, C. and Nishikata, T. Effects of mitochondrial inhibitors on ascidian ooplasmic segregation. FIBER Forum 2012, Kobe, Japan (November, 2012).
17. 白井琢馬, 石井宏和, 西方敬人. ホヤ卵細胞質再配置における精子星状体形成、移動対すアジ化ナトリウムの影響. 日本動物学会近畿支部研究発表会, 大阪 (2013 年, 5 月).
18. 白井琢馬, 石井宏和, 西方敬人. ホヤ卵細胞質再配置における精子星状体移動に対するアジ化ナトリウムの影響. 第四回生命機能研究会, 滋賀 (2013 年, 9 月).
19. 国広潮里, 石井宏和, 谷川亜里沙, 井上貴裕, 野嶋尚俊, 西方敬人. 卵巣内および海水中におけるホヤ卵成熟過程の比較観察. 第四回生命機能研究会, 滋賀 (2013 年, 9 月).
20. 石井宏和, 白井琢馬, 牧野千里, 西方敬人. ミトコンドリア因子複合体が引き起こすホヤ卵細胞質内における母性因子輸送機構の解析. 第四回生命機能研究会, 滋賀 (2013 年, 9 月).

Others

1. 石井宏和 受賞歴： FIBER 学生研究賞 (2008)
2. 石井宏和 外部研究資金： 財団法人日本科学協会 平成 23 年度笹川科学研究助成 研究代表 (2011.4 - 2012.2)
3. 石井宏和 学会旅費支援金： 日本発生生物学会 APDBC 2012 フェローシップ （2012）
4. 石井宏和 外部研究資金： 財団法人日本科学協会 平成 24 年度笹川科学研究助成 研究代表 (2012.4 - 2013.2)